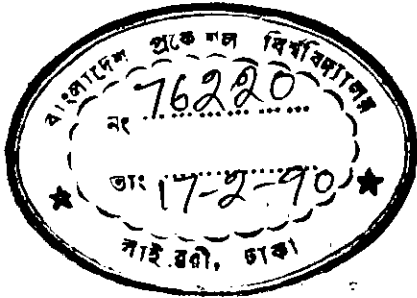# ANALYSIS OF SPINE BEAM BRIDGE DECK

A Thesis

by

SUSANKAR CHANDRA ACHARJEE, B.Sc.Engg. (Civil)

Submitted to the Department of Civil Engineering

Bangladesh University of Engineering and Technology, Dhaka

in partial fulfilment of the requirements for the degree

of

MASTER OF SCIENCE IN CIVIL ENGINEERING
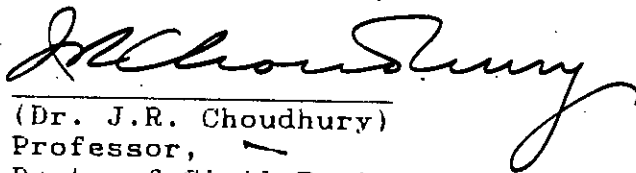
May, 1989

ANALYSIS OF SPINE BEAM BRIDGE DECK

A Thesis
by
SUSANKAR CHANDRA ACHARJEE, B.Sc.Engg. (Civil)
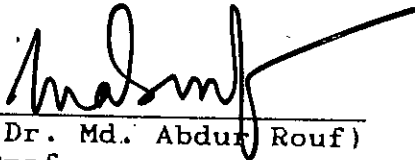
Approved as to style and content by:

(Dr. Md. Alee Murtuza)   Chairman
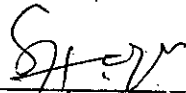Professor and Head,
Dept. of Civil Engg.,
BUET, Dhaka.

(Dr. J.R. Choudhury)   Member
Professor,
Dept. of Civil Engineering,
BUET, Dhaka.

(Dr. Md. Abdur Rouf)   Member
Professor,
Dept. of Civil Engineering,
BUET, Dhaka.

(Mr. A.K.M. Shamsul Haque)   Member
Chief Engineer,   (External)
Jamuna Multipurpose Bridge Authority,
Ganabhaban, Sher-e-Bangla Nagar,Dhaka.

May, 1989

ABSTRACT

Linear elastic analysis of simple Spine Beam Bridge Deck was carried out by Finite Element method and compared with approximate methods such as simple beam theory, method of Kollbrunner, Hajdin and Heilig and beam on elastic foundation analogy. Loading used in the analysis is HS_{20}. The analysis shows that the simple beam theory underestimates the longitudinal stress than that obtained by finite element method. The difference decreases with the increase of span length. But simple beam theory can not predict torsional and distortional warping stresses. The overall effect by approximate methods is predicted by superimposing the results as obtained by the simple beam theory with that of beam on elastic foundation analogy and the method of Kollbrunner, Hajdin and Heilig. After superimposing the results the combined stresses for the spine beams analysed in this study are 16 to 34% lower at top and 4 to 14% higher at bottom of webs than that obtained by Finite element method at midspan for eccentric loading.

Analytical model for analysis of Spine Beam Bridge Decks by Finite Element method is presented by representing the diaphragms by restraining the translational displacements to reduce the computational time. It is found that more than 50% time can be saved by the modelling of the diaphragms in this manner. A parameter study (such as width, thicknesses of' different elements) was performed to highlight the effects of these on the design of a Spine beam bridge deck. The analysis shows that the longitudinal stresses decrease with the increase of web thickness and the ratio of change is more than one.

CONTENTS

ACKNOWLEDGEMENTS

LIST OF FIGURES

LIST OF TABLES

LIST OF SYMBOLS

a_{dis}	Vertical deflection of web associated with distortion
a_t	Vertical deflection of web occuring in torsion without distortion
a_{vlg}	Differential longitudinal deflection in flange associated with shear lag
a_x, a_y, a_z	Displacement in element axes
A	Total area of cross-section including side cantilevers
A_{bot}	bh_{bot} = area of bottom flange
$A_{bot,eff}$	Area of bottom flange of one equivalent beam
A_{cant}	$b_{cant}h_{top}$ = area of cantilever
A_{enc}	bd=area enclosed by mid-line of webs of closed portion of cross-section
A_{top}	bh_{top} = area of top flange
$A_{top,eff}$	Area of top flange of one equivalent beam
$(Ay)_{1/2}$	First moment of area of partial half-cross-section about centroidal x axis
b	Breadth between mid-lines of webs
b_{cant}	Width of cantilever
b_1, b_2	Dimensions relating to lateral position of load
B_{dwr}	Distortional warping bimoment
B_{twr}	Torsional warping bimoment
C_{dwr}	Distortional warping moment of inertia of cross-section
C_{svt}	Torsional moment of inertia of cross-section in St Venant torsion
C_{twr}	Torsional warping moment of inertia of cross-section
d	Depth between mid-lines of top and bottom slabs
d_{shc}	Depth of shear centre below mid-line of top slab
D_x, D_y	Flexural rigidities in the x and y directions
D_1, D_2	Coupline rigidities with respect to x and y directions
D_{xy}, D_{yx}	Torsional rigidities in x and y directions
E	Young's modulus of elasticity
EI_{fra}	Frame stiffness

f_{dwr}	Distortional warping stress
f_{lbg}	Longitudinal bending stress, calculated by engineer's theory of bending
f_{trb}	Torsional warping stress
F_y	Concentrated applied load in the direction of the y axis
G	Shear modulus of elasticity
h	Thickness of web
h_{bot}	Thickness of bottom slab
h_{top}	Thickness of top slab
h_{web}	thickness of web
I_x	Moment of inertia of entire cross-section about the centroidal x axis
I_y	Moment of inertia of entire cross-section about the centroidal y axis
L	Span
m	Poisson's ratio
M_{trb}	Transverse bending moment
M_x	Internal bending moment about the x axis
M_y	Internal bending moment about the y axis
n	Index in summation of series
n_y	Intensity of distributed loading in the y direction
s_{per}	Peripheral coordinate along mid-line of wall
T	Internal torsional moment
T_{svt}	Internal torsional moment in St. Venant torsion
v_{lbg}	Shear stress in longitudinal bending
v_{svt}	Shear stress in St. Venant torsion at mid-line of wall
V_y	Shear force in the y direction
U,V,W	Displacement in global axes
x,y,z	Element axes
X,Y,Z	Global axes
w_{dwr}	Distorsional warping coordinate
w_{twr}	Sectorial coordinate in torsional warping, referred to the shear centre
$\int_A dA$	Integral over the entire cross-sectional area

CHAPTER 1

INTRODUCTION

1.1 GENERAL

Reinforced concrete is particularly adaptable for use in highway bridges because of its less maintenance cost, rigidity and economy as well as the comparative ease with which a pleasing architectural appearance can be secured. For small to medium range spans, reinforced concrete bridges are extensively used. The present practice in Bangladesh is to design bridges on major highways for the AASHTO HS_{20} loading. However, the lighter loadings are used only for structures on secondary roads, on which the occurence of heavily loaded traffic is a remote possibility.

1.2 BACKGROUND OF THE RESEARCH

A spine beam bridge deck is one with a single box beam in the centre with large cantilevers on the sides. In spine beam bridge deck design, if relatively large web and thicker flanges are used, simple beam theory and St. Venant torsion theory can be applied for the analysis. However to attain economy, reduction in the thickness of the elements are required which ineffect increases the warping and distortional stresses. A number of analytical methods have been developed for analysing of this type of problems. Most of these analytical methods are applicable to

rectangular, straight box-beams of uniform cross-section. A spine beam bridge deck is subjected to torsion and warping stresses in addition to bending and shear-stresses. Moreover shear lag effects are more important with wide single-cell box-beams in comparison to narrow one. The simple beam theory gives no information on transverse bending stress due to eccentric loading which can result severe torsional and distortional stresses in the structure. Many of the available simple analytical methods can not predict accurate information of the combined action of the complex behaviour of spine beam bridge deck. For better understanding of the combined effects of these stresses finite element method may be used for analysis whcih takes care of these stresses.

1.3 OBJECTIVE OF STUDY

A spine beam bridge deck usually has diaphragms. Analysis of a spine beam bridge deck by finite element method having diaphragms is a time consuming process from the computational points of view, because of the large band width of the overall stiffness matrix. If the diaphragms can be modelled in the analysis by avoiding the physical presence of diaphragms, the band width of the stiffness matrix is reuced significantly thereby reducing the computational time. In this study this aspect of analytical model is investigated. Parameter study (Such as width, thicknesses of different elements) is also performed to highlight the effects of these on the design of the spine beam bridge deck.

Correlation of the behaviour of the spine beam bridge deck will be investigated in this study by analysing the bridge decks by finite element method and by simple methods. So that the results of the study can be used to study the behaviour of these type of bridge decks where large computational facilities are not easily available.

CHAPTER 2

CELLULAR STRUCTURE AND ITS BEHAVIOUR

2.1 INTRODUCTION

The feature survey by Swan [18] shows that for medium to long spans, the concrete box girder is a popular variety. The spine beam bridge is one of the most commonly occuring forms in the family of the box girder bridges. The design of concrete box-girder bridges usually is based on analysis of the structure by linear elastic methods, where displacements are assumed to be linearly proportional to loads, irrespective of the level of the loads. The elastic loads are then increased by overload factors to calculate the sections and reinforcements in the ultimate strength design.

The response of a given structure under loading can in principle be predicted by a number of analytical techniques, all of which are derived from common fundamental rules. These are the satisfaction of conditions of equilibrium, compatibility and the constitutive relationship of material.

Conventional methods of strength of materials and theory of structures use a number of simplifications in order to make the problem tractable. The most important of these, from an engineer's point of view, is that of linearity. In this, it is

assumed that all displacements and internal actions are linear functions of applied loading. As most structures behave in an approximately linear manner upto working load level, this approach is useful and makes the analysis a great deal easier. Structural design of members on this basis is related to permissible working stress, which in turn are related to failure by a factor of safety.

2.2 DEVELOPMENT OF CELLULAR CONSTRUCTION [12]

Concentrated loading necessitates a thorough analysis of bridge decks. For structural efficiency, a bridge deck must have a high strength/weight ratio. With longer spans, the need for efficiency in resisting longitudinal bending and shearing forces is greater. Due to the incidence of heavy concentrated loading, the need for good load distribution has also increased.

Cellular construction evolved to meet these requirements. It can be considered as the result of development from a solid concrete slab to a more efficient structural form by eliminating the less efficient part of the slab (close to the neutral axis) to obtain maximum efficiency of material coupled with a maximum weight reduction. The development of cellular construction is shown in Fig. 2.1. Voided or cored slabs (Fig. 2.1b) are developed from solid slabs, since the removal of the material from the region of neutral axis has little effect on the flexural or torsional strength, but makes the structure lighter. However, the use of

(a) Solid Slab
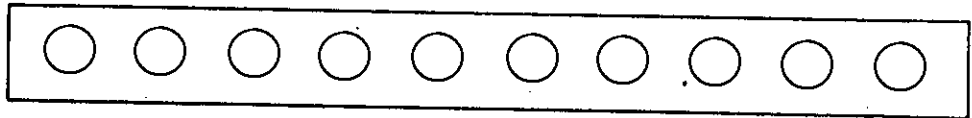
(b) Cored Slab
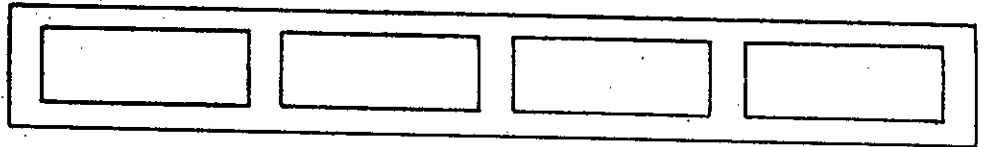
(c) Multi- Cellular Slab
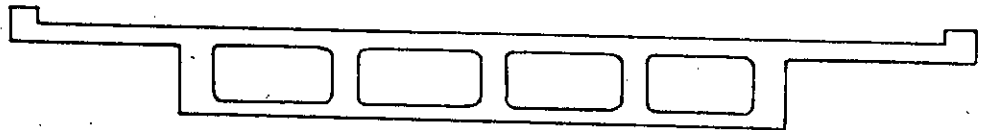
(d) Cellular Slab with Cantilever.
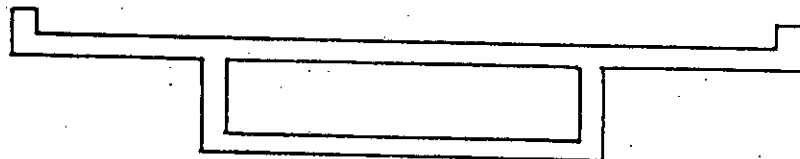
(e) Spine Beam

Fig. 2.1   The development of bridge decks from solid slab
to spine beam.

circular voids limits the amount of material that can be removed from the slab.

The next step is to use rectangular voids (Fig. 2.1c) which allows removal of all the structurally least efficient part of the slab. The material thus removed does not cause any difficulties in interpreting the longitudinal action of the bridge, since the webs still carry the main shear. In the transverse direction, however, the structural action of the medium is somewhat complex since no through webs are present.

As the torsional stiffness of cellular construction is large, the structural efficiency of a deck can be increased by incorporating cantilever slabs (Fig. 2.1d). The special form of box girder is shown in Fig. 2.1e. This type of bridge deck with side cantilevers having a central beam (spine) is called spine beam bridge deck. The cost of a wide deck is thus greatly reduced due to the reduction of number of cells and dead weight of structure.

Box girder decks are thus structurally economic solutions for medium to long spans, especially where headroom limitations are a major design consideration. Box girder decks tend to be more streamlined and slender than other types. This type of bridge is pleasing in appearance, a consideration for their adaptability to most urban flyovers. They are particularly adaptable to prefabrication and standardisation of detail which are especially advantageous when many similar spans have to be built.

2.3 TYPES OF STRUCTURAL ACTION OF SPINE BEAM BRIDGE DECK [3]

In addition to simple beam action, there are two types of structural action whcih can occur in spine beam bridge decks. These are called distortion or deformation of the cross-section and warping of the cross-section.

2.3.1 Distortion or Deformation of the Cross-Section

This is illustrated in Figs. 2.2 and 2.3 which show the effects of symmetric and antisymmetric loading respectively. Any eccentric point load or longitudinally distributed load can be resolved into the two load system shown.

In both cases, the shape of the cross-section has been altered by transverse bending of the webs of the box beam, and this has come about because of the absence or non-rigidity of transverse diaphragms. The torsional stiffness of a spine beam bridge deck is reduced by distortion of the cross-section.

2.3.2 Warping of the Cross-section

This is an out of the plane displacement of points on the cross-section, and arises under torsional loading as follows. Firstly a box beam whose cross-section cannot distort because of the existence of rigid transverse diaphragm all along the span can be
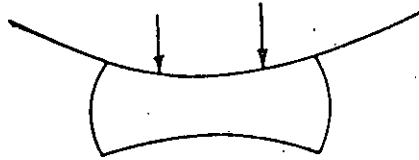
Fig. 2.2 Distorition of cross-section due to symmetric (bending)loading.
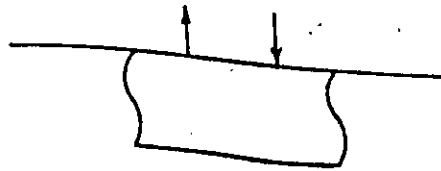
Fig.2.3.Distortion of cross-section due to antisymmetric (torsional)loading.

undeflected position
of cross-section
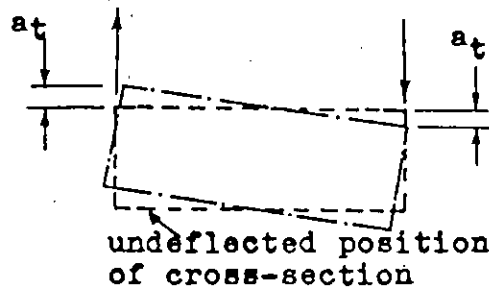
Fig.2.4:Twisting of midspan cross-section without distortion.

considered. These, however, are assumed not to restrict longitudinal displacements. Fig. 2.4 shows how the cross-section of such a box beam twists under torsional loading.

The chain dotted configuration in Fig. 2.5 shows how this leads to out-of-plane (longitudinal) displacements of cross-sections, except at midspan where, by symmetry, the cross-section remains plane. These longitudinal displacements are called torsional warping displacements, and are associated with shear deformations in the planes of the flanges and webs. The midspan vertical deflection of each web occuring in torsion without distortion is denoted by a_t. The term warping torsion is also used to denote the state of loading and stress associated with torsional warping displacements. Now, as a further stage in the deforation of the structure it can be assumed that the rigid transverse diaphragms are removed, so that the cross-section can distort. Fig. 2.6 shows the additional twisting of cross-section that now results center torsional loading.

The additional vertical deflection of each web at midspan due to distortion is denoted by a_{dis} (Fig. 2.5). This in turn increases the out-of-plane displacements of cross-sections not at midspan, as shown by the solid line configuration in Fig. 2.5. These additional warping displacements are called distortional warping displacements, and are associated with in-plane bending of the flanges and webs.

Key
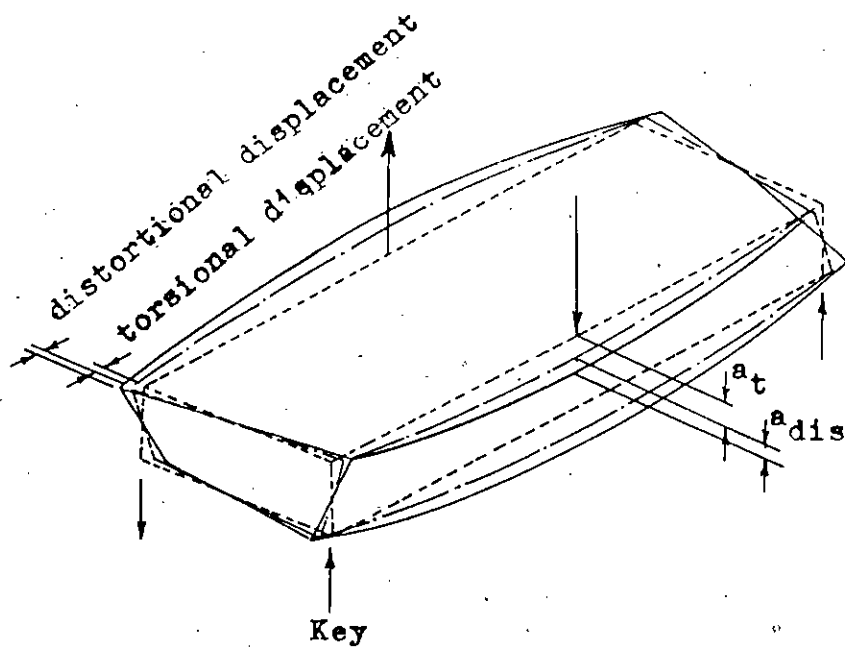
----- undeflected form of structure

_ . _ deflected form of structure with rigid
transverse diaphragms all along the span

_____ deflected form of structure after removal
of diaphragms between supports

Fig.2.5:Torsional and distortional warping
of boxbeam under torsional
loading.
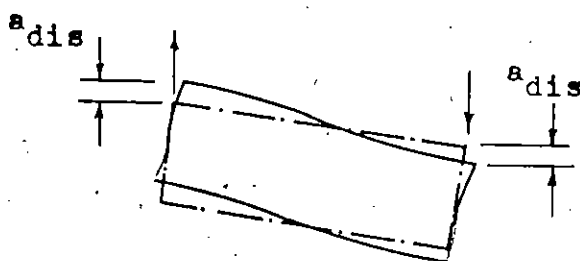
Fig.2.6: Additional twisting of midspan
cross-section when distortion is permitted.

Thus, concrete spine beam bridge decks with no diaphragms except at supports, when subjected to torsional loading, can undergo warping displacements which composed of two components viz. torsional warping displacements and distortional warping displacements. But these components give rise to longitudinal normal stresses (warping stresses) when the warping is constrained, e.g. by symmetry at the midspan section of a box beam, or at a continuous or built-in support, or by changes in cross-section or in applied torsional moment. In these circumstances, the significance of the warping stresses depends on the geometry of the structure as well as on the nature of the loading and support conditions. The warping stresses can form a significant addition to the ordinary bending stresses resulting from the symmetrical component of loading. Distortion of cross-section is the main source of warping stresses in concrete box beam construction where distortion is resisted mainly by the transverse bending strength of the webs.

2.3.3 Shear Lag

Another form of warping arises when a spine beam bridge deck is subjected to bending without torsion, as with symmetrical loading. This type of warping is known as shear lag in bending, and is illustrated in Figs. 2.7 and 2.8. The differential longitudinal deflection between points A and B in the top flange due to shear lag is denoted by a_{vlg}. This type of behaviour results from shear deformation in the planes of the flanges, and
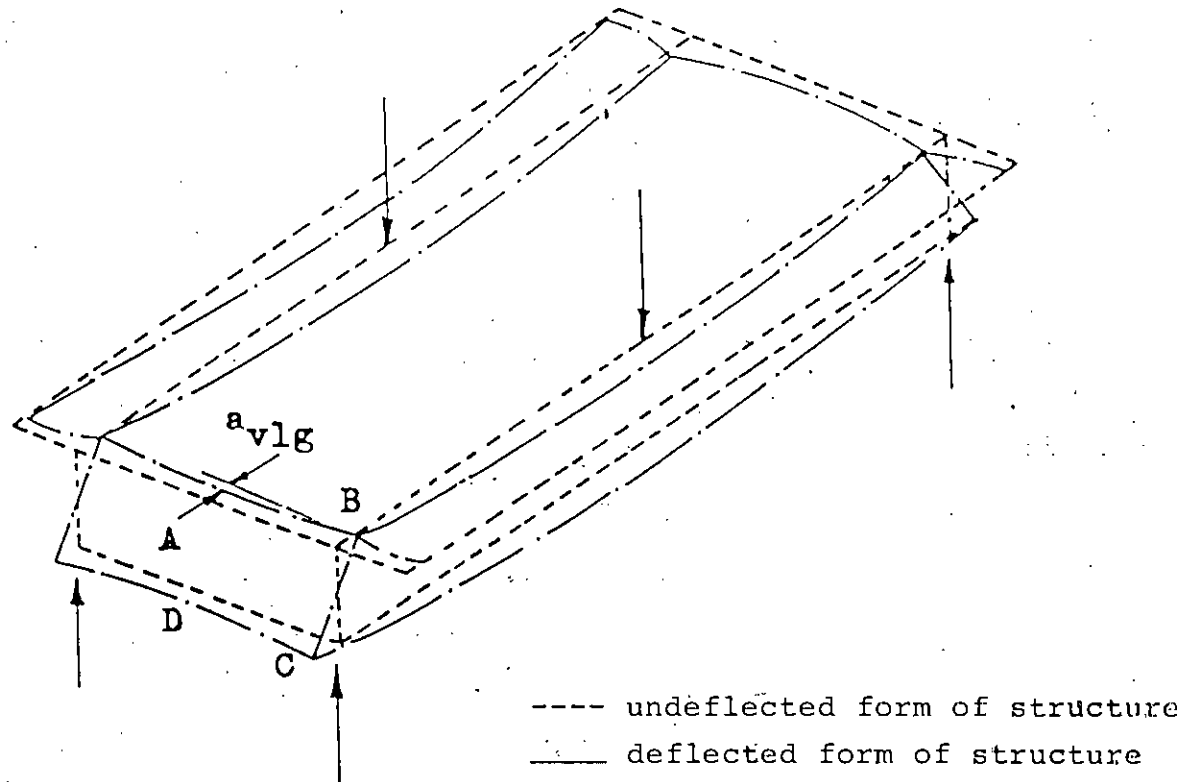
Fig. 2.7   Shear lag in bending.
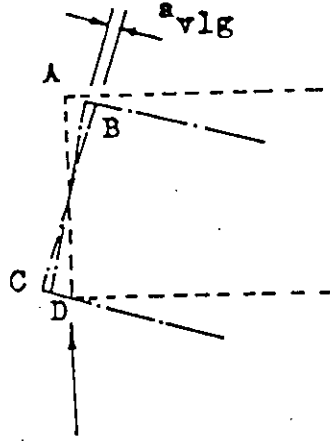
Fig.2.8: Enlarged elevation of region
of boxbeam near support,
showing out-of-plane displa-
cements of end cross-section
due to shear lag in bending.
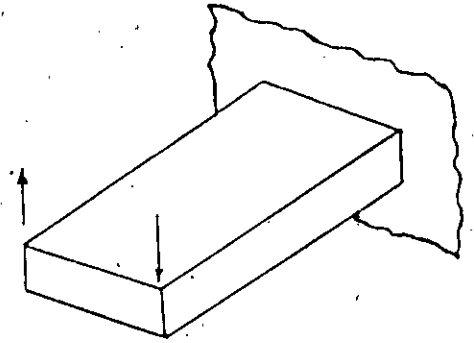
Fig. 2.9: Torsional load applied
with warping restraint
at support.

leads to a decrease in longitudinal bending stress away from the webs, which in turn affects the effective widths of the flanges in bending, especially when there are extensive large side cantilevers.A finite element analyses of the West Gate bridge(3) demonostrated shear lag effects of upto 80%, i.e. the calculated stress was 80% greater than that obtained by engineer's bending theory.

Shear lag can also arise in torsion, for example when one end of a box beam is restrained against warping and a torsional load is applied away from the end, as shown in Fig. 2.9. The restraint against warping induces longitudinal stresses in the region of the built-in end, and the shear stress in this area is redistributed as a result. This is also an effect of shear deformation, and is sometimes called a shear lag effect.

2.3.4 Stress Patterns Arising in Bending and ST Venant Torsion

Engineers' theory of bending leads to the normal and shear stress distributions are shown in Fig. 2.10. Shear deformation is not taken into account in this theory.

As discussed in connection with Fig. 2.7, when shear deformation is taken into account in the bending analysis, shear lag effects arise, as indicated in Fig. 2.11. The variation of normal stresses across the flanges has been drawn according to the

midspan
point load

A

A

(a)Elevation of simply supported beam

C

T
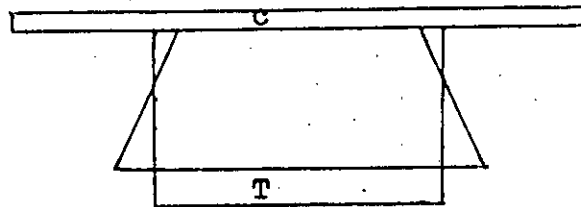
(b) Section A-A showing variation of
     normal stress round the perimeter
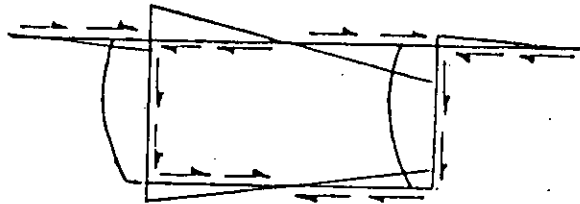
(c) Section A-A showing variation of shear
     stress round the perimeter.

Fig. 2.10   Bending and shear stress distribution
            at a corss-section by simple beam theory.

analytical results obtained by finite element method considering shear lag effect.

The theory of St. Venant torsion (pure torsion) assumes that there is no constraint on warping. Thus only shear stresses arise in the cross-section, and no (longitudinal) warping stress. These shear stresses are called St. Venant shear stresses and are shown in Fig. 2.12 for a spine beam bridge deck loaded by two equal and opposite concentrated torsional moments, one at each end. The St. Venant shear stresses are usually taken as constant through the wall thickness of the closed box, although a more refined calculation, which considers the linear variation through the web thickness shown in Fig. 2.12 is possible.

2.3.5 Local Effects in the Top and Bottom Slabs

These effects are particularly associated with the occurence of point loading between the webs or on the side cantilevers. With large spine beam bridge deck carrying two levels of traffic where the bottom slab can also be loaded. The stresses arising from local bending may be calculated by the use of influence surfaces for plates, independently of the overall spine beam brdige deck analysis.
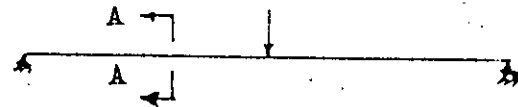
(a)Elevation of simply supported beam

(b)Section A-A showing variation
ofrnormal stress round the perimeter.

Fig.2.11:Bending stress distribution at
cross-section,considering shear lag
effects.

antisymmetric distribution about mid-
line of web in cantilevers

trapezoidal
distribution
in webs of box
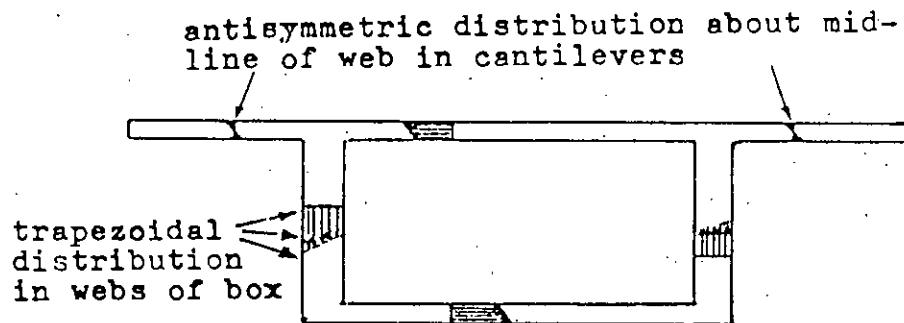
Fig.2.12: St Venant shear stress
distribution.

2.3.6 Transverse Normal Stresses Constant Through the Web Thickness

Of minor significance in the analysis of rectangular section, single-cell, non-prestressed spine beam bridge decks, is a set of transverse normal stresses constant through the web thickness. These arise from differential shear stresses on cross-sections.

CHAPTER 3

ELASTIC ANALYSIS OF CELLULAR STRUCTURE
AND RIVIEW OF DIFFERENT METHODS

3.1 INTRODUCTION

Elastic methods of analysis are based on the principle that displacements are linearly proportional to load at that all stages of loading. Linear elastic methods are still the most popular approach to analysis and design of bridge structures. In the case of open type ribbed construction the load is transmitted from an immediately loaded web to the other webs by the transverse flexure of the top slab. For greater load capacity, design results in an increased number of ribs or a greater thickness of the top slab or a combination of both. In the case of closed type box girders, the transmission of load is effected by shear stresses which develop around the box. The existing elastic solutions are based on simplifying assumptions.

3.2 DIFFERENT METHODS OF ELASTIC ANALYSIS

The following are the principal methods of analysis available for elastic analysis of box girder bridge decks.

i)   Simple beam theory

ii)   Load distribution factor method.

iii) Knittel's [8] method

iv) Equivalent beam method (Richmond [14]

v) Kupfer's [11] method

vi) Kollbrunner, Hajdin and Heilig [10,7]

vii) Beam on elastic foundation analogy

viii) Reissner [15] method

ix) Influence surfaces for plates and frame analysis for local transverse bending effects.

x) Grillage theory

xi) Orthotropic plate method

xii) Shear weak orthotropic plate method

xiii) Three dimensional frame work method.

xiv) Folded plate method

xv) Finite strip method.

xvi) Shell theory

xvii) Finite element method

All of the above methods, except the finite element approach, are based on the following assumptions.

a) The thickness of each plate is small compared with its breadth and length so that the thin plate theory can be applied to individual plates.

b) Each plate of the box bridge deck is rectangular, uniform in thickness, and is made of elastic, isotropic and homogeneous material.

Table 3.1 shows the field of application of each of the above methods.

3.2.1 Simple Beam Theory

This method is sometimes known as 'engineer's method'. In this method the elementary beam theory based on the following assumptions is used to determine the stresses and strains.

a) Longitudinal strains and stresses are linear over the cross-section.

b) There is no shear lag across the flanges hence all fibres located same distance from neutral axis are equally strained.

c) Since all fibres' are equally strained, the transverse deflection of all points in a cross-sections are the same, so there is no distortion of the cross-section.

According to this theory, the following expression is obtained for the normal stresses in longitudinal bending of a thin-webed beam whose cross-section has a vertical axis of symmetry (Fig. 3.1).

Table 3.1 Different methods of elastic analysis and their field of
application [18]

Analytical method	Type of structural action considered						
	Longitudinal bending	St.Venant torsion	Distortional (transverse bending)	Torsional warping	Distortional warping	Shear lag	Local effects
1. Simple beam theory	✓						
2. Load distribution factor method	✓	✓					
3. Knittel's [8] method			✓				
4. Equivalent beam (method(Richmond[14]))			✓		✓		
5. Kupfer's [11] method			✓				
6. Kullbrunner and Hajdin,[10] Heilig [7]				✓			
7. Beam on elastic foundation analogy			✓		✓		
8. Reissner [15] method						✓	

Analytical method	Type of structural action considered						
	Longi-tudinal bending	St.Venant torsion	Distortional (transverse bending)	Torsional warping	Distor-tional warping	Shear lag	Local effects
9. Influence surfaces for plates and frame analysis for local transverse bending effects.							
10. Grillage theory	✓	✓	✓				
11. Orthotropic plate method	✓						
12. Shear weak orthotropic plate method	✓		✓				
13. Three dimensional frame work method	✓		✓	✓	✓		
14. Folded plate method	✓	✓	✓	✓	✓	✓	✓
15. Finite strip method	✓	✓	✓	✓	✓	✓	✓
16. Shell theory	✓	✓	✓	✓	✓	✓	✓
17. Finite element method	✓	✓	✓	✓	✓	✓	✓

$$f_{lbg} = \frac{M_x y}{I_x} + \frac{M_y x}{I_y} \qquad\qquad (3.1)$$

f_{lbg} = normal longitudinal stress in longitudinal bending (positive tensile)

x,y = coordinate of a point on the mid-line of the web of cross-section, referred to centroidal axes (Fig. 3.1).

M_x = bending moment about x axis (Fig. 3.3)

M_y = bending moment about y axis (Fig. 3.3)

I_x = moment of inertia of entire cross-section about centroidal x-axis.

I_y = moment of inertia of entire cross-section about centroidal y-axis.

For the shear stresses arising in bending due to vertical loading only, by symmetry about the vertical axis of cross-section the longitudinal shear stress is zero at this axis, hence the complementary shear stress V_{lbg} in the plane of cross-section is also zero at $x = 0$, as shown in Fig. 3.2. Half the open-closed section (ABCDE in Fig. 3.2) may therefore be analysed as an open section, since the boundary conditions for open sections are now

satisfied i.e zero longitudinal shear stress in bending at the ends of the cross-section (A, C and E).

Kollbrunner and Basler [9] give a formula which may be applied here in the form:

$$(V_{1\,b\,g}h) = \frac{V_y\,(A_y\,)_{1/2}}{I_x} \tag{3.2}$$

where,

$(V_{1\,b\,g}h)$ = shear flow in longitudinal bending

$V_{1\,b\,g}$ = shear stress in longitudinal bending

h = thickness of web

V_y = shear force on cross-section in the y direction (Fig. 3.3)

(A_y) = first moment of area of the partial half-cross section about the centroidal x-axis (Fig. 3.4).

I_x = moment of inertia of entire cross-section about centroidal x-axis.

I_y = moment of inertia of entire cross-section about the centroidal y axis.
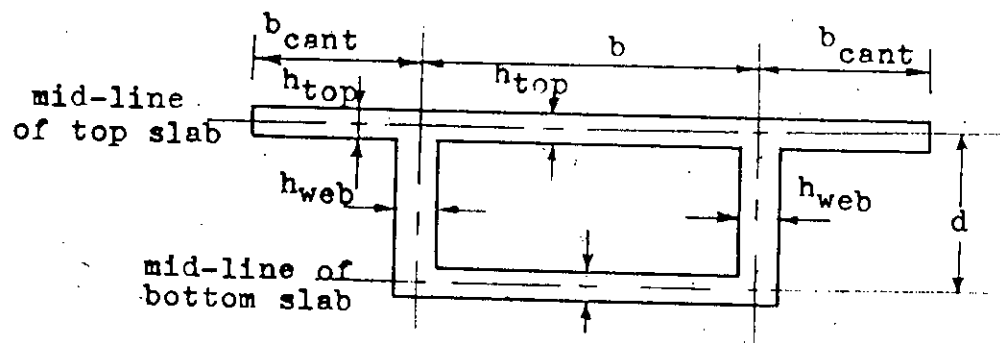
Fig.3.1:Dimensions of cross-section
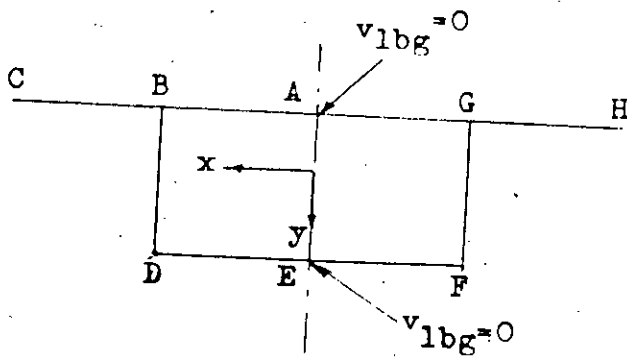
Fig.3.2: Zero bending shear stress v_{lbg} on axis of symmetry,for vertical loading.

For the St. Venant torsion of thin-webed beams of open-closed section, Kollbrunner and Basler [9] give the following expression:

$$(V_{svt}h) = \frac{T_{svt}}{2A_{enc}} \qquad (3.3)$$

where,

$(V_{svt}h)$ = shear flow in St. Venant torsion of thin-webed section

V_{svt} = Shear stress in St. Venant torsion at mid-line of web.

h = thickness of web of closed portion of cross-section

T_{svt} = torsional moment at cross-section in St. Venant torsion

A_{enc} = area enclosed by mid-line of web of closed portion of cross-section

= bd. (Fig. 3.1);

This leads to the stress distribution shown in Fig. 3.5 which is a simplification of that in Fig. 2.12. For thin-webed cross-sections, the distribution of Fig. 3.5 is adequate, in that it assumes V_{svt} to be constant through the wall thickness of the closed portion of cross-section, and zero in the open portions. For thicker-welded sections, Kollbrunner and Basler [9] give the

following more accurate formula corresponding to Fig. 2.12 and
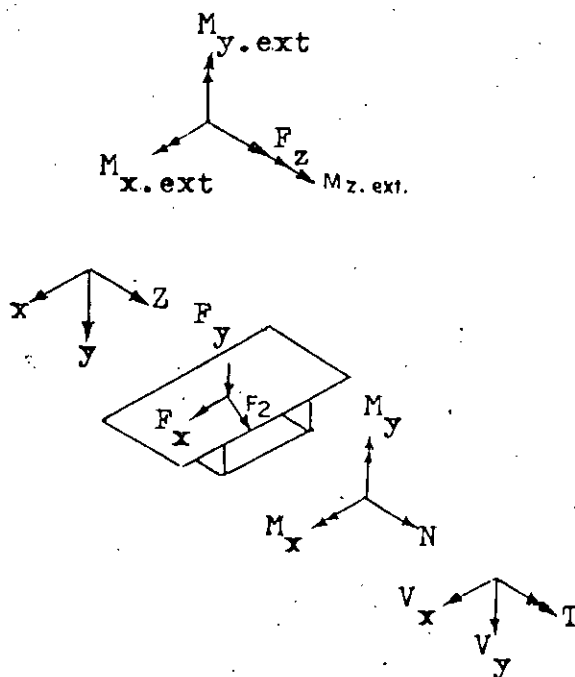
Fig.3.3: Positive directions of internal stress-resultants and external loading.
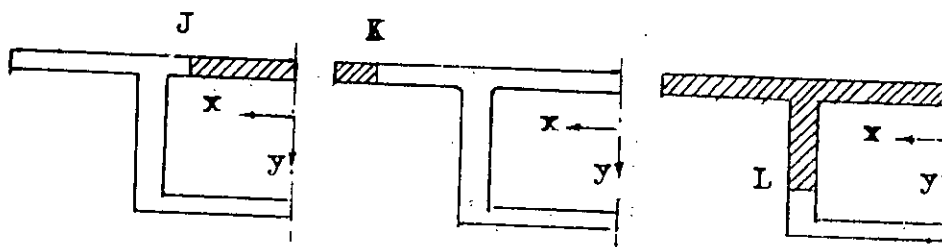
Fig. 3.4: Evaluation of $(\overline{Ay})_{\frac{1}{2}}$, the first moment of the partial half-cross-section about the centroidal x axis.
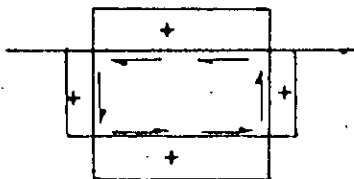
Fig.3.5: Diagram of St.Venant shear stress at mid-line of web at midspan

3.6.

$$\Delta V_{svt} = h \, T_{svt}/c_{svt}$$

where,

ΔV_{svt} = increment in V_{svt} over half thickness of web (Fig. 3.4)

h = thickness of web (open or closed portion of cross-section)

T_{svt} = torsional moment at cross-section in St. Venant torsion

c_{svt} = torsional moment of inertia of cross-section in St. Venant torsion.

$$= 4A^2_{enc}/\oint(ds_{per}/h)$$

(3.5)

$$\oint(ds_{per}/h) = b/h_{top} + b/h_{bot} + 2d/h_{web}$$

b = breadth between mid-lines of webs (Fig. 3.1).

d = depth between mid-lines of top and bottom slabs (Fig.3.1).

h_{top} = thickness of top slab (Fig. 3.1)

h_{bot} = thickness of bottom slab (Fig. 3.1)

h_{web} = thickness of web (Fig. 3.1)

S_{per} = peripherical coordinate along mid-line of web

= integral along the mid-line of wall of the closed portion
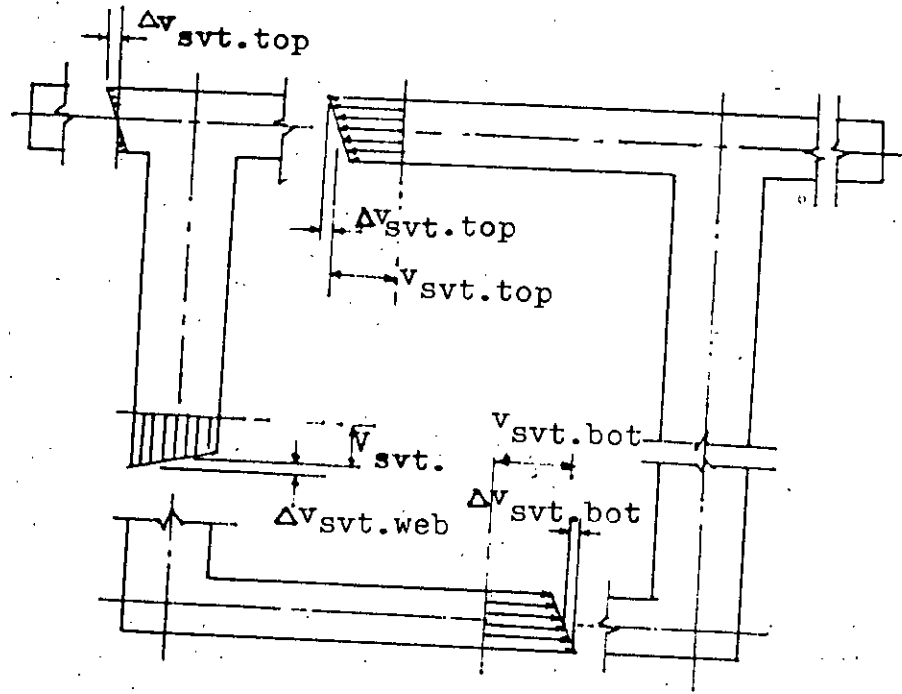
Fig.3.6:Notation for St Venant shear stress
distribution,considering linear variation of stress
through thickness of web,

of cross-section.

The following criterion for a thin-webed section may now be formulated in a more general form. From equations 3.3 and 3.4 it follows that

$$\Delta V_{svt}/V_{svt} = h^2/2A_{enc}(b/h_{top}+b/h_{bot}+2d/h_{web}) \qquad (3.6)$$

It can also be shown that

$$\Delta T_{svt}/T_{svt} = (b(h^3_{top}+h^3_{bot})+2d\ h^3_{web})/(3c_{svt}) \qquad (3.7)$$

where ΔT_{svt} = increment in T_{svt} due to the antisymmetric shear
stress distribution measured by ΔV_{svt}

Thus equations 3.6 and 3.7 may be used to evaluate the proportional errors in stress and moment arising from the use of the simplified stress distribution of Fig. 3.5 instead of the more accurate one of Fig. 2.12. If the error in torsional moment T_{svt} exceeds 10%, the section may be considered to be thick-webed. For sections tending towards the thick-webed, C_{svt} may be replaced by $(c_{svt} + \Delta c_{svt})$, where

$$\Delta c_{svt} = ((b+2b_{cant})h^3_{top}+bh^3_{bot} + 2dh^3_{web})/3 \qquad (3.8)$$

b_{cant} = width of cantilever (Fig. 3.1).

The results obtained from this method are considerably in error because of the above simplified assumptions. Spine beam bridge decks usually consist of thin plate and transverse distorsion invariably occurs. The external loads are usually eccentric resulting in bending and torsion, and distortion of cross-section.

3.2.2 Load Distribution Factor Method

This method is particularly applicable to simply supported, straight (not skewed) multi-cell box girder bridge slabs with transverse diaphragms. In this method the box girder is considered to consist of repeating I-shaped girders made up of a web and a top and bottom flange equal in width, except for the external web, where the bottom flange extends only on one side and the top flange extends from the kerb to the centre of the top flange. All the dead loads due to kerb and railing are equally distributed among individual girders. The wheel loads are distributed by empirical distribution factors related to the girder spacing, based on tests and experience. The distribution is generally of the form:

Load carried by an interior girder

$$W_i = \text{wheel load} \times \frac{\text{spacing of the girder}}{\text{constant } C}$$

Load carried by an exterior girder

$$w_e = w_i \times \frac{\text{Top flange width of exterior girder}}{\text{Top flange width of interior girder}}$$

This method is over-simplified and does not take into account distortion of the cross-section.

3.2.3 Analysis of Simple Bending, Torsion and Distortion by Knittel's Method [8]

The structural effects neglected here are torsion and distortional warping and shear lag.

Loading:

Knittel's method is formulated in terms of line loads along the webs of the spine beam. It is shown below how to represent practical loadings by equivalent sinosoidally distributed loadings.

Resolution of Loading:

(a) Resolution of loading applied at web

(b)Resolution of loading applied between webs

(c)First fourier component of symmetric loading

(d)First fourier component of antisymmetric loading
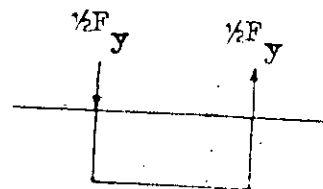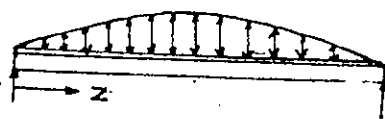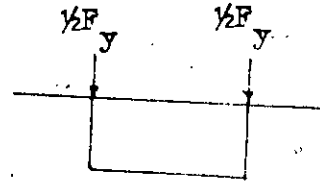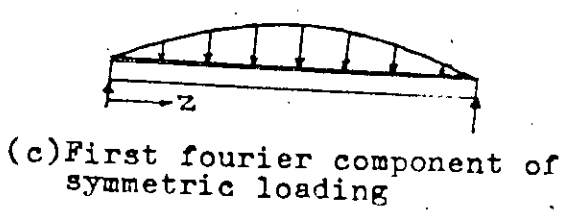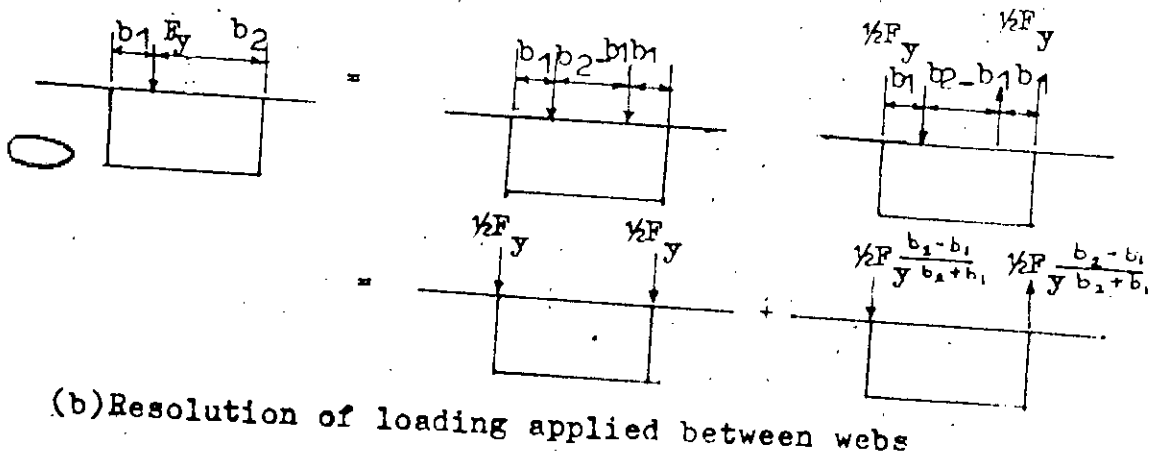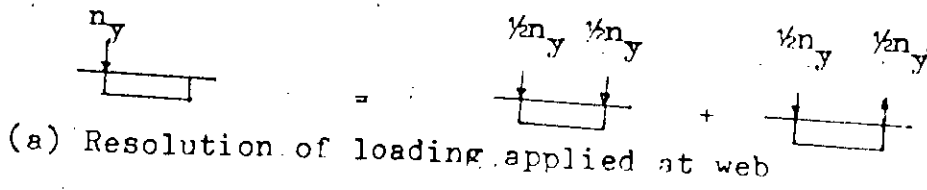
Fig. 3.7: Resolution of loading

If the given loading is line loading, this is replaced by a statically equivalent combination of symmetric and antisymmetric line loading at the webs. Thus, for a line load n_y at a web, the resolution shown in Fig. 3.7a is obtained.

If there is point loading on the structure, this is resolved in Fig. 3.7b, obtaining symmetric and antisymmetric point loading at the webs, and this is replaced by Fourier components of equivalent line loading, as indicated in Figs. 3.7c and d.

Summary of Procedure for Analysis:

1) For the symmetric load case (Fig. 3.7c), the structure is analysed by simple beam theory, which has been presented in connection with equations 3.1 and 3.2. Consideration of transverse normal forces are included, as discussed below.

2) For the antisymmetric load case (Fig. 3.7d), the following two effects are analysed separately:

a) Pure (St. Venant) torsion, giving rise to shear stresses in the cross-section, as shown by equations 3.3 and 3.4;
b) Distortion, giving rise to transverse bending of the flanges and webs, and transverse normal forces.

3.2.4 Analysis of Distortion and Distortional Warping by the Equivalent Beam

The structural effects neglected here are torsional warping and shear lag.

Loading:

The given loading is resolved into statically equivalent distributed loading along the webs, as shown in Fig. 3.7. Only the antisymmetric load case is considered in the equivalent beam method and the action under symmetric loading is treated by simple beam theory.

Summary of Procedure for Analysis:

For the antisymmetric load case, the following two effects are analysed separately as explained in Ref. 3.

a) Pure (St. Venant) torsion, giving rise to shear stress v_{svt} in the cross-section.

b) Distortion and distortional warping, giving rise to transverse bending stress f_{trb}, transverse normal stress f_{trn} and (longitudinal) distortional warping stress f_{dwr}.
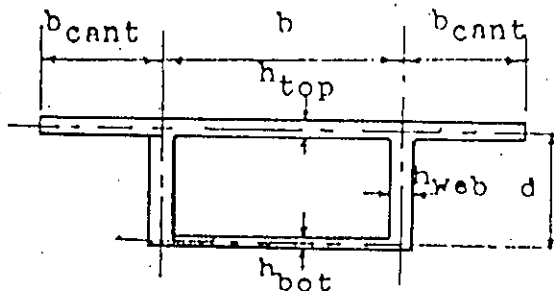
(a) Dimensions of actual cross-section
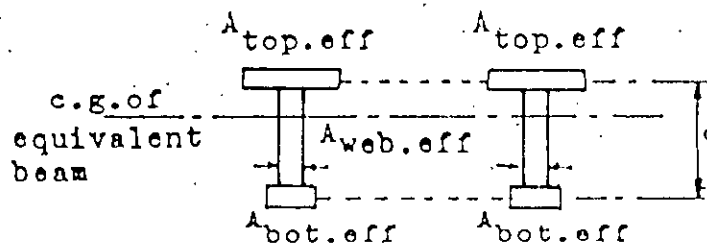
(b) Cross-section of two equivalent beams

Fig. 3.8: Cross-section of actual and equivalent beams.

3.2.5 Analysis of Distortion and Distortional Warping by Kupfer's Method [10]

The structural effects neglected here are torsional warping and shear lag.

Loading:

The vertical loading is assumed to be applied over a web, and is resolved into three systems as shown in Fig. 3.9. These systems generate (a) longitudinal bending, (b) torsion and (c) distortion, Kupfer recommends that the first two be treated by Knittel's method and St. Venant torsion theory respectively and develops an analysis refering mainly to the action in distortion and distortional warping. The method is formulated in terms of distributed loading, and Fourier components are used to represent the loading. However, the point loading is treated as such when evaluating transverse bending stresses and distortional warping stresses in the vicinity of the point load.

Summary of Procedure for Analysis:

In system (b) of Fig. 3.9 for a square section box beam of constant web thickness around the perimeter there are no transverse bending effects in pure torsion. However, for a rectangular section box beam in whcih the web thickness varies

around the perimeter, small transverse bending moments arise in pure torsion. There occurs the St. Venant shear stresses in addition.

In treating the distortional system (c) of Fig. 3.9 the procedure is to subdivide the load of this system between two mutually independent structural systems 1 and 2 which are deformationally compatible. In system 1, (Fig. 3.10) the spine beam is treated as a hinged folded plate structure subjected to a load in the plane of each web, sinusoidally distributed along the beam. Only the longitudinal structure action of the webs is considered, with each web behaving as a longitudinal beam in inplane bending. The influence of shear deformation is neglected.

System 2 is a rigid jointed closed-frame structure and also subjected to a load in the plane of each web, sinusoidally distributed along the beam. Only the transverse structural action is considered, with each web developing transverse bending stresses. The subdivision of the distortional load system (c) of Fig. 3.9 between systems 1 and 2 of Fig. 3.10 is determined by specifying that the deflections at the corners of all cross-sections must be compatible as between sytem 1 and 2.

3.2.6 Analysis of Torsional Warping by the Method of Kollbrunner,

Fig.3.9: Resolution of loading

a)System 1(Hinged folded plate) (b)System 2 (Rigid jointed closed frame
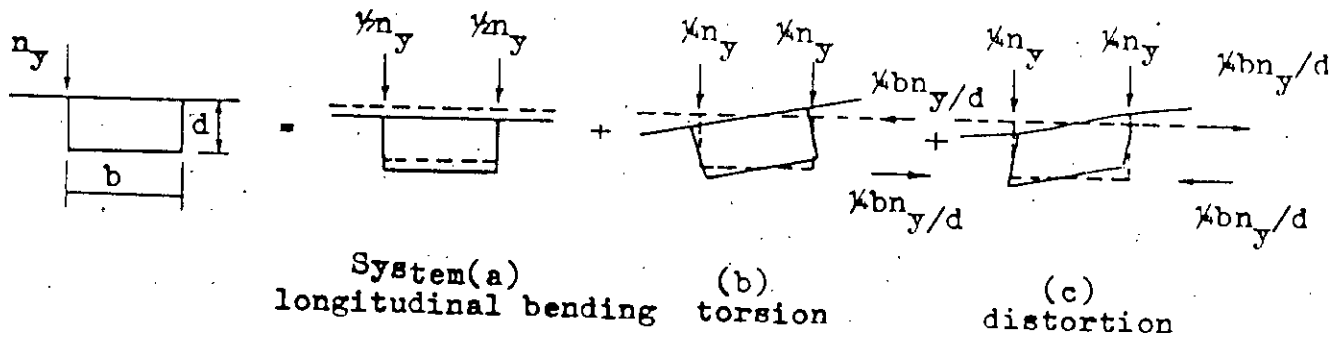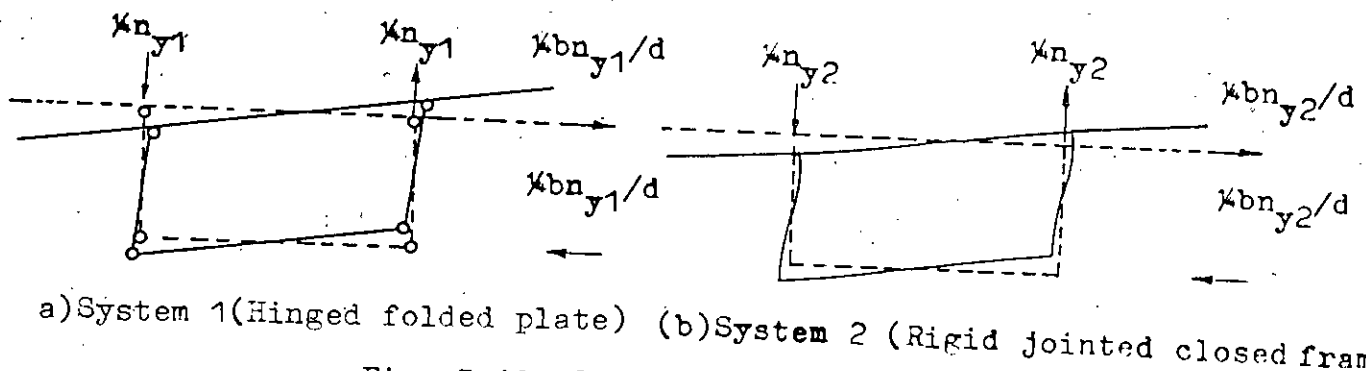
Fig. 3.10: Subdivision of distortional system.

Hajdin and Heilig (10,7)

This is a rigorous analysis of torsional warping, in which it is assumed by definition that there is no distortion of cross-section. The only other structural effect neglected is the minor one giving rise to transverse normal stresses constant through the web thickness.

Loading:

The analysis considers only the torsional system of Fig. 3.9b. The torsional component of the actual loading is used, and not a Fourier representation of it.

Summary of Procedure for Analysis:

Following Vlasov [23], Kollbrunner and Hajdin [10] have developed the theory of warping torsion of thin-webed beams of closed or open closed, undeformable cross-section. The torsional warping (longitudinal) stresses and torsional warping shear stresses are obtained in terms of the applied torsional moment, the bimoment and section properties known as the sectorial coordinate and the torsional warping moment of inertia.

3.2.7 Analysis of Distortion and Distortional Warping by the
Beam-on-Elastic Foundation Analogy

The structural effects neglected here are torsional warping and shear lag and the minor one giving rise to transverse normal stresses constant through the web thickness.

This method is based on Vlasov's [23] thin-walled beam theory. It is based on the following assumptions.

a)   The thickness of each plate is small compared with its width and length.

b) The box section is symmetrical about its vertical axis and the individual plates are symmetrical about their centroidal axes.

Among all the approximate methods, this method takes into account warping and distortional stresses and is suitable for hand computation. It is therefore, described in some detail. In this method any applied loading P and be split up into two force systems in Fig. 3.11(ii).

a) The symmetrical force system P_B causes bending in the vertical plane of the cross-section. The stresses can be determined by conventional beam theory neglecting deformation due to shear.

b) The antisymmetrical force system causes twisting of the cross-sections. This force system can be subdivided again into the following two sub-systems as shown in Fig. 3.11(iii).

i) Pure torsion system, consisting of P_T forces in different plates, so as to equilibriate the applied torsion of the antisymmetrical force system.

ii) The self equilibriating pure shear system P_s, so that in combination with pure torsion system they balance the externally applied load to each web.

The components of antisymmetrical force system are found by simple statics.

1. Pure Torsion P_T

Saint Venant's shear flow per unit length computed by Bredit's formula

$$= p.b_t.x/(2(b_t+b_b)d)$$

$$Pc_t = pb_t c/(2(b_t+b_b)d) \qquad\qquad (3.9)$$

$$Pt_t = b_t\ pc_t/c \qquad\qquad (3.10)$$

$$Pb_t = b_b\ pc_t/c \qquad\qquad (3.11)$$

2. Pure Shear Force P_s

$$Pc_s = pb_b \ c/(2d(b_t + b_b))$$
(3.12)

$$Pt_s = - b_b \ pc_s/c$$
(3.13)

$$Pb_s = b_t \ pc_s/c$$
(3.14)

The effect of pure torsion P_T is determined by using St. Venant's torsion theory asuming a rigid body rotation of the cross-section but no distortion. The warping stresses associated with St. Venant's shear flow are usually neglegible in the case of reinforced concrete box girders.

The box section under the influence of pure shear, undergoes deformation as shown in Fig. 3.12 due to frame action. The transverse stresses due to this deformation are called distortional stresses. The measure of the distortion may be defined either as w or c as shown in Fig. 3.12. If this distortion is non-uniform along the span, due to nonuniformity of torsional load, or because of non-symmetrical external load, each plate will displace unequally in its plane along the span.

This non-uniform distortion gives rise to longitudinal bending of individual plates in their own planes, thus causing distortional warping stresses.

A fourth order differential equation can be set up from energy consideration in terms of w, as was done by Wright [23], or in
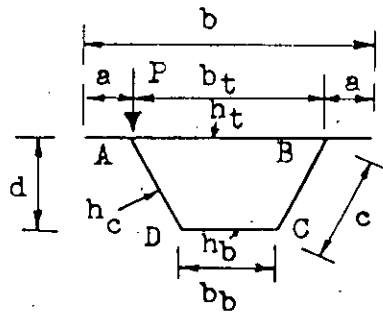
(a) Section A-A
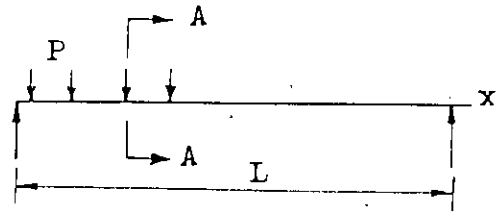
(b)

(i)Cross-section and external load of box girder.
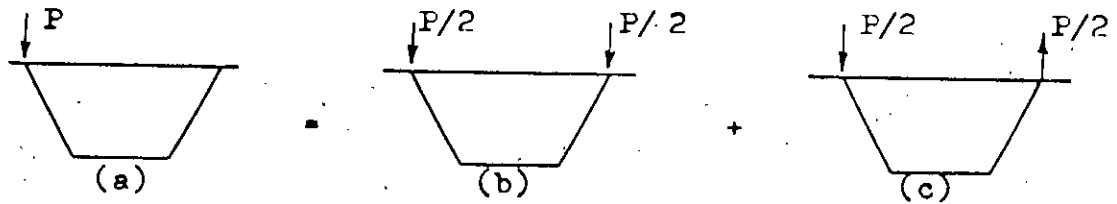
(ii) Symmetrical and antisymmetrical components of load
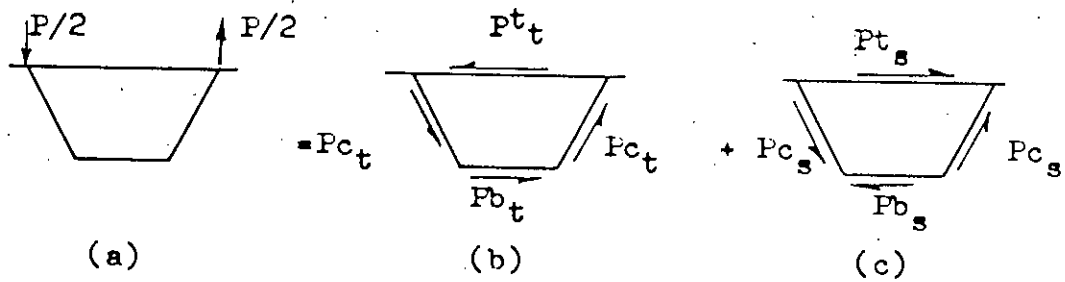
(iii) Pure torsion and pure shear systems.
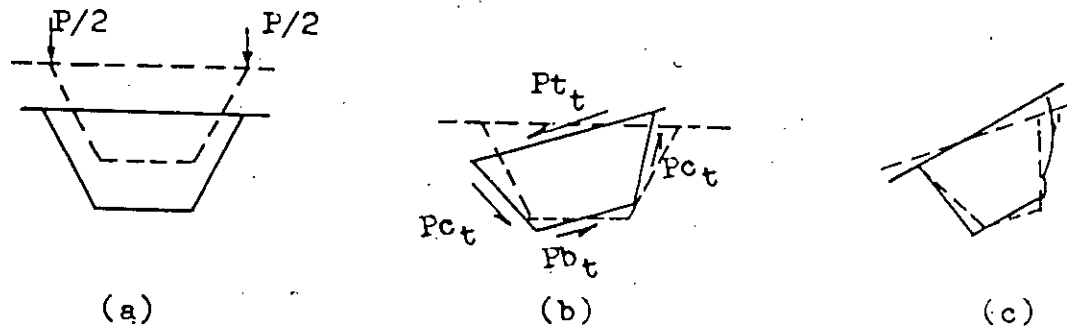
(iv) Displacement of a typical cross-section

Fig. 3.11: Forces and displacements of a box section
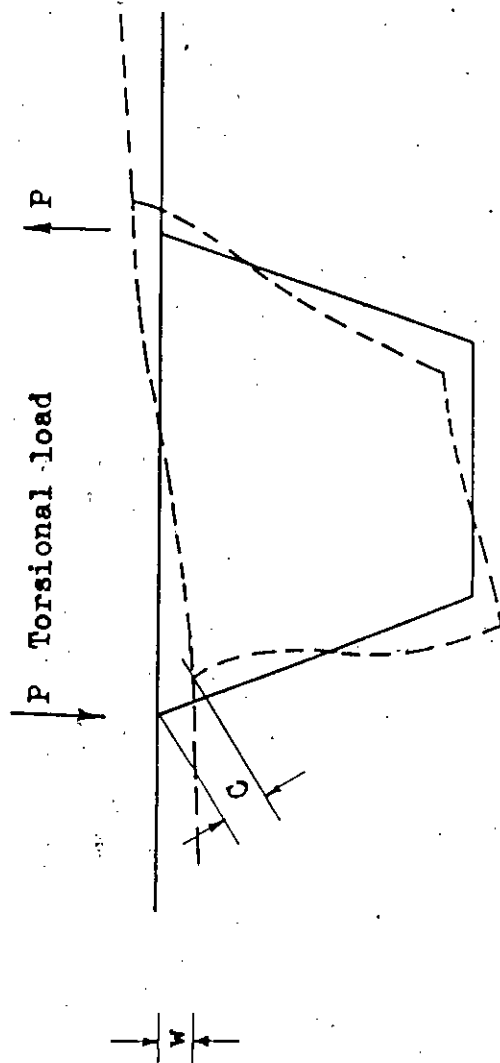
Fig. 3.12: Deformation of cross-section

terms of inplane displacement of the web plate Δc, as was done by Tung (21), from statics and compatibility considerations. The equation developed in terms of Δc is given by:

$$d^4 \Delta c/dx^4 + 4 \ ^4\lambda c = pc_s \qquad (3.15)$$

where $\lambda = 4 \ K/4EI_{ce}$

where K is known as foundation stiffness, which is related to geometric properties of the box section. I_{ce} and P_{cs} are the moment of inertia of the box section and pure shear force on web. The distortional bending and warping stresses can now be found by analogy with the beam on elastic foundation. The analogy between the behaviour of box girder and that of beam on elastic foundation is shown in Fig. 3.13 and 3.14. Wright, Samad and Robinson [23] presented simplified formulae for different types of diagram, and presented solutions of the beam on elastic foundation in dimensionless parameters in the form of graphs.

3.2.8 Orthotropic Palte Method

In this method, the box girder is replaced by an equivalent anisotropic plate, of dimensions determined by empirical relationships. The analysis is performed by orthotropic plate theory, assuming plate rigidities D_x, D_y, D_1 and D_{xy}. The stresses obtained from the analysis are then related to the actual structure. This method is not capable of taking into

Distributed Loading w

Beam EI$_b$

Foundation Modulus k

Support Spacing

Support Stiffness Q=qk
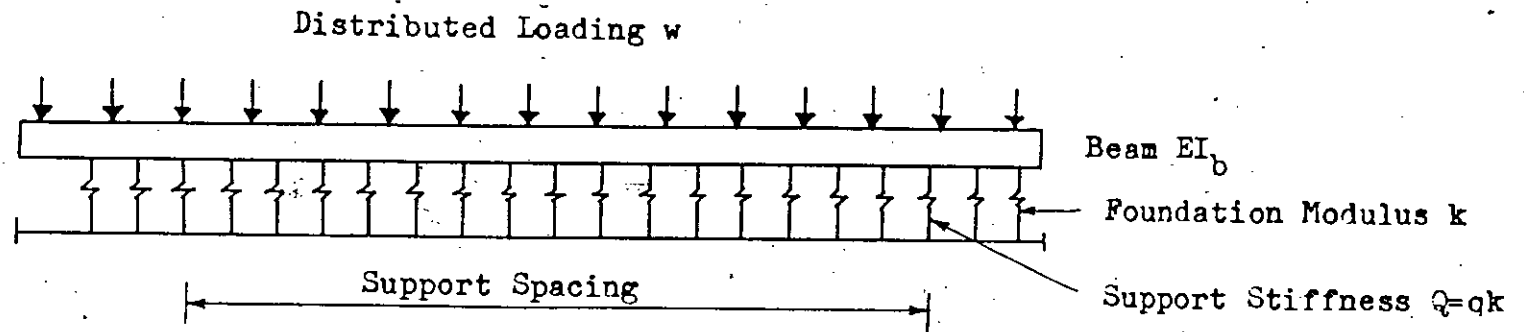
Fig. 3.13: Beam on Elastic Foundation analogy
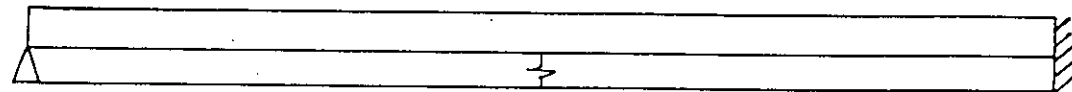
Shear Rigid
Diaphragm
Free to warp

Flexible diaphragm
free to warp

Rigid diaphragm
no warping

Fig. 3.14: Analogy between box girder and Beam on Elastic Foundation.

account distortion, and stresses associated with it. The method can at best evaluate the approximate longitudinal and lateral stresses.

3.2.9 Shear-Weak Plate Method

In this method the behaviour of the box girder is idealised to that of quasi-slab and a substitute structure is analysed. It simulates the stress distribution of cellular slab by simulating the transverse bending of cell wall by a shear parameter. Cope, Harris and Sawko [16] used this approach using shear analogy to simulate cell distortion of the box section. The resulting slab was solved by the finite element technique. They reported good agreement of results for 3 and 6 cell decks with simple and fixed supports. This method is economical in comparison with three-dimensional finite element or finite difference technique. Intermediate supports do not present difficulties as they do in the case of folded plate or finite strip methods. However, the method cannot predict local transverse bending stresses directly, and these are determined by applying displacements, obtained from the quasi-slab analysis, to the web of a plane-framework representation of the cross-section.

3.2.10 Three Dimensional Framework

In a slight modification of the Orthotropic plate method, the actual box girder is replaced by an equivalent orthogonal grid-work of beams rigidly connected at joints to form a three-dimensional rigid frame. These grid members are assigned axial, bending and torsional stiffnesses to simulate the two-way plate behaviour. Each joint has six degrees of freedom and the equivalent system is solved for internal forces and moments which are used to interpret the two-way behaviour of the plates of the box girder. In addition to complexities of inter-relation and the problem of solving a large number of equations, the grid behaviour is only an approximation to that of the actual structure.

3.2.11 Folded Plate Method

The theory of folded plates was originally put forward by Goldberg and Leve [6] and implemented using matrix stiffness method of analysis of the box girder by Scordelis [17]. Chu and Elliot [13] used the same method for the analysis of multicell box girders. The following is a brief description of the method.

a) A box girder is considered to consist of an assemblage of isotropic rectangular plates inter-connected along the longitudinal edges.

b) The applied loads, with any arbitrary longitudinal distribution, are resolved into Fourier series. The analysis is carried out for all load components of each harmonic, and the

process is repeated for all harmonics. The final results are obtained by superposition of the results from all of the harmonics.

c) As the harmonic load component produces displacements of the same variation as that of the loading, single values may be used to represent and force or displacement in the longitudinal direction. Thus each longitudinal joint may be treated as a single nodal point.

d) Each longitudinal joint has four degrees of freedom, viz. translation in horizontal, vertical and longitudinal directions, and rotation about the longitudinal edge axis.

e) Each plate is first isolated and fixed along its longitudinal edges and analysed for surface loads. The internal forces of the plate, and fixed edge forces are obtained by the use of equations of elasticity and plate theory in flexure, for tangential and normal components of load. The internal forces for each plate are similarly related to edge displacements.

f) The stiffness matrix for the whole structure is formulated from the stiffness matrix of individual plates using the appropriate transformation matrices.

g) Using the compatibility of edge displacements, and equilibrium of edge forces, leads to a set of linear simultaneous equations

with loads as the known vector. These equations are then solved for displacement of edges.

h) Final stress resultants for each plate are obtained by adding the internal forces calculated for fixed edges and internal forces for edge displacements.

The final solution is obtained by summing results of the analysis for each harmonic of the applied loads.

The method possesses the advantage of simplicity and involves few degrees of freedom, but it suffers the limitation of being suitable only for right simple spans with shear rigid diaphragms at each end. The method loses its simplicity when intermediate supports or internal diaphragms have to be treated.

3.2.12 Finite Strip Method

The Finite Strip method [4] may be considered as a special form of the well-known finite element method, in whcih the box girder cross-section is divided into a number of strips of length equal to the span of the box girder. The displacement function of the finite strip consists of two parts, a polynomial in the transverse direction and a continuously differentiable smooth trigonometric series in the longitudinal direction. The series is so selected that it satisfies, a priori, the boundary conditions at the ends of the strips. The relation between strains and

displacements are obtained from the theory of elasticity and the load is represented by Fourier series. Finally, the relations between load and displacements are obtained by minimising the total potential energy, i.e. strain enrgy stored in the body and the potential energy of the loads. This leads to a set of linear simultaneous equations which are then solved for the displacements. The solution is obtained by solving the equations for each harmonic and the total displacement is obtained by adding the displacements for a number of harmonics. Cheung [4] was the first to use this method for the analysis of box girder bridges by combining the bending and inplane stiffness of the strips. This method is suitable for simple spans, but becomes uneconomic for multispan structures due to coupling of terms.

3.2.13 Finite Element Method

The finite element method [24] is now a well-established method for the analysis of continuum structures. In this approach the continuum is divided into elements inter-connected only at a finite number of points. At these points fictitius forces representative of the distributed stresses actually acting on the element boundaries are assumed to act. With such an idealisation the local displacement characteristics for the elements are determined. The solution of structural continua, plates and shells etc., lies in the solution of these force displacement relationships by numerical procedures. Among all the elastic methods of analysis, this method is the most versatile and

includes torsional, distortional and warping stresses in the formulation. The general derivation of this method is not discussed here, and can be referred to elsewhere [24].

Because of its versatility, this approach has been selected for the analysis of the box girder used in this study. A brief description of the finite element program used is given in the next chapter.

CHAPTER 4

ANALYSIS OF SPINE BEAM BRIDGE DECK

4.1 INTRODUCTION

A spine beam bridge deck may be analysed by different analytical methdos as discussed in Chapter 3. Of the different methdos of analyses of spine beams, the simplest one is the simple beam theory or the engineer's bending theory which is used in many cases for calculation of bending and shear stresses. A spine beam is subjected to torsion and warping stresses in addition to bending and shear stresses. Moreover shear lag effects are important with wide single-cell box-beams in comparison with narrow one. The simple beam theory can not predict accurate information of the combined action of the complex behaviour of spine beams.

Many of the simplified methods are used to predict individual action of different stresses which have been shown in Table 3.1. The method of Kollbrunner, Hajdin and Heilig [10,7] is used to calcualte the torsional warping stresses and the beam on elastic foundation analogy is used to calculate the distortional warping stresses. These two methods are simple and used in most cases. Of all the methods the finite element method is the most sophisticated method. To obtain accurate results of the combined

effects of different stresses, the finite element method has been used for the analysis of spine beam bridge decks.

4.2 ANALYSIS BY SIMPLE BEAM THEORY, METHOD OF KOLLBRUNNER, HAJDIN AND HEILIG (10,7) AND BEAM ON ELASTIC FOUNDATION ANALOGY

Three simply supported spine-beam bridge decks having diaphragms only at the ends were considered in the analysis. The span length and the cross-sectional dimensions were fixed up with reference to normal sizes of this type of bridge [18]. The feature survey by Swann [18] shows that the economic span range of this type of bridge decks is usually greater than 80', the popular span being between 80 and 160 ft. Most of the spans smaller than 80 ft. are for subsidiary structure such as entry and exist ramps to viaducts. Economy has been achieved in some small spans by forming the cells of the box with permanent cylindrical void-former, virtually resulting in a voided slab with side cantilevers. From the above consideration three span of 84, 96 and 120 feet were selected in the analysis.

Three examples are presented in Appendix-A. For all the spine beams considered in the analysis, the span/depth ratio is 10. The breadth/depth ratio for the cell is 2 and the thicknesses of top flange, bottom flange and webs are taken to be the same. The total width of section with side cantilevers is twice the distance between centre line of webs. Cross-sectional dimensions

and distribution of loads are shown in Fig. 5.1 to 5.9. In all cases HS_{20} loading was considered at midspan.

Longitudinal bending stresses at midspan, bending and torsional shear stresses at support section were calculated by simple beam theory and St. Venant torsion theory. These stresses are shown in Fig. A.3, A.11 and A.19 in Appendix-A.

Torsional warping stresses at midspan section were calculated by the method of Kollbrunner, Hajdin and Heilig [10,7] placing the loading on the end of cantilever to produce the maximum torsional warping stress. Distortional warping stresses and transverse bending stresses were calculated by the beam on elastic foundation analogy. For simplicity total weight of HS_{20} loading i.e, 72 kips load was assumed to act at midspan on one web to calculate distortional warping and transverse bending stresses at midspan. Torsional warping, distortional warping and transverse bending stresses are shown in Fig. A.5, A.7, A.8; A.13, A.15, A.16; A.21, A.23 and A.24 for the three examples respectively in Appendix-A.

4.3 DESCRIPTION OF THE FINITE ELEMENT PROGRAMME AND ELEMENT STIFFNESS MATRIX

A rectangular finite element stiffness matrix, with inplane and flexure terms, known as a 'shell element', was used for the development of the programme. It is assumed that there is no

interaction between inplane and flexure stresses. The stiffness
matrix of the shell element was obtained by superposition of the
stiffness matrix of the Melosh [12] rectangular plane stress (2
degrees of freedom per node) element and the Zienkiewicz [24]
plate bending (3 degrees of freedom per node) element. Each
element thus has five degrees of freedom, three translations and
two rotations per node. The stiffness matrix for an element is
stored in a 24x24 matrix: The terms in each 6x6 submatrix (terms
relating the forces at a node to the deflections at a node) are
given by the following relations to facilitate operations later
in the programme.

$$
\begin{bmatrix} P_x \\ P_y \\ P_z \\ \hline T_x \\ T_y \\ T_z \end{bmatrix} = \left[\begin{array}{ccc:ccc} K_m & K_m & 0 & 0 & 0 & 0 \\ K_m & K_m & 0 & 0 & 0 & 0 \\ 0 & 0 & K_b & K_b & K_b & 0 \\ \hdashline 0 & 0 & K_b & K_b & K_b & 0 \\ 0 & 0 & K_b & K_b & K_b & 0 \\ 0 & 0 & 0 & 0 & 0 & 1 \end{array} \right] \begin{bmatrix} U \\ V \\ W \\ \hline x \\ y \\ z \end{bmatrix} \qquad (4.1)
$$

where K_m and K_b parameters refer to terms of the inplane and
bending stiffness matrices respectively.

In general, adjacent shell elements may not be co-planner,
therefore the nodal point displacements and forces must be
expressed in terms of a common co-ordinate system before
compatibility and equilibrium conditions can be established.

The co-ordinate system of a particular element is denoted by (x,y,z) and referred to as element axes, and the common co-ordinate system of the complete structure is denoted by (X,Y,Z), referred to structure axes as shown in Fig. 4.1. The forces, displacements, moments and rotations can be represented by vectors acting in the co-ordinate directions and it is, therefore only necessary to determine the transformation matrix for any set of vectors acting in these directions. Denoting the angle between the x and Y axes by xY etc. The displacement in the element axes can be expressed in terms of those of structural axes by equation 4.2.

$$
\begin{bmatrix} U_e \\ V_e \\ W_e \end{bmatrix} = \begin{bmatrix} Cos\ xX & Cos\ xY & Cos\ xZ \\ Cos\ yX & Cos\ yY & Cos\ yZ \\ Cos\ zX & Cos\ zY & Cos\ zZ \end{bmatrix} \begin{bmatrix} U_s \\ V_s \\ W_s \end{bmatrix} \qquad (4.2)
$$

where subscript e and s stands for element and structure respectively. The direction cosines Cos (xX) etc. are determined by the following:

Let I,J,K be unit vectors in the X,Y,Z directions and (x_2, y_2, z_2) and (x_3, y_3, z_3) be co-ordinates of nodes 2 and 3 in structure axes with node 1 taken as origin. Unit vectors in the element axes are given by:
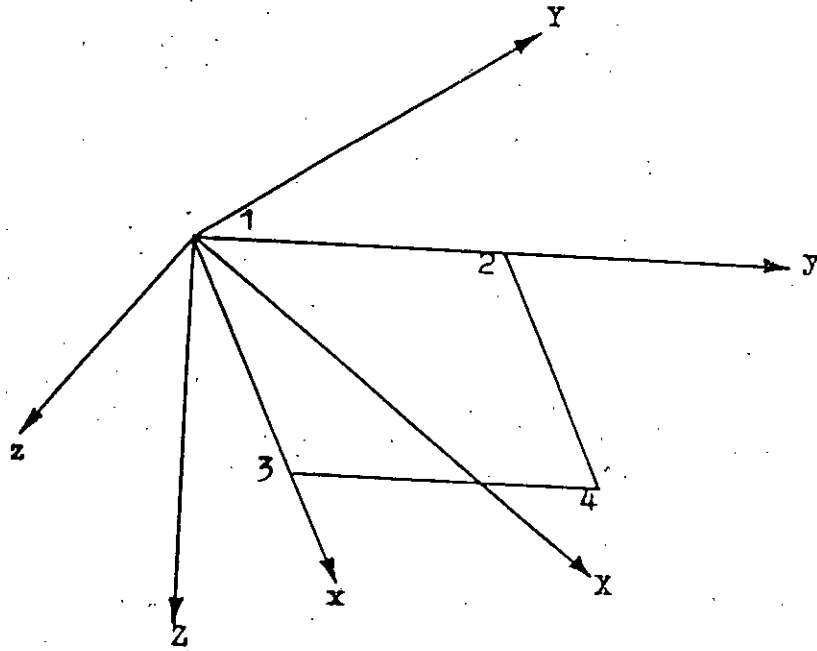
Fig.4.1: Axes of element and structure.

$$i = 1/a \ (x_3 I + y_3 J + z_3 K)$$

$$j = 1/b \ (x_2 I + y_2 J + z_2 K)$$

$$k = 1/ab \begin{bmatrix} I & J & K \\ x_3 & y_3 & z_3 \\ x_2 & y_2 & z_2 \end{bmatrix}$$

where a and b are length of element sides and given by:

$$a = (x_3{}^2 + y_3{}^2 + z_3{}^2)^{1/2}$$

$$b = (x_2{}^2 + y_2{}^2 + z_2{}^2)^{1/2}$$

The direction cosines are obtained by taking scalar products such as $i.I = Cos(xX) = x_3/a$ etc. to give:

$$\begin{bmatrix} U_e \\ V_e \\ \\ W_e \end{bmatrix} = \begin{bmatrix} x_3/a & y_3/a & z_3/a \\ x_2/b & y_2/b & z_2/b \\ \\ \dfrac{\begin{vmatrix} y_3 & z_3 \\ y_2 & z_2 \end{vmatrix}}{ab} & \dfrac{\begin{vmatrix} z_3 & x_3 \\ z_2 & x_2 \end{vmatrix}}{ab} & \dfrac{\begin{vmatrix} x_3 & y_3 \\ x_2 & y_2 \end{vmatrix}}{ab} \end{bmatrix} \begin{bmatrix} P_6 \\ V_6 \\ \\ W_6 \end{bmatrix} \qquad (4.3)$$

The square matrix of equation 4.3 is termed as transformation matrix and is denoted by T.

$$\left[d_e \right] \quad = \quad \left[T \right] \quad \left[d_s \right] \qquad (4.4)$$

where d_e are displacements in local axes

d_s are displacements in structural axes

The corresponding forces can be similarly transformed by:

$$\left[F_e \right] \quad = \quad \left[T \right] \quad \left[F_s \right] \quad \circ$$

$$(4.5)$$

$$\left[F_s \right] \quad = \quad \left[T^{-1} \right] \quad \left[F_e \right]$$

For orthogonal transformation $T^{-1} = T^T$. The complete transformation is performed by operating separately on each 3x3 sub-matrix S of an element stiffness matrix.

$$\text{Thus,} \quad \left[F_s \right] \quad = \quad \left[T \right]^T \quad \left[S \right] \quad \left[T \right] \quad \left[d_s \right] \qquad (4.6)$$

By applying the above process to each element in turn, the element stiffness matrices are transformed to structural axes, ready for assembling the overall stiffness matrix.

As shown in Eqn. 4.1, at each node, six degrees of freedom have been permitted, but only five components of displacement and force have been used to formulate the element stiffness matrix with respect to local axes. These forces and displacements are resolved into the six directions of the structural axes. For nodes at which only co-planner elements meet, the resolution produces six equations from sets of five and one of them is linearly dependent upon on of the others. This makes the overall stiffness matrix singular and therefore incapable of solution. To maintain regularity in the method the redundant equations are set up by the computer programme, but they have no influence as their co-efficients are set equal to zero before solution. For nodes at which non-co-plannar elements meet resolution produces six equations from each of five equations and when they are combined six independent equations are formed.

4.4 SOLUTION OF EQUATIONS

Once the stiffness matrix is formed the next step is to solve the equations for displacement. These displacements are then used for calculating the stresses in the individual elements. Since in a box girder bridge the number of equations solved is quite large, the whole assembled stiffness matrix cannot be stored in the live core of the computer, because of core limitation for any job. The assembled stiffness matrix is, therefore, stored in backing store in a square matrix of size equal to that of half band-width. The solution of the equations are then carried out by Cholesky

decomposition. The programme for the analysis of spine beam bridge deck by using the above procedure was obtained from Murtuza [13].

4.5 NUMBER OF ELEMENTS

To determine the number of elements in the cross-section, a subroutine subprogramme for an automatic mesh generation was used in the finite element programme. Only the number of elements in the cross-section and the number of segments in the span were given as input. The number of elements in the cross-section was 16 for all of the cases, with 2 elements in each web and 4 elements in top and bottom flange and 2 in each cantilever. The number of segments in the span was 12.

The number of elements in the cross-section increases the band-width of the stiffness matrix and the number of segments in the span increases the size of the stiffness matrix. Since the solution time is a square of band width, the abvoe sequence of the number of elements and segments was selected in the analysis by the finite element methods to obtain the output in a reasonable time.

4.6 ANALYTICAL MODEL STUDY

Analysis of a spine beam bridge deck having diaphragms is a time consuming process from the computational points of view because of the large band width of the overall stiffness matrix. If the diaphragms can be modelled in the analysis by omitting the physical presence of diaphragms, the band-width of the stiffness matrix is reduced significantly thereby reducing the computational time. For this purpose a simply supported spine beam bridge deck of span 84 feet, inconformity (18) with the usual single span spine beam, was analysed with four types of boundary conditions. The plan, cross-section and the end boundary conditions are given in Figs. 4.2 and 4.3. For simplicity, the web and flange thicknesses are taken to be the same. The structure was analysed by the finite element method. HS_{20} loading was used and the loading arrangements are shown in Fig. 4.4a.

Fig. 4.2 represents the dimensions of spine beam and load position. Fig. 4.3 represents the corss-sectional geometry and Figs. 4.3a to 4.3d represent the end boundary conditions of spine beam. Fig. 4.3a represents the presence of end diaphramgs and the end diaphragm is omitted in Fig. 4.3b to Fig. 4.3d.
Fig. 4.3c and 4.3d indicate the modelled diaphragms. The modelling has been done by restraining the translational displacements of the joints at the diaphragmed section. After the analysis by the finite element method for this loading case (Fig.
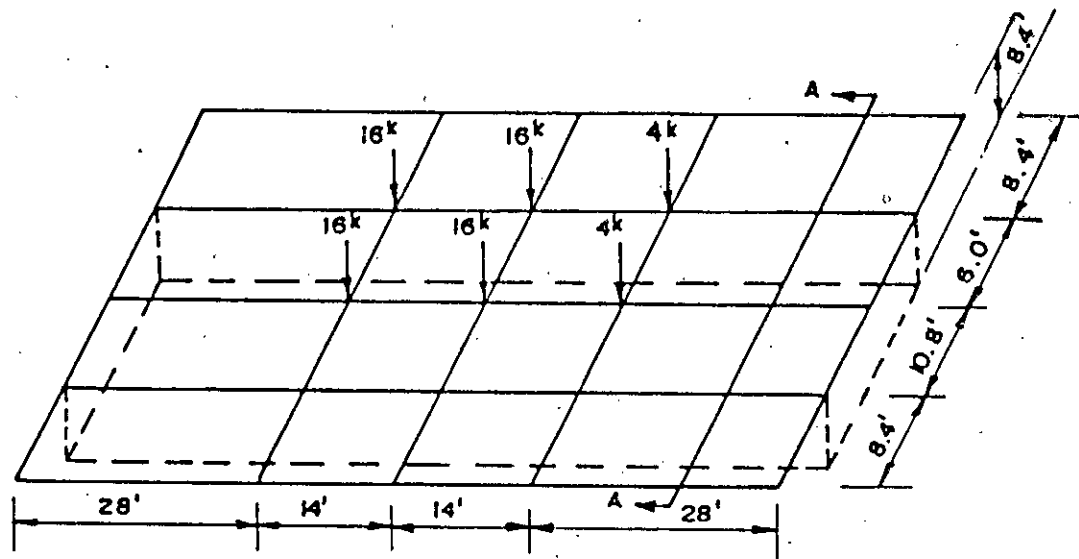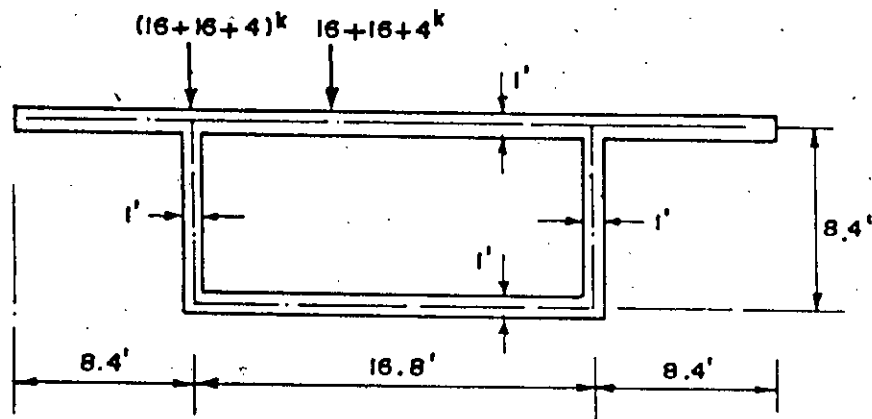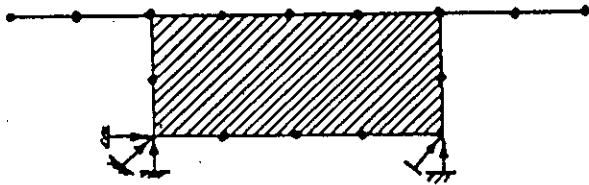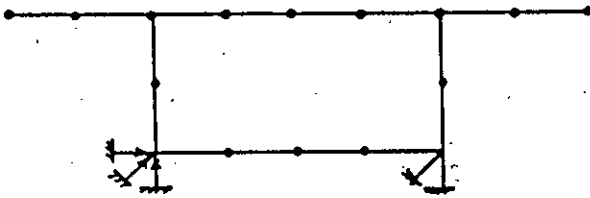
(a) Plan and Geometry

Section A - A

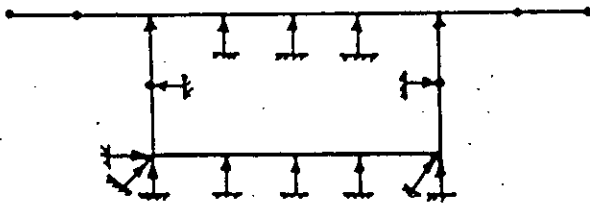Fig. 4.2 Plan, geometry and loading of analytical
model study.

Left support, u = 0, V = 0, W = 0
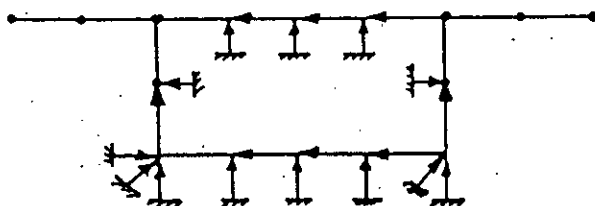
Right support, V = 0, W = 0

With end diaphragm.

(a)

Left support, u=0, V = 0, W = 0

Right support, V=0, W=0

Without end diaphragm

(b)

Left support, u =0, V=0, W=0

Right support, V=0, W=0

In top and bottom flange, vertical translations and in webs horizontal translations are zero only at nodes.

(c)

Left support, u=0, V=0, W=0

Right support, v =0, W=0

In all nodes, vertical and horizontal translations are zero.

(d)

Fig. 4.3   End's boundary conditions of analytical model study.

4.2) only the vertical deflections of the loaded web for four cases (Fig. 4.3a to 4.3d) are shown in Table 4.1. For the same

loading and cross-sectional configuration, the longitudinal bending stresses of loaded and unloaded webs at the bottom points at midspan for the four types of boundary conditions are given in Table 4.2. From these Tables (4.1 and 4.2) it is found that the spine beam with boundary conditions as shown in Fig. 4.3d behaves just like as case one (Fig. 4.3a) i.e with the presence of end diaphragms. For this element configuration, the band-width of the case one is 138 and that for the case two, three and four is 120. Computational time for the first case was 21 minutes and that for the other three cases was 10 minutes for the finite element programme [13] used in this analysis. But computational time also depends upon the total number of nodes. Therefore higher time will be required for smaller size of elements to obtain better results.

This shows that a diaphragm can be modelled reasonably by restraining the translational displacements of joints at the section where a diaphragm is present. Therefore less computational time will be required to analyse such a structure by the finite element method. In this analysis more than 50% time was saved by this modelling.

Table 4.1   Vertical deflection of loaded web (span = L=84')

Case Distance	Case 1 Fig. 4.3a (ft)	Case 2 Fig. 4.3b (ft)	Case 3 Fig. 4.3c (ft)	Case 4 Fig.4.3d (ft)
0	0.00	0.00	0.00	0.00
L/6	0.00149	0.0017	0.0015	0.00148
2L/6	0.0027	0.0031	0.0028	0.00270
3L/6	0.00310	0.0036	0.0032	0.00310
4L/6	0.0025	0.0029	0.0026	0.00249
5L/6	0.0014	0.0016	0.0014	0.00136
L	0.00	0.00	0.00	

Table 4.2 Longitudinal stresses at bottom of loaded and unloaded webs at mid-span

	Case 1 Fig. 4.3a (ksf)	Case 2 Fig. 4.3b (ksf)	Case 3 Fig. 4.3c (ksf)	Case 4 Fig. 4.3d (ksf)
Loaded web	8.6	10.0	9.0	8.7
Unloaded web	5.4	4.0	5.0	5.3

4.6 ANALYSIS BY THE FINITE ELEMENT METHOD

The three examples which were analysed by simple beam theory, the method of Kollbrunner, Hajdin and Heilig [10,7] and the beam on elastic foundation analogy in Appendix-A, were analysed by the finite element method to compare the results obtained by the finite element method to the results obtained by these methods. This comparison has been discussed in Chapter 5.

Results as obtained by finite element method depend on the aspect ratio of the elements. Table 4.3 gives the ratio of the stresses as obtained by finite element method to that obtained by simple beam theory for symmetrical case with respect to the longitudinal

axis at the bottom of webs at midspan for different aspect ratio of elements.

Table 4.3 Ratio of stresses as obtained by SBT to FEM for
         different aspect ratio

ASpect ratio	Stress by FEM/Stress by SBT
1.0	1.038
0.6	1.005
0.5	0.969
0.3	0.955
0.17	0.89
0.15	0.8257
0.10	0.7320

From this table an aspect ratio 0.6 is taken for finite element analysis.

To obtain the variation of longitudinal stresses at midspan across the width of deck, HS_{20} loading was placed on different position. The position of loads and corresponding stress diagrams of the mid-section across the width of deck are shown in Fig. 5.1 to 5.9. Magnitude of Poisson's ratio was taken as 0.18.

CHAPTER 5

RESULTS OF ANALYSIS AND DISCUSSION OF RESULTS

5.1 INTRODUCTION

This investigation presents the analysis of spine beam bridge decks and interpretation of results as obtained by the simple beam theory, the method of analysis proposed by Kollbrunner, Hajdin and Heilig [10,7], beam on elastic foundation analogy and the finite element method. The simple beam theory, the method of Kollbrunner, Hajdin and Heilig [10,7] and the beam on elastic foundation analogy are simple to use. The finite element method gives accurate results but it is a time consuming process and is only suitable where computer facilities are available. Torsional and distortional warping stresses may arise due to eccentric loading on spine beam bridge decks. These type of stresses can not be predicted by simple beam theory. Therefore the method of Kollbrunner, Hajdin and Heilig [10,7] was used to calculate the torsional warping stresses and the beam on elastic foundation analogy was used to calculate the distortional warping stresses and the transverse bending stresses. Amount of these stresses which may arise in case of spine beams with respect to longitudinal bending stresses are shown in percentage form for HS_{20} loading. The same spine beams were analysed by the finite element method to obtain the longitudinal stresses. The comparison of longitudinal stresses as obtained by the simple beam theory and the finite element method are shown in Tables 5.1, 5.2 and 5.2

Lastly a parameter study of 81 spine beams has been performed by the finite element method and the effects of changing of cross sectional geometry on the longitudinal and distortional stresses are presented in section 5.3.

5.2 COMPARATIVE STUDY OF THE RESULTS AS OBTAINED BY THE METHOD OF KOLLBRUNNER, HAJDIN AND HEILIG, BEAM ON ELASTIC FOUNDATION ANALOGY AND FINITE ELEMENT METHOD

Three simply supported spine beams having diaphragms only at the ends of different span lengths and cross-sectional geometry were analysed by the simple beam theory, the method of Kollbrunner, Hajdin and Heilig [10,7] and the finite element method. These analyses are shown in Appendix-A. Longitudinal bending stresses, bending and torsional shear stresses were calculated by simple beam theory and St. Venant torsion theory. Torsional warping stresses were calculated by the method of Kollbrunner, Hajdin and Heilig [10,7] and the distortional warping and the transverse bending stresses were calculated by the beam on elastic foundation analogy.

The simple beam theory is very simple to use. But this theory does not consider distortion, warping and shear lag effects. Moreover this theory is not applicable to deep beams. The method of Kollbrunner, Hajdin and Heilig and the beam on elastic foundation analogy are used for analysis of individual actions

and the combined effects of bending, torsion and distortion are obtained by superimposing the results obtained by these methods with the simple beam theory. However these methods are conservative for individual actions of different stresses. The finite element method is the most sophisticated one.

Figures 5.1 to 5.9 represent the geometry, position of loads and longitudinal bending stresses at midspan across the width of deck and at the bottom of the loaded and the unloaded web along the span of deck as obtained by the simple beam theory and the finite element method. The simple beam theory is abbreviated as SBT while the finite element method is abbreviated as FEM and used in the text in the following. These stress diagrams represent the variation of stress level as obtained by SBT and FEM. Since the longitudinal bending stress is the same at a particular section across the width of deck for different load position at a particular section across the width of deck as obtained by the simple beam theory, therefore longitudinal bending stress diagrams are of the same type. These are shown in clearly in Figs. 5.1 to 5.3, 5.4 to 5.6 and 5.7 to 5.9 for examples one, two and three respectively. The detail calculations of stresses for these diagrams are given in Appendix-A.

Figs. 5.1 to 5.9 represent the variation of longitudinal bending stresses across the width of deck at the midspan and at the bottom of webs along the span. These diagrams show that the variation of the longitudinal bending stresses as obtained by the
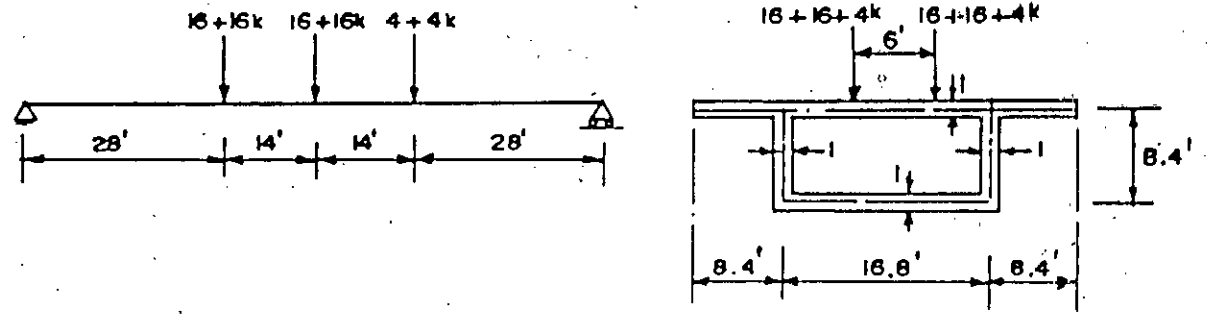
(a) Loading and geometry.
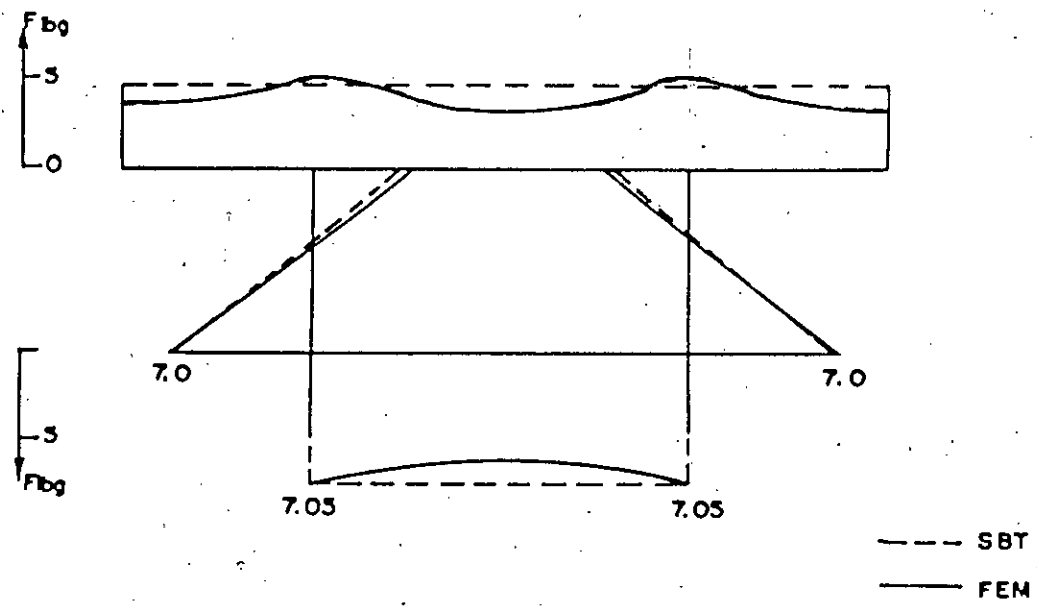
(b) Longitudinal bending stress across the width of deck at midspan(ksf)
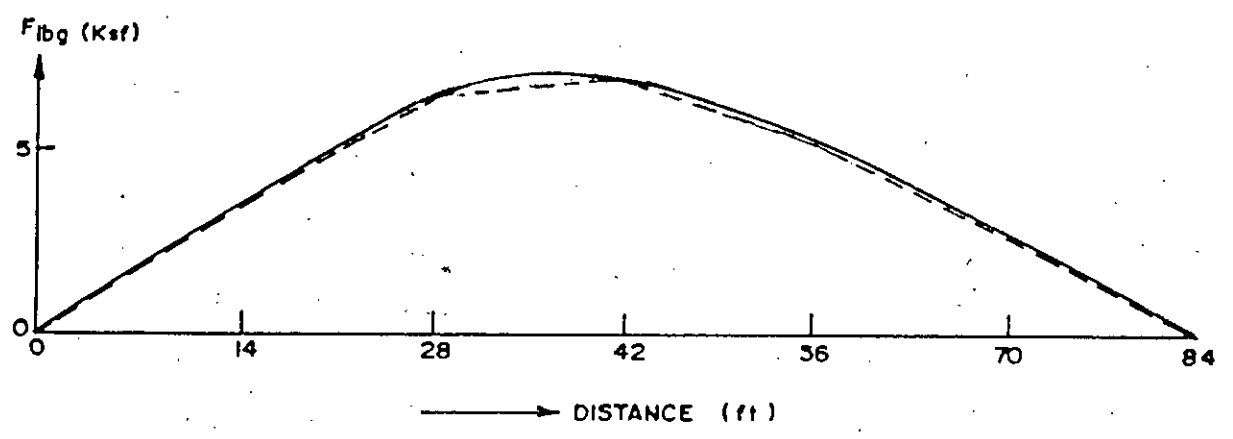
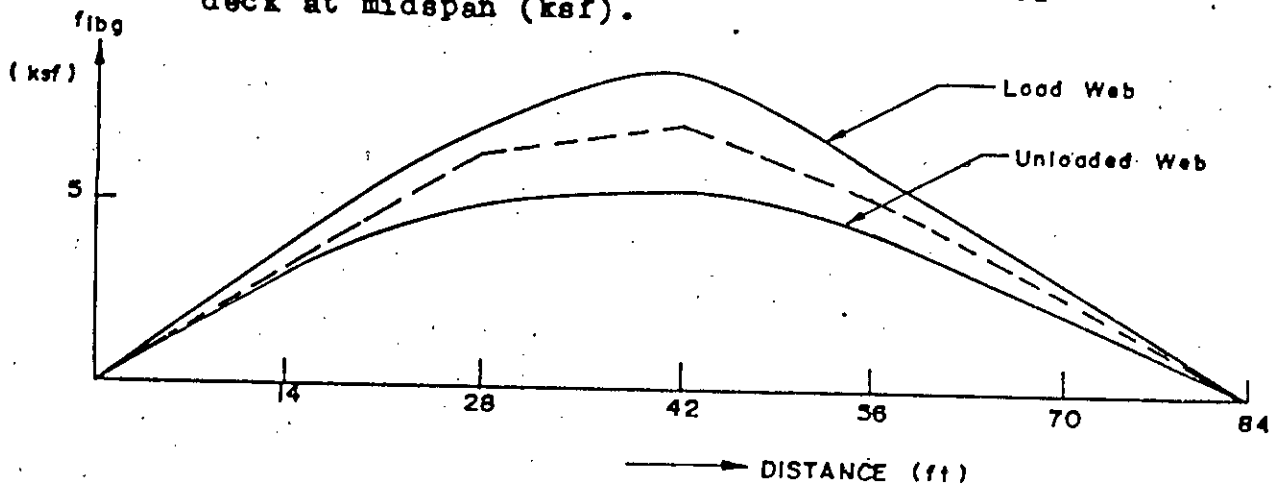(c) Longitudinal bending stress along the span at the bottom of web.

Fig. 5.1 Loading, geometry and longitudinal bending stress at midspan and along the span.
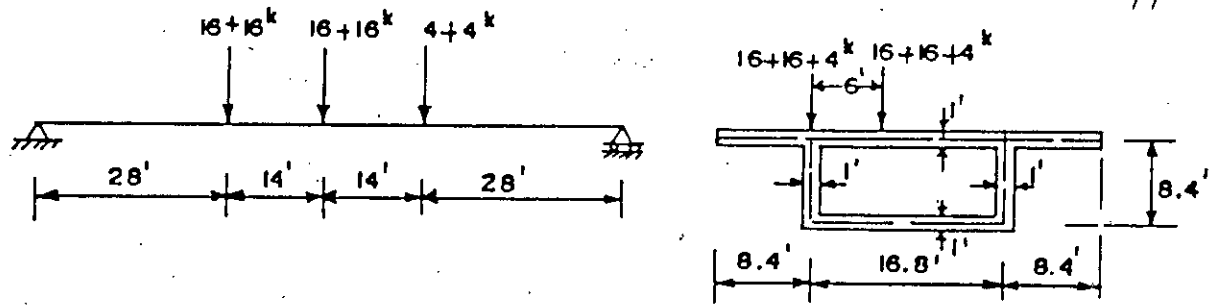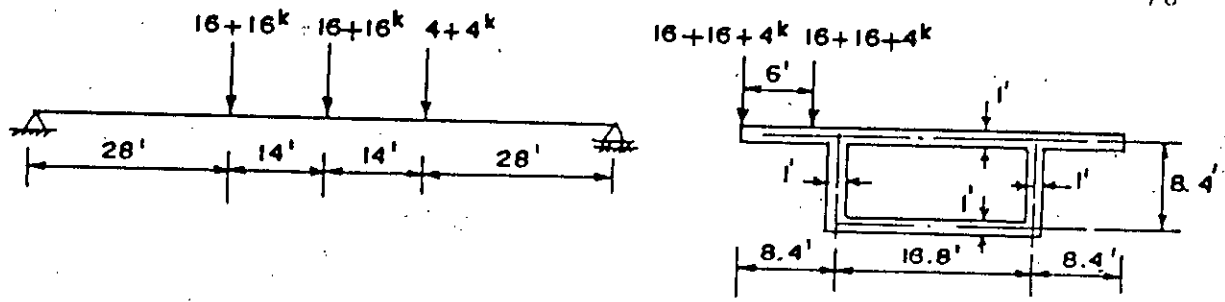
(a) Loading and geometry.
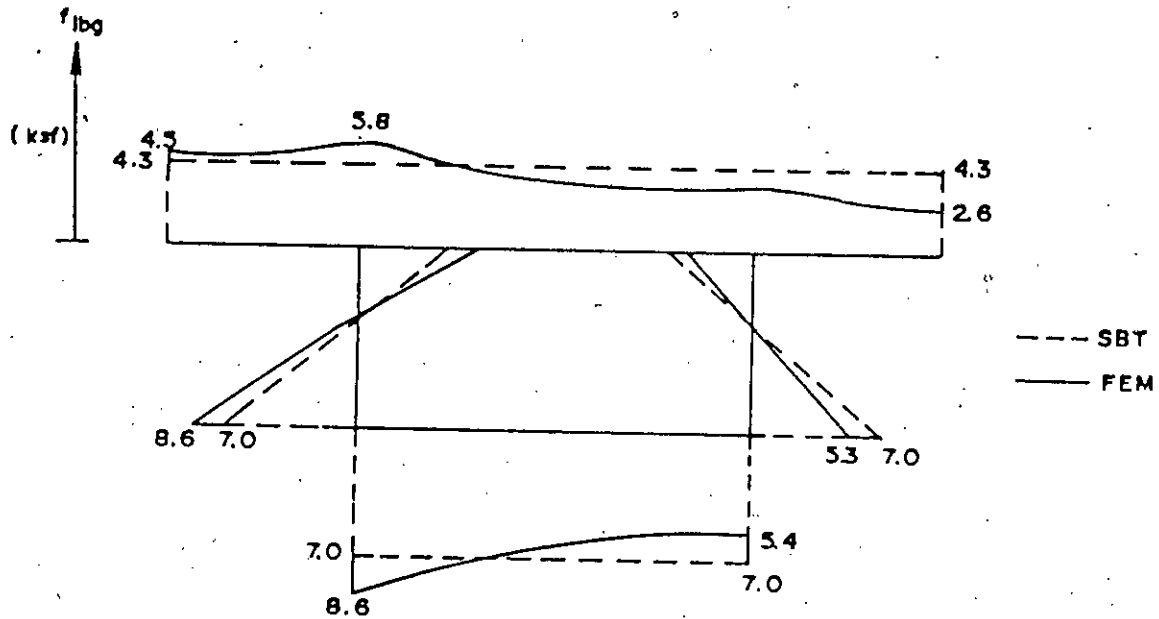
(b) Longitudinal bending stress across the width of deck at midspan (ksf).
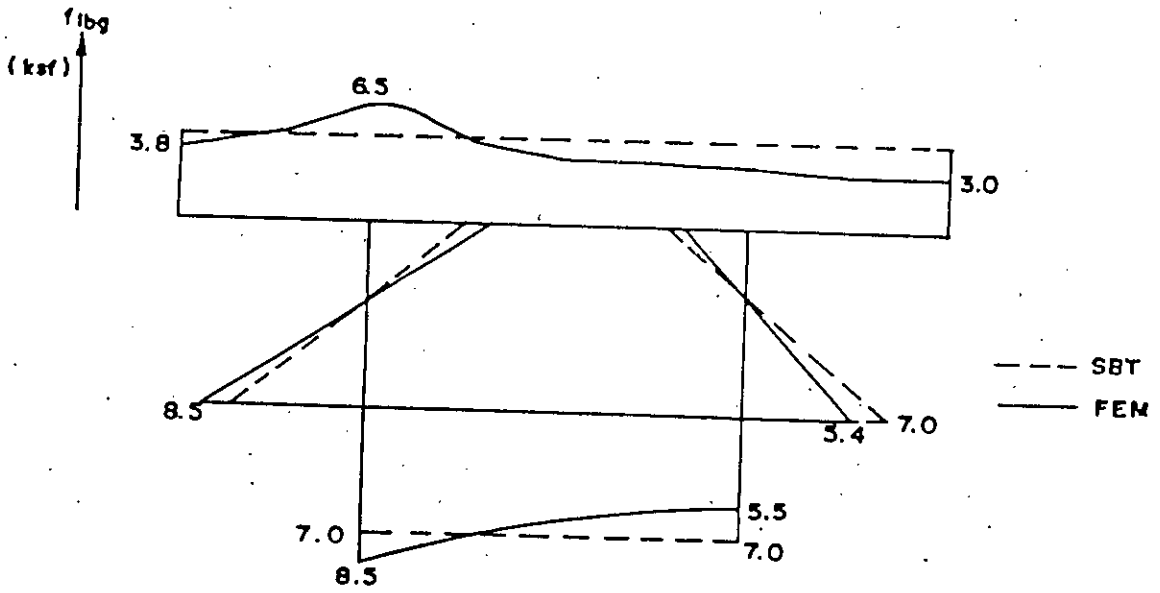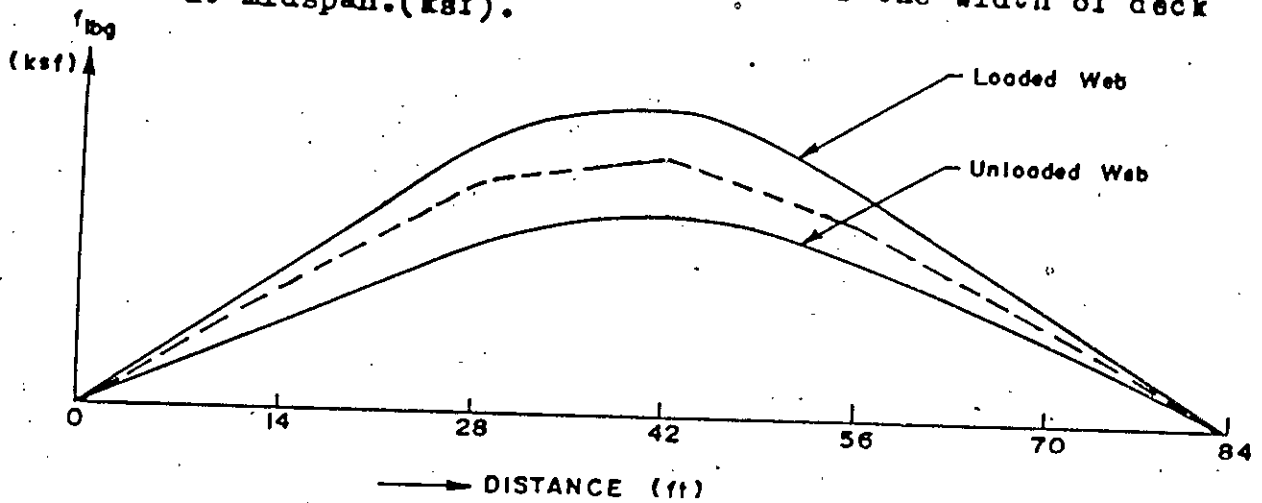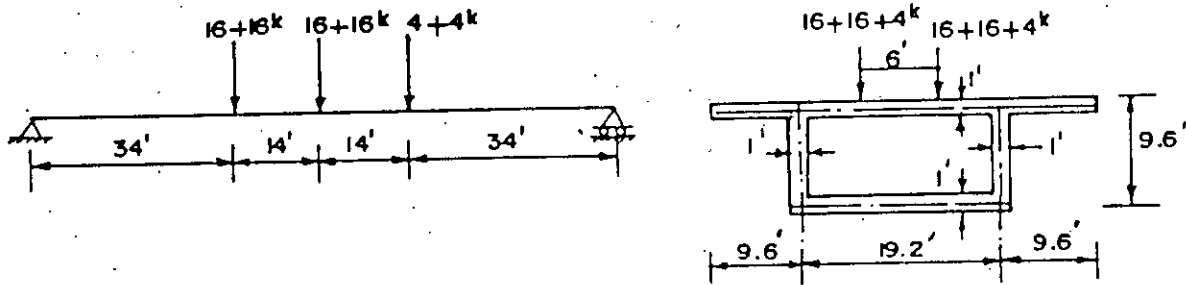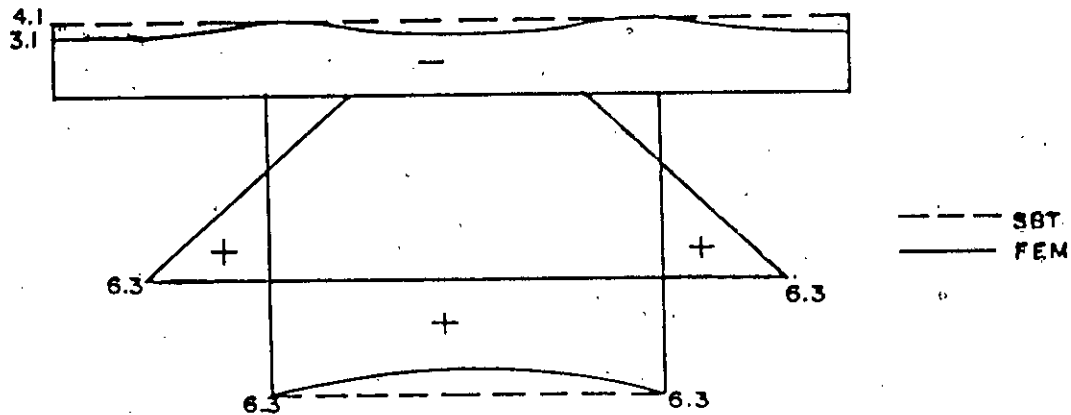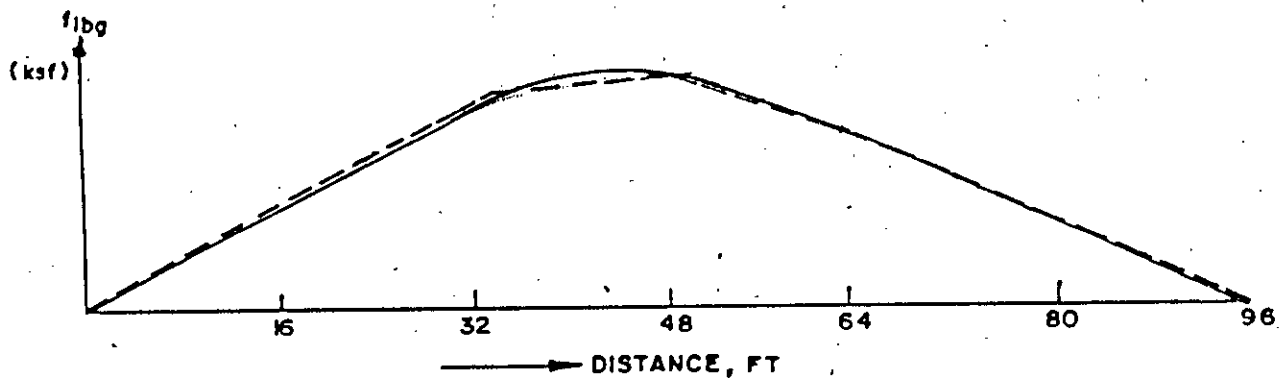

(c) Longitudinal bending stress along the span at the bottom of web.

Fig. 5.2 Loading geometry and longitudinal bending stress at midspan and long the span.
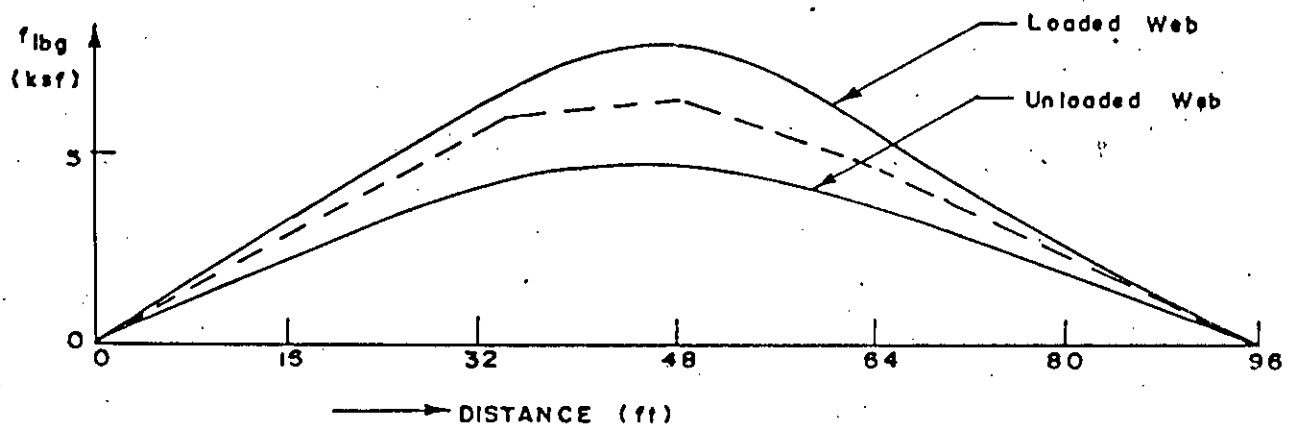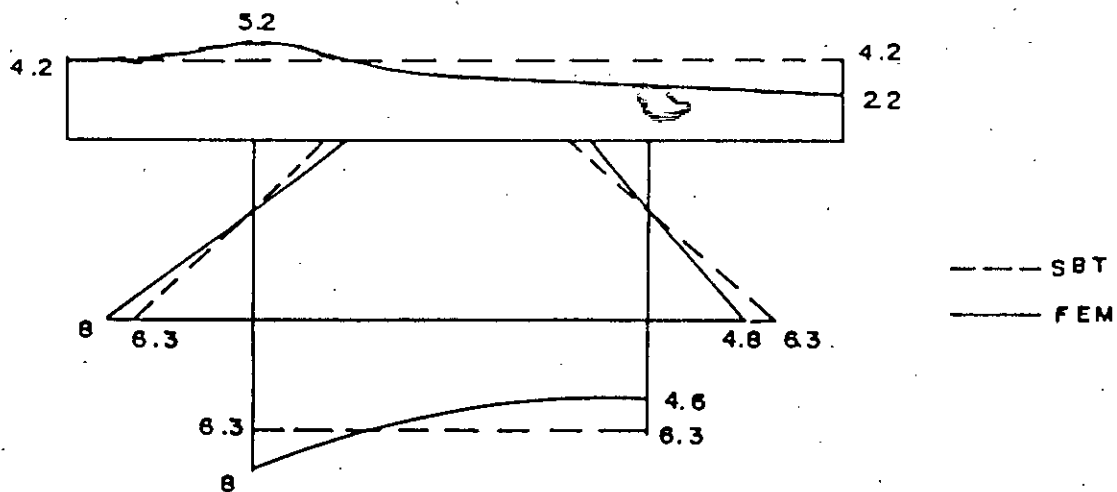
(a) Loading and geometry

(b) Longitudinal bending stress across the width of deck at midspan.(ksf).

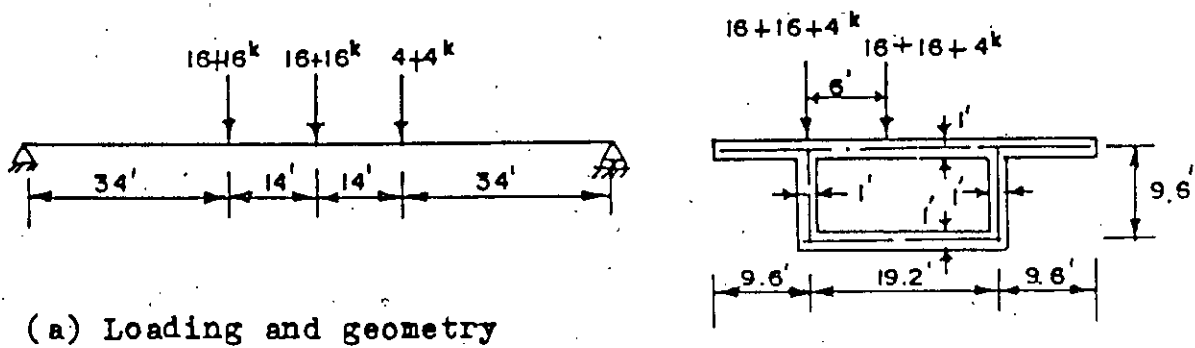(c) Longitudinal bending stress along the span at the bottom of web.

Fig. 5.3   Loading geometry and longitudinal bending stress at midspan and along the span.

(a) Loading and geometry

(b) Longitudinal bending stress across the width
of deck at midspan(ksf).

(c) Longitudinal bending stress along the span at the
bottom of web.

Fig. 5.4   Loading, geometry & longitudinal bending stress
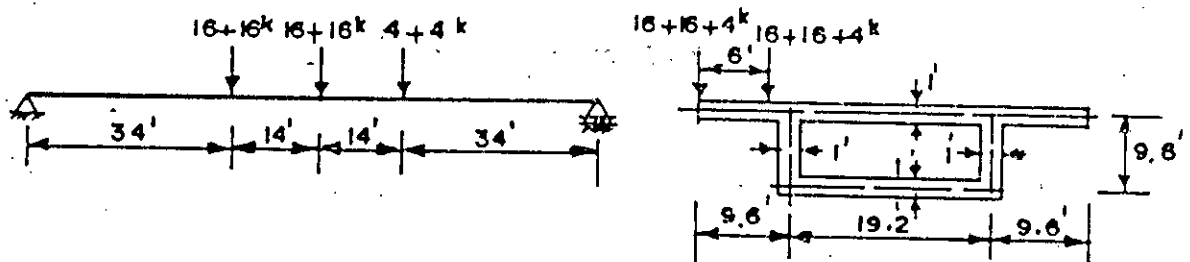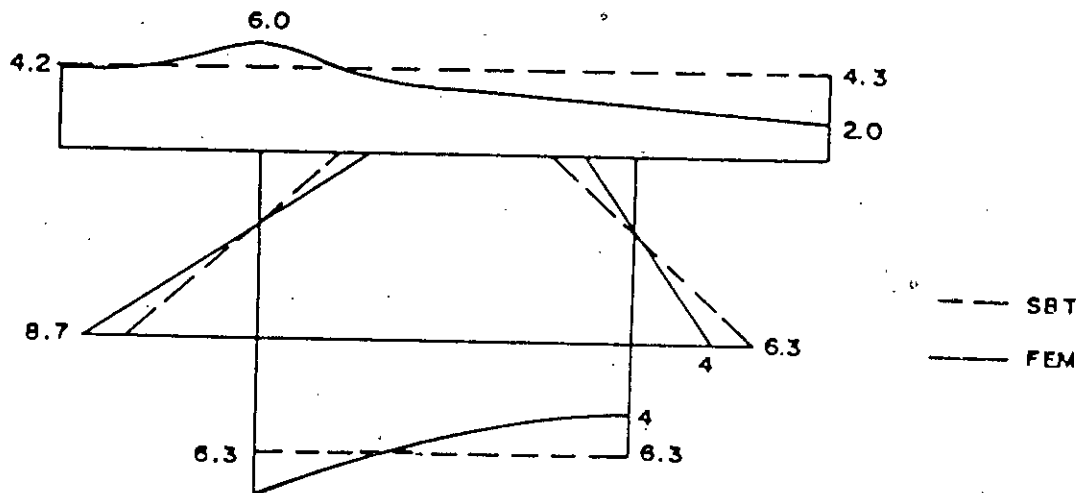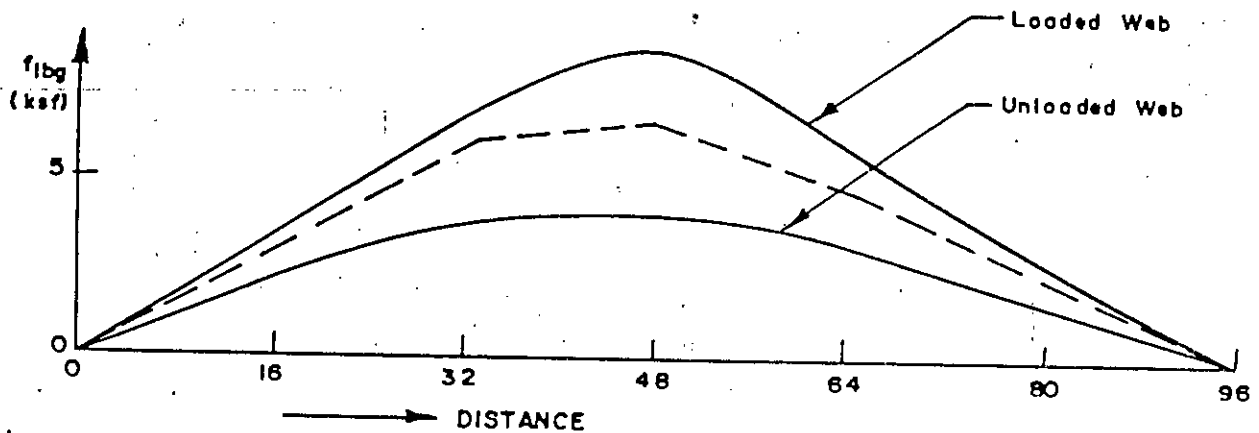at midspan and along the span.

(a) Loading and geometry

(b) Longitudinal bending stress across the width of deck at midspan (ksf).

(c) Longitudinal bending stress along the span at the bottom of web.

Fig. 5.5 Loading, geometry and longitudinal bending stress at midspan and along the span. Span = 96'.

(a) Loading and geometry.

SBT

FEM

(b) Longitudinal bending stress across the width of deck at midspan (ksf).

(c) Longitudinal bending stress along the span at the bottom of web.

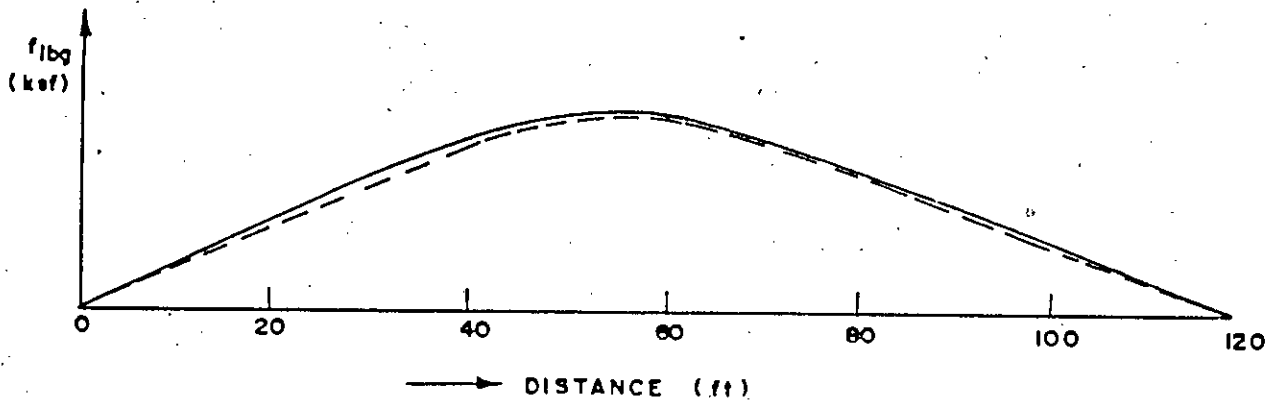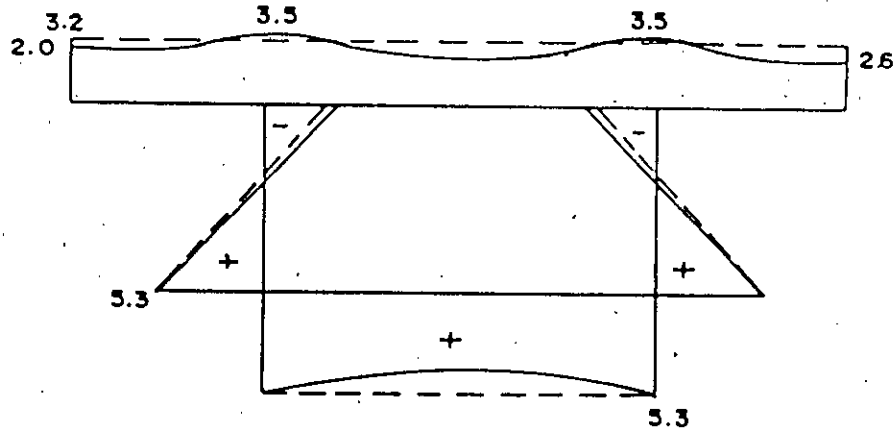Fig. 5.6 Loading, geometry and longitudinal bending stress at midspan and along the span. Span = 96'.

(a) Loading and geometry.

(b) Longitudinal bending stress across the width of deck at midspan(ksf).

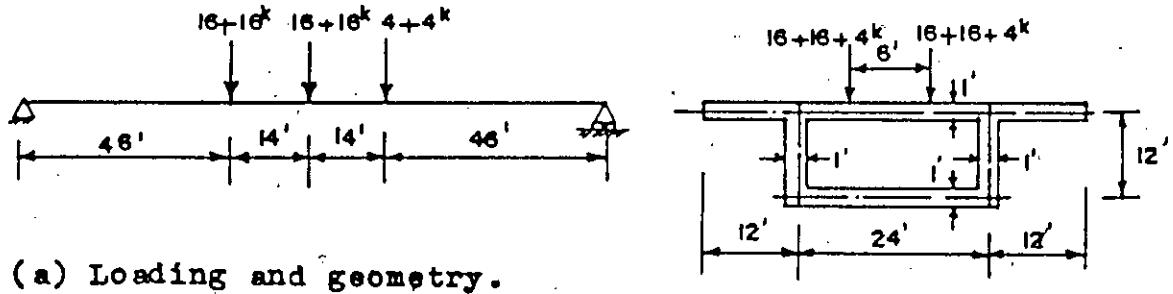(c) Longitudinal bending stress along the span at the bottom of web.
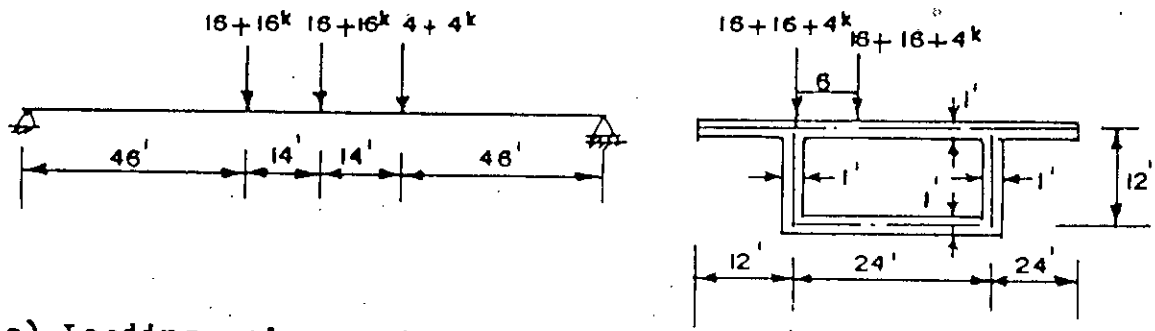
Fig. 5.7   Loading, geometry & longitudinal bending stress at midspan and along the span. Span = 120'

(a) Loading and geometry.

(b) Longitudinal bending stress across the width of deck at midspan (ksf).

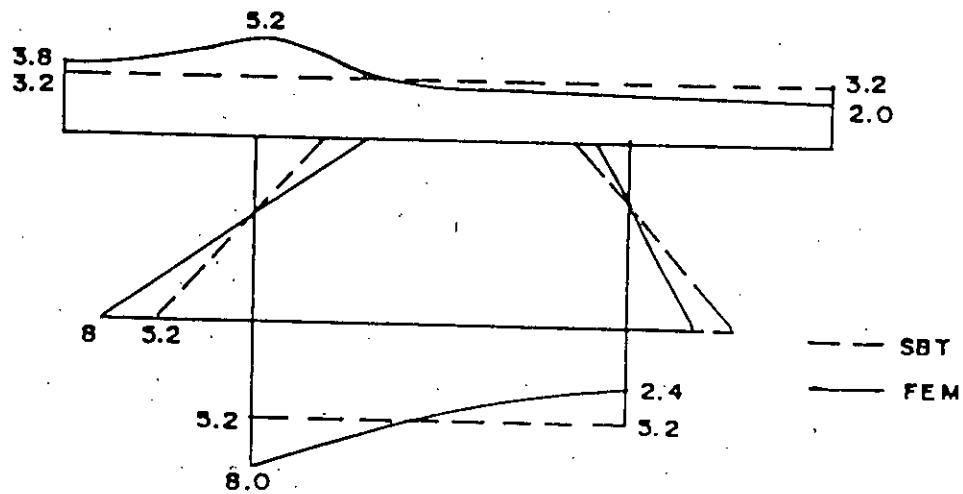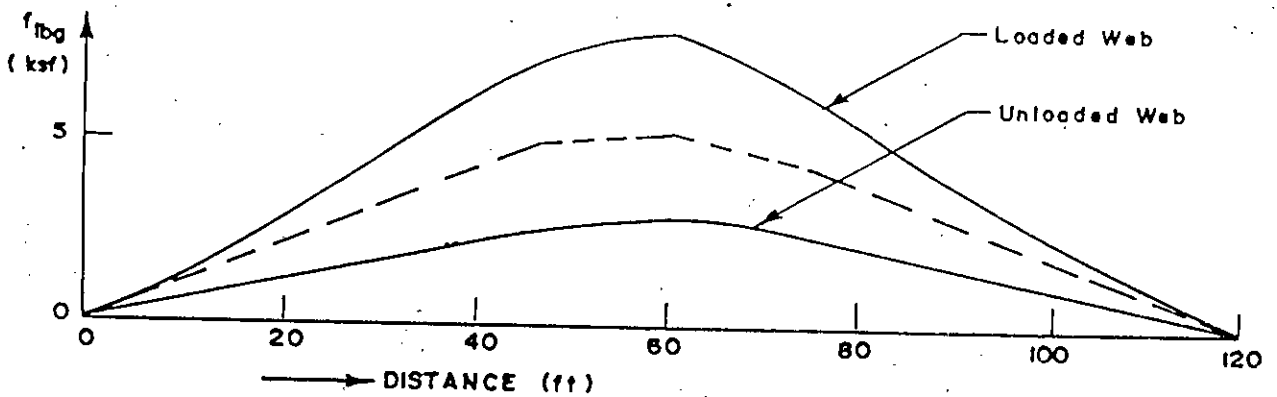(c) Longitudinal bending stress along the span at the bottom of web.

Fig. 5.8 Loading, geometry longitudinal bending stress at midspan and along the span. Span = 120'.
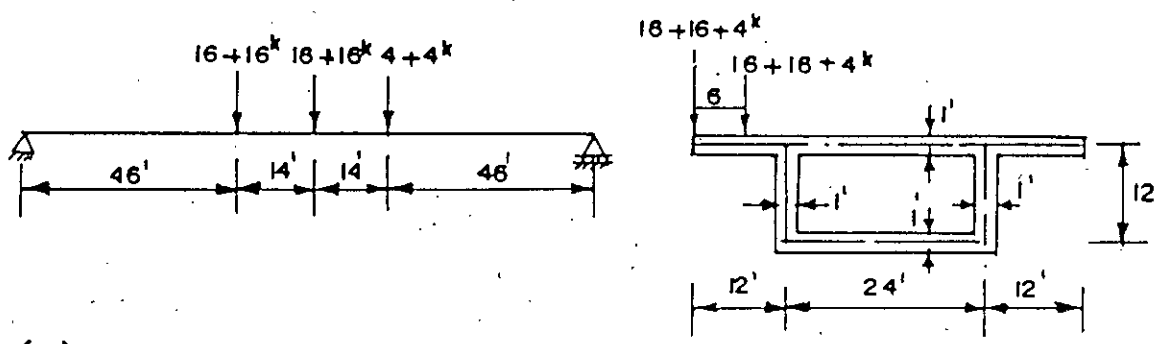
(a) Loading and geometry.

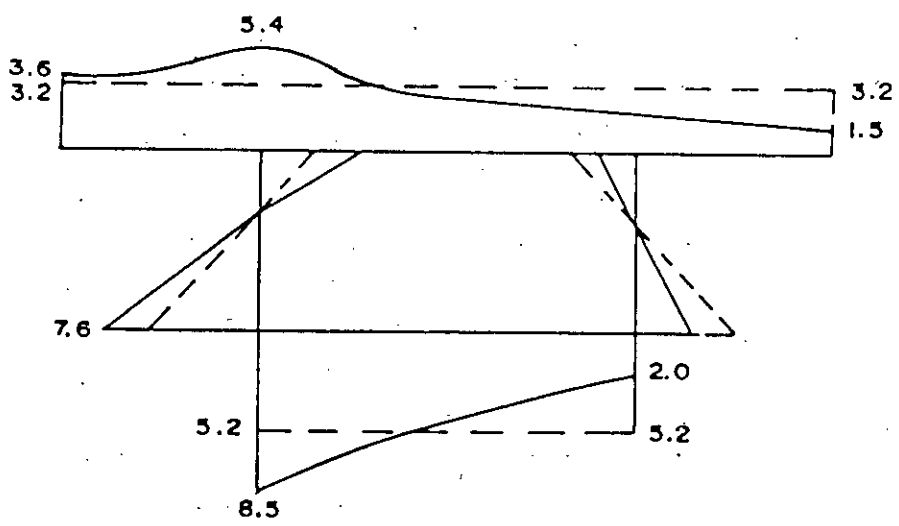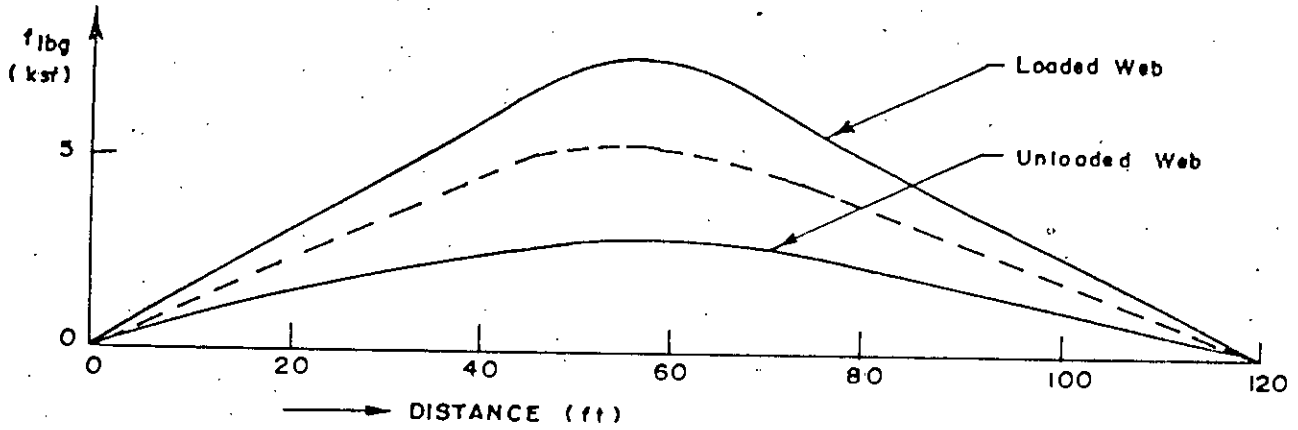(b) Longitudinal bending stress across the width of deck at mid span (ksf).

(d) Longitudinal bending stress along the span at the bottom of web.

Fig. 5.9 Loading, geometry and longitudinal bending stress at midspan and along the span. Span = 120'.

finite element method is not linear. These diagrams also represent the shear lag effects. Tables 5.1 to 5.3 represent the variation of longitudinal bending stresses at top and bottom of webs at midspan as obtained by SBT and FEM of the three examples as described in previous chapter. These tables (5.1 to 5.3) show that the calculated stresses as obtained by SBT are higher at unloaded web and lower at loaded web than that of obtained by FEM. This variation increases with the increasing span length. Table 5.1 (for example one) shows that the calculated longitudinal bending stresses as obtained by SBT and FEM are nearly the same in case of symmetrical loading but there is slight difference due to shear lag effect. And this difference increases with the increasing eccentricity of loading but average stress level remains the same. For eccentric loading the differences are -29% and -20% at top and bottom of laded web and 35% and 34% at top and bottom of unloaded web.

In this situation severe torsional and distrotional warping stresses arise. Table 5.4 and Table 5.5 show the ratio of torsional and distrotional warping stresses to longitudinal bending stresses whcih are 62% at the top and (30+12) 42% at the bottom of webs at midspan for Example 1. Table 5.2 and 5.3 represent the longitudinal bending stresses for Example 2 and 3 respectively. But the variation of above stresses are increased than example one. Table 5.2 shows that for eccentric loading longitudinal bending stresses are 35% and 27% higher at top and bottom of loaded web and 62% lower at top and bottom of unloaded

Table 5.1   Variation of longitudinal bending stresses as obtained by
SBT and FEM at midspan for Example one

Figure for load position, cross-sectional dimension	Stresses obtained by SBT		Stresses obtained by FEM				Excess than FEM			
	Top of web (ksf)	Bottom of web (ksf)	Left web Top (ksf)	Bottom (ksf)	Right web Top (ksf)	Bottom (ksf)	Left web Top (%)	Bottom (%)	Right web Top (%)	Bottom (%)
5.1	-4.32	7.0	-4.5	7.05	-4.5	7.05	-4	0	-4	0
5.2	-4.32	7.0	-5.8	8.6	-3.5	5.3	-25	-18	23	32
5.3	-4.32	7.0	-6.1	8.8	-3.2	5.2	-29	-20	35	34

Table 5.2 Variation of longitudinal bending stresses as obtained by
          SBT and FEM at midspan for Example Two

Figure for load position, cross-sectional dimension	Stresses obtained by SBT		Stresses obtained by FEM				Excess than FEM			
	Top of web (ksf)	Bottom of web (ksf)	Left web Top (ksf)	Bottom (ksf)	Right web Top (ksf)	Bottom (ksf)	Left web Top (%)	Bottom (%)	Right web Top (%)	Bottom (%)
5.4	-3.9	6.35	-4.13	6.38	-4.13	6.38	-5	0	-5	0
5.5	-3.9	6.35	-5.22	7.9	-3.2	4.8	-25	-19	21	32
5.6	-3.9	6.35	-6.0	8.7	-2.4	3.9	-35	-27	62	62

Table 5.3 Variation of longitudinal bending stresses as obtained by SBT and FEM at midspan for Example Three

Figure for load position, cross-sectional dimension	Stresses obtained by SBT		Stresses obtained by FEM				Excess than FEM			
	Top of web (ksf)	Bottom of web (ksf)	Left web Top (ksf)	Bottom (ksf)	Right web Top (ksf)	Bottom (ksf)	Left web Top (%)	Bottom (%)	Right web Top (%)	Bottom (%)
5.7	-3.2	5.27	-3.5	5.3	-3.5	5.3	-8	0	-8	0
5.8	-3.2	5.27	-5.11	8.0	-2.0	2.7	-37	-34	60	95
5.9	-3.2	5.27	-5.4	8.2	-1.8	2.4	-40	-35	77	119

web as obtained by FEM than SBT. Table 5.3 shows the above values as 40%, 35% 77% and 119% respectively for example three.

Table 5.4 and 5.5 show the ratio of torsional and distortional warping stress to longitudinal bending stress remain the same level for the three cases at different points across the width of deck at the midspan section. Table 5.6 represents the ratio of the transverse bending stresses to the longitudinal bending torsional and distortional warping stresses at the top and bottom of webs at midspan for the three examples. This table shows that the ratio of the above stresses are the same but are different at top and bottom of webs.

Table 5.7 represents the ratio of combined longitudinal bending stresses by superimposing the results as obtained by the simple beam theory, method of Kollbrunner, Hajdin and Heilig [10,7] and the beam on elastic foundation analogy to the finite element method at top and bottom of loaded web at midspan. This table shows that the magnitude of combined effect of stresses are higher than that obtained by FEM at bottom of webs and lower at top of webs. This variation increases with the increasing of bridge span. But this variation is higher at the top of webs than at bottom of webs. In example one, this variation is 16% at top and 4% at bottom of webs. In example two, this variation is 13% at top and 3% at bottom of webs. In example three the above values are 34% and 14% respectively.

Table 5.4   Ratio of torsional warping stress (f_{twr}) to longitudinal bending stress (f_{lbg}) at different points for the midspan section

Position	Example 1 d=8.4 span=84	Example 2 d=9.6 span=96	Example 3 d=12 span=120
At top of web	32	32	32
At ends of cantilever	40	40	40
At bottom of web	12	12	12

Table 5.5   Ratio of distortional warping stress (f_{dwr}) to longitudinal bending stress (f_{lbg}) at different points of the midspan section.

Position	Example 1 d=8.4 span=84	Example 2 d=9.6 span=96	Example 3 d=12 span=120
At top of web	30	30	30
At ends of cantilever	60	62	65
At bottom of web	70	72	76

Table 5.6 Ratio of transverse bending stress (f_{trb}) to $(f_{lbg} + f_{twr} + f_{dwr})$ at different points of midspan section.

Position	Example 1 $d = 8.4'$ Span=84' (%)	Example 2 $d=9.6'$ Span=96' (%)	Example 3 $d=12'$ Span=120' (%)
At top of web	111	111	111
At bottom of web	60	60	60

Table 5.7   Ratio of combined longitudinal stress by super-
imposing the results as obtained by SBT, method of
Kollbrunner, Hajdin and Heilig [10,7] and Beam on
elastic foundation analogy to FEM at midspan section.

Example	Position	Combined effect,ksf	FEM ksf	Excess than combined effect(%)
One	Top of loaded web	-5	-5.8	16
	Bottom of loaded web	9	8.6	-4
Two	Top of loaded web	-4.6	-5.22	13
	Bottom of web	8.3	8.0	-3
Three	Top of loaded web	-3.8	-5.11	34
	Bottom of loaded web	7.0	8.0	14

5.3 PARAMETER STUDY

In the design of structures generally, the decision on overall configuration is the most important, as for as effect on cost is concerned, and prolonged background work is usually necessary if a realistic assesment of the merits of alternative configurations is to be obtained. Therefore in designing a spine beam bridge deck for an anticipated traffic volume, where the site conditions and the economic of construction are known, decision can be made regarding the overall breadth of top flange, the lengths of individual spans and the depth of webs. It then remains to select the distance between webs and the web thickness. A parameter study could be performed to assist in this selection, but would require knowledge of the particular conditions of the design project.

A parameter study has been performed here, in which the overall width of section and the span are assumed known. Altogether, 81 geometrical configurations of rectangular, simply supported straight spine beam bridge decks have been analysed by the finite element method and the results are presented below. The structures are assumed to have diaphragms at the supports only, where there is full torsional and distortional restrant exists. The range of geometrical proportions has been selected with reference to a feature survey by Swann [18]. For all the spine beams analysed in this section, the span/depth ratio is 10. Spans of 84', 96' and 120' are used, the breadth/depth (b/d) ratio for the cell varies from 1.0 to 2.0 and the flange thickness/web
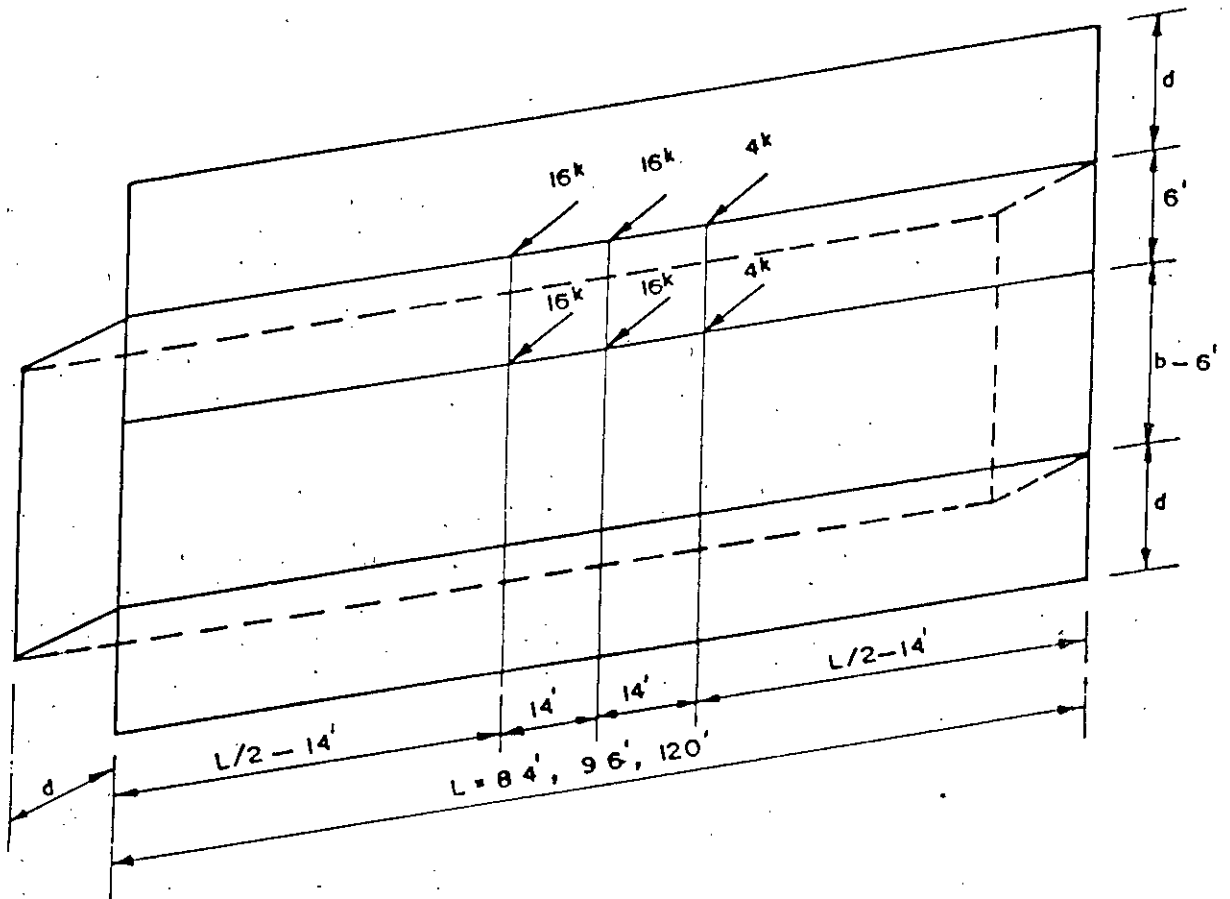
Fig. 5.10   Position of HS$_{20}$ loading on the bridge deck for parameter study.

depth ratio (h/d) varies from 0.1 to 0.2. The bottom flange thickness is taken equal to the top flange thickness in all cases.

In the analysis HS_{20} loading is considered as shown in Fig. 5.10. The finite element method was used for the analysis and the shear lag effect is taken into account by the analysis.

Curves of Figs. 5.11 to 5.13 show the variation of longitudinal bending stresses at the bottom of the loaded web at midspan due to the variation of breadth/depth (b/d) ratio of the cell to the thickness/depth (h/d) ratio. These curves show that the longitudinal bending stress at the bottom of the loaded web decreases with the increase of b/d ratio. Similarly the longitudinal bending stress at the bottom of loaded web decreases with the increase of h/d ratio. But the latter decreasing rate is faster than that of the earlier case.

Figs. 5.14 to 5.22 represent the variation of longitudinal bending stresses at the bottom of the loaded web at midspan due to the variation of web thickness to flange thickness. Individual curve is plotted for b/d ratio of 1 to 2 for span length of 84, 96 and 120 feet. From these curves, it is observed that the longitudinal bending stress decreases with the increase of web thickness. But this decreasing rate is not linear.
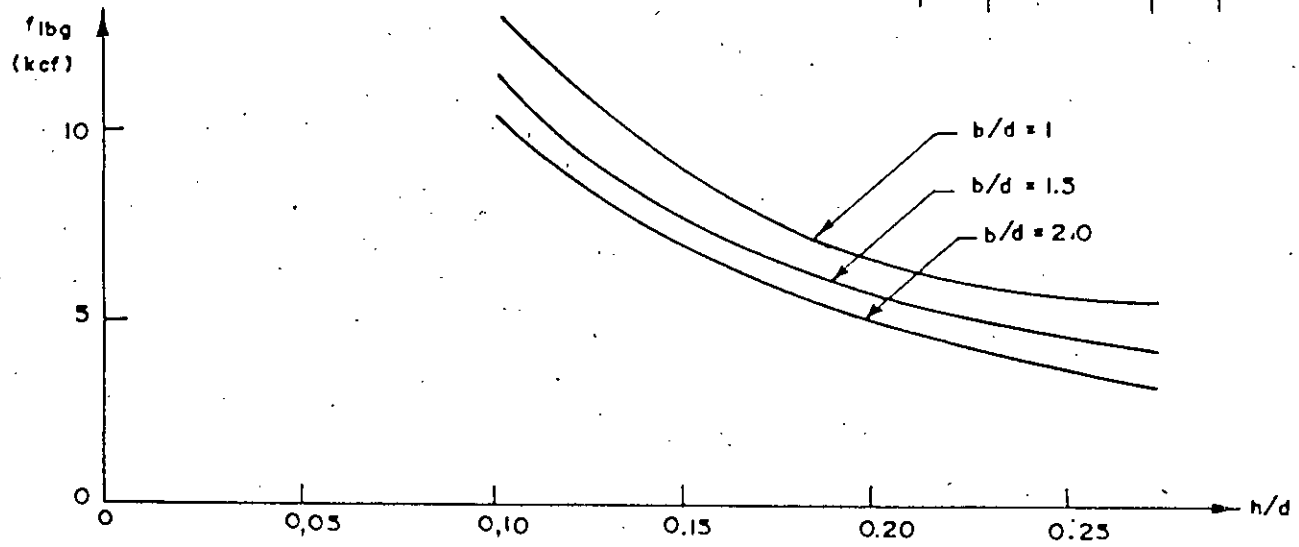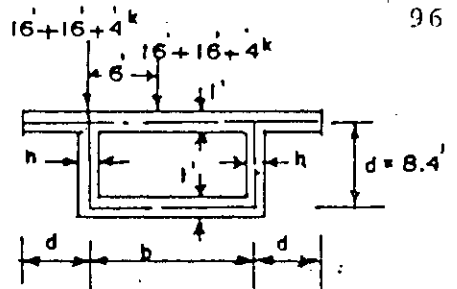
Fig. 5.11 Variation of longitudinal stress at bottom of
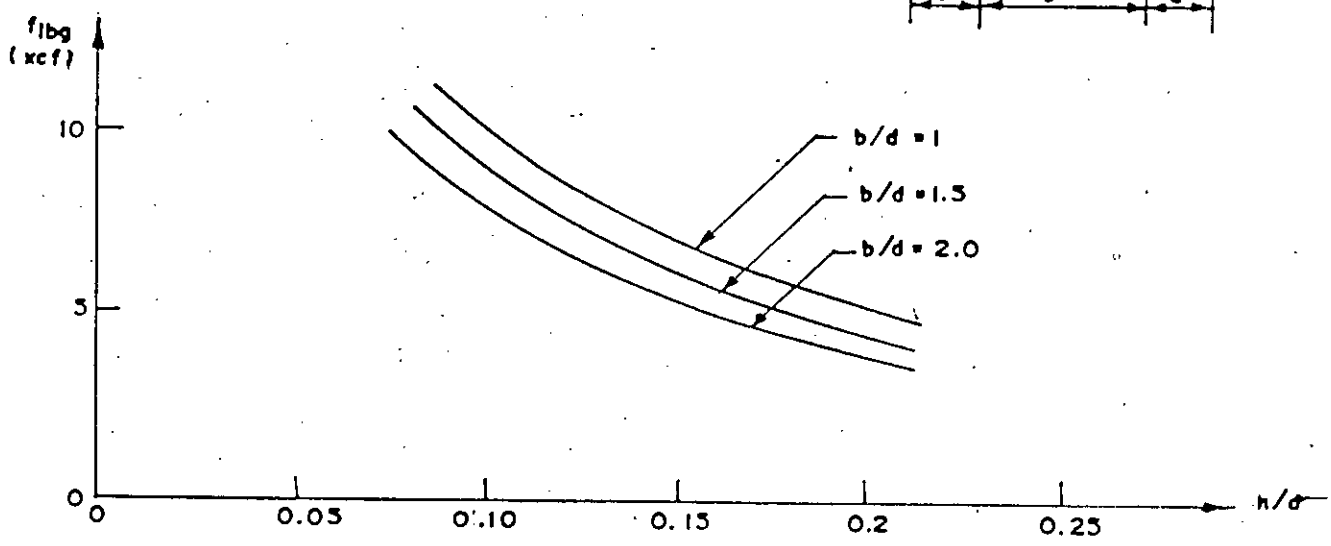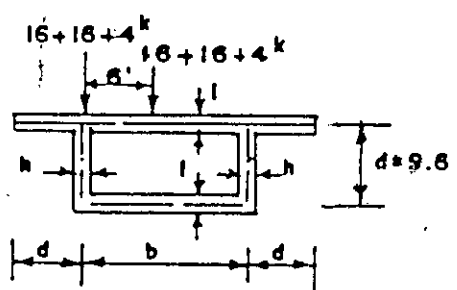loaded web for different b/d w.r.t. h/d, Span=84'.

Fig. 5.12 Variation of longitudinal stress at bottom of loaded
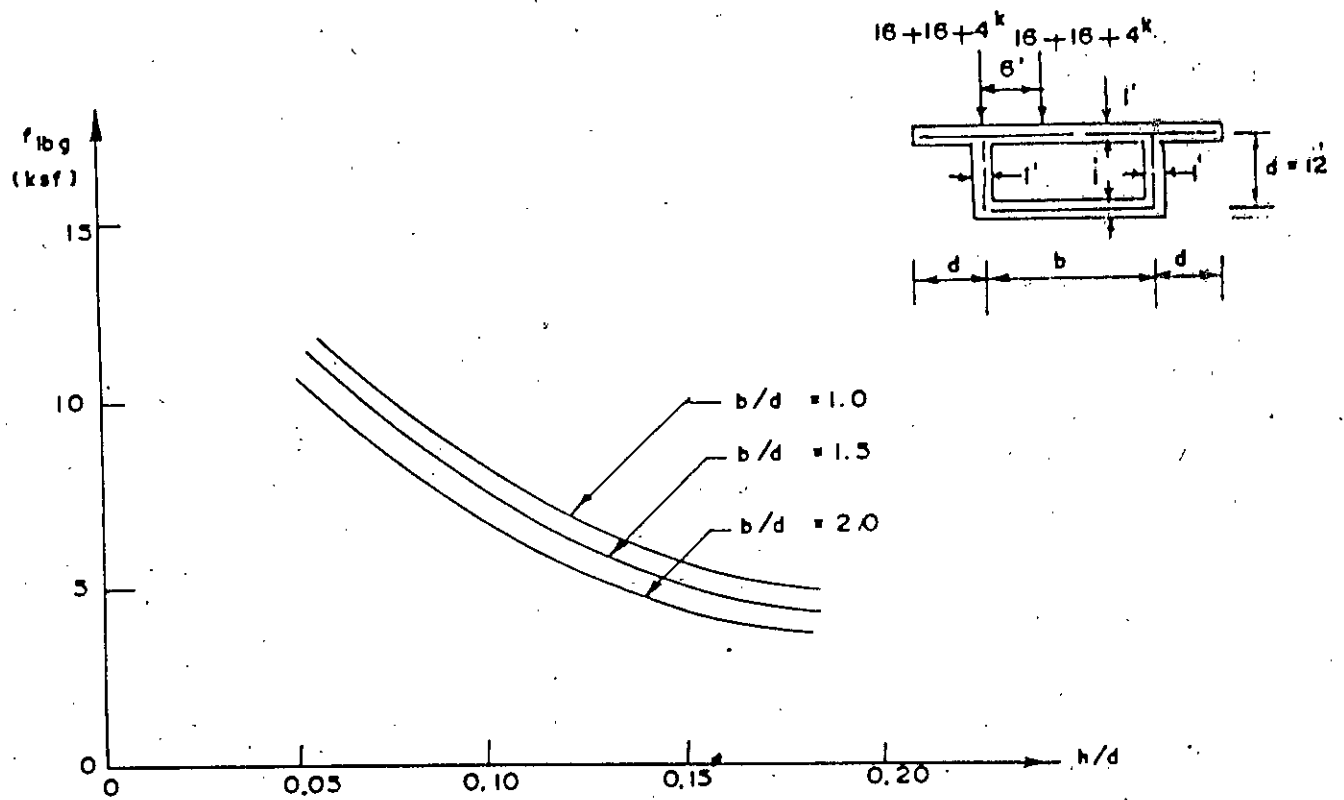web for different b/d w.r.t. h/d, Span = 96'.

Fig. 5.13 Variation of longitudinal bending stress at bottom
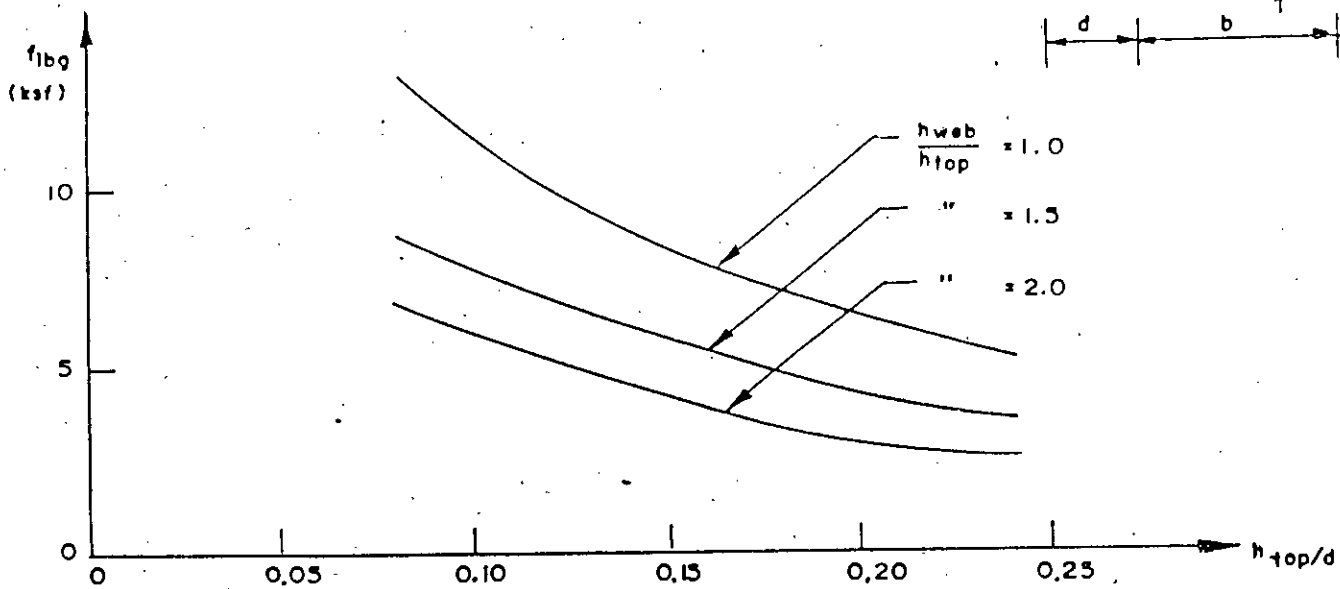of loaded web for different b/d w.r.t h/d.
Span = 120'.

Fig. 5.14   Variation of longitudinal bending stress at bottom
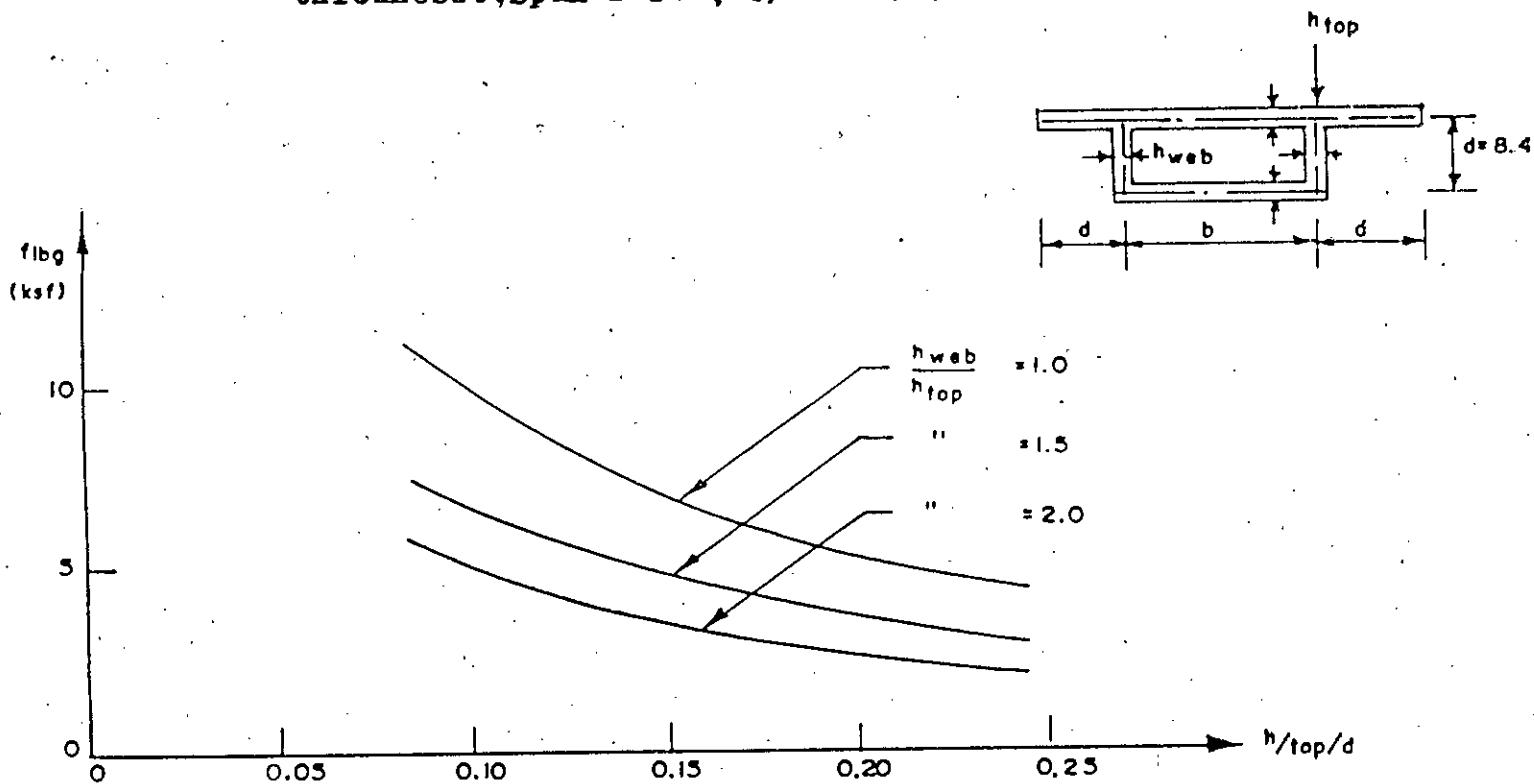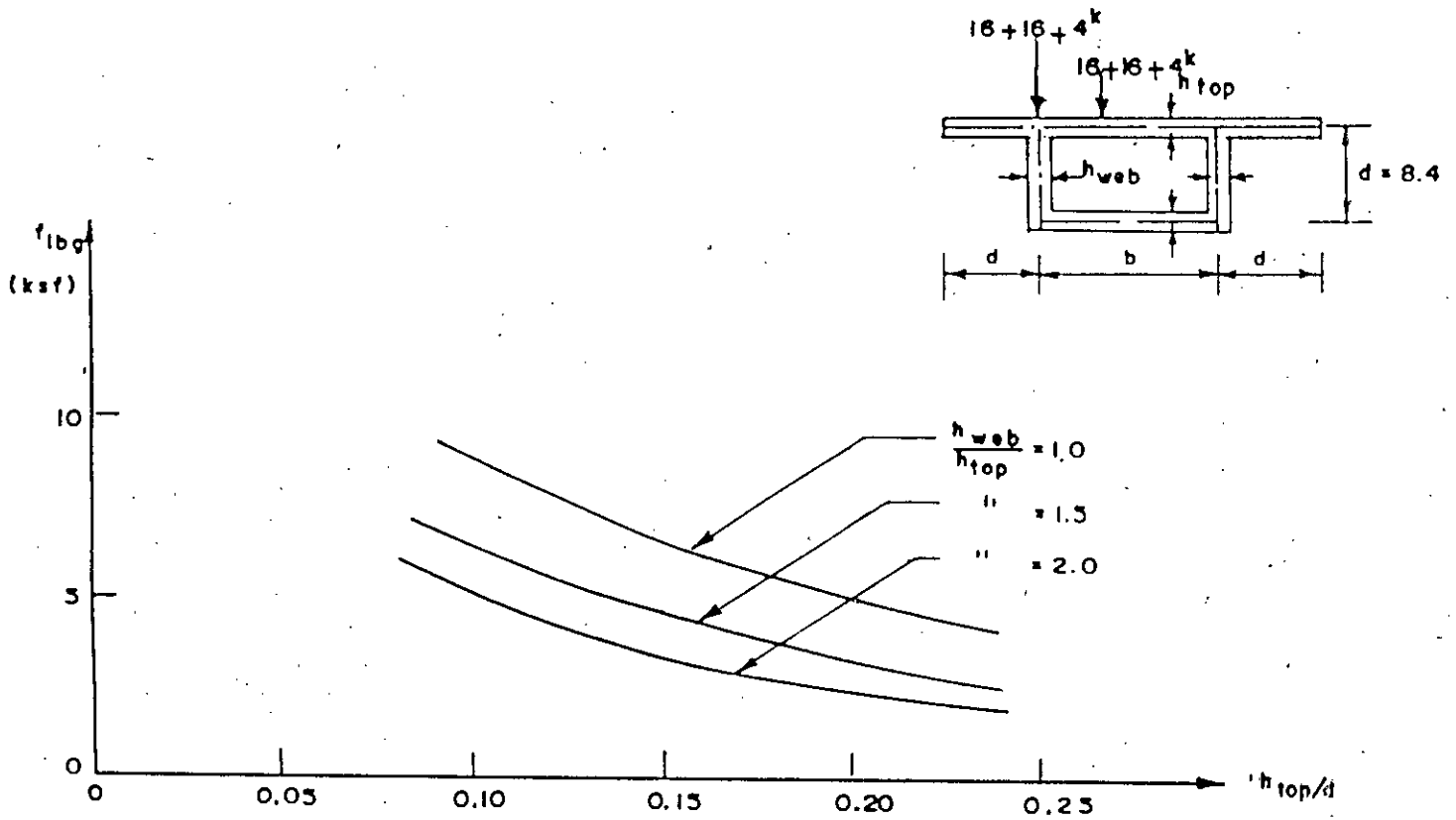of loaded web for different web thickness to flange
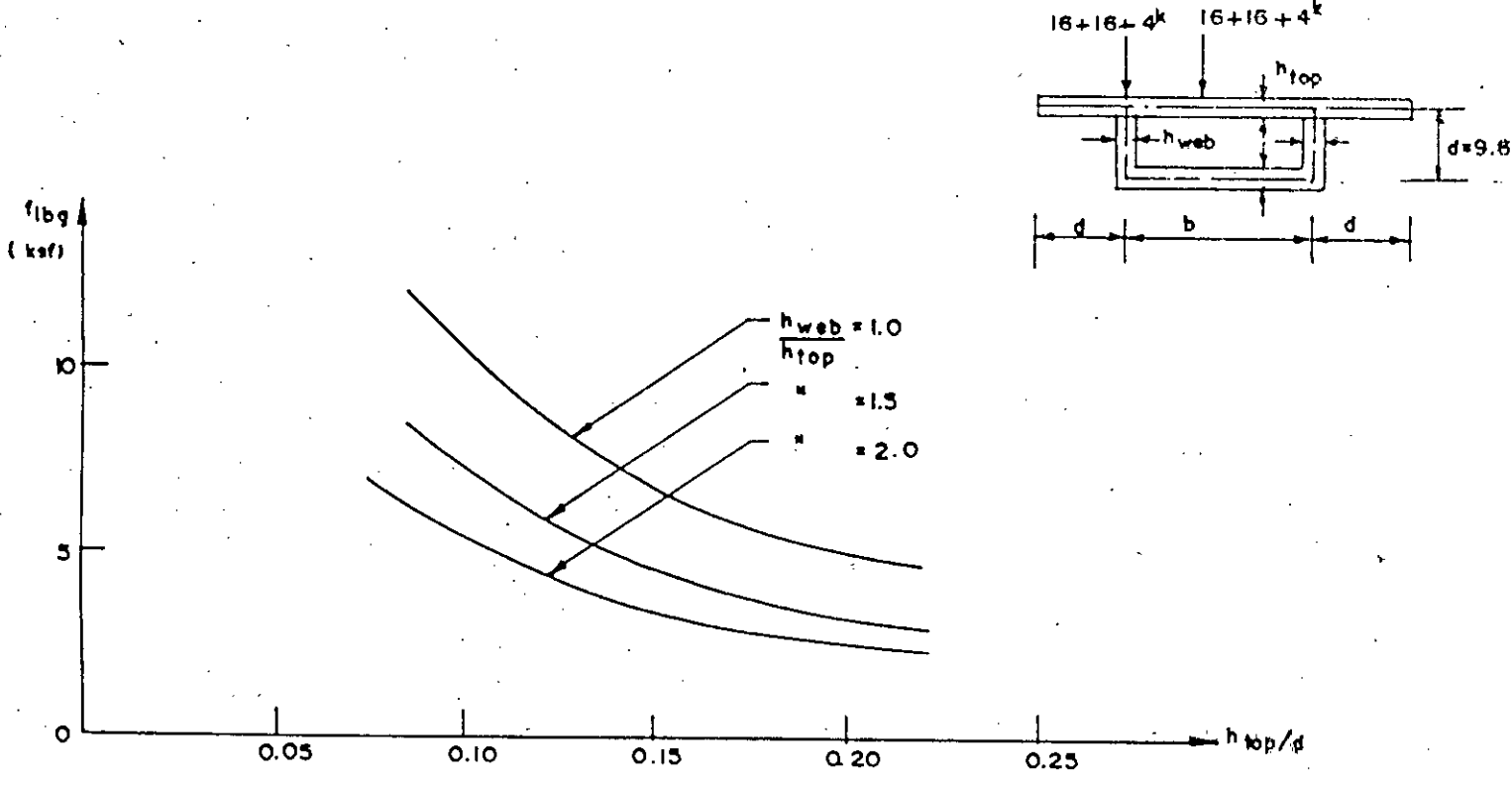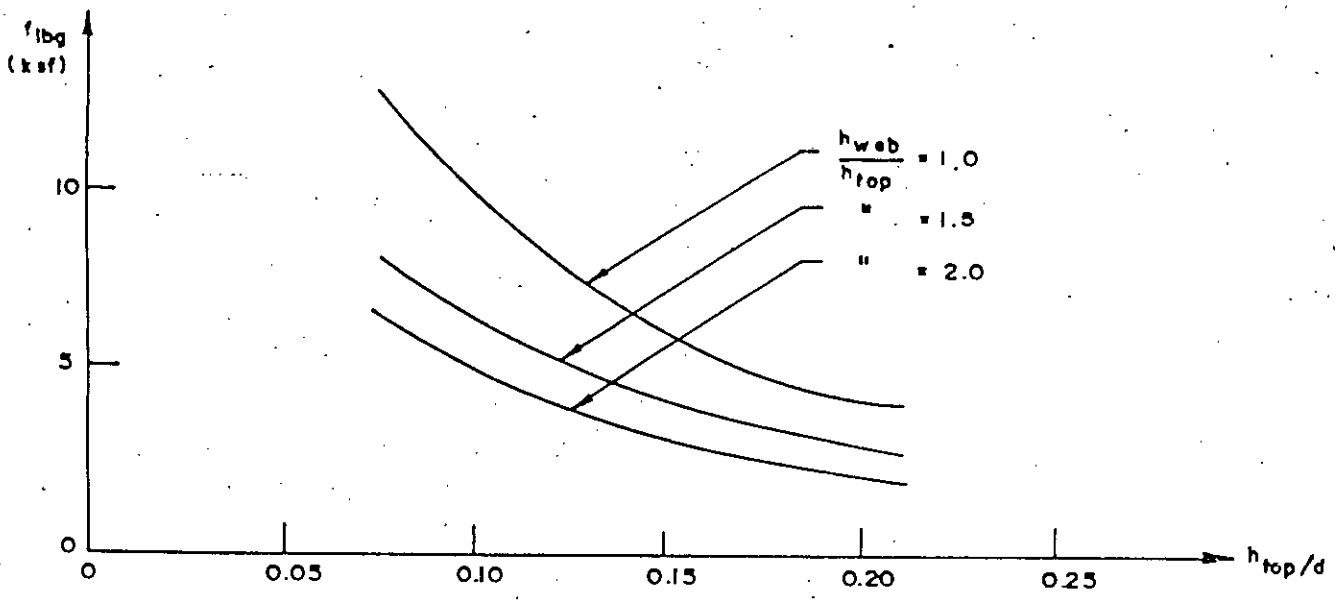thickness, Span = 84', b/d = 1.0.

Fig. 5.15   Variation of longitudinal bending stress at bottom of
loaded web for different web thickness to flange
thickness. Span = 84', b/d = 1.5.

Fig. 5.16   Variation of longitudinal bending stress at bottom
of loaded web for different web thickness to flange
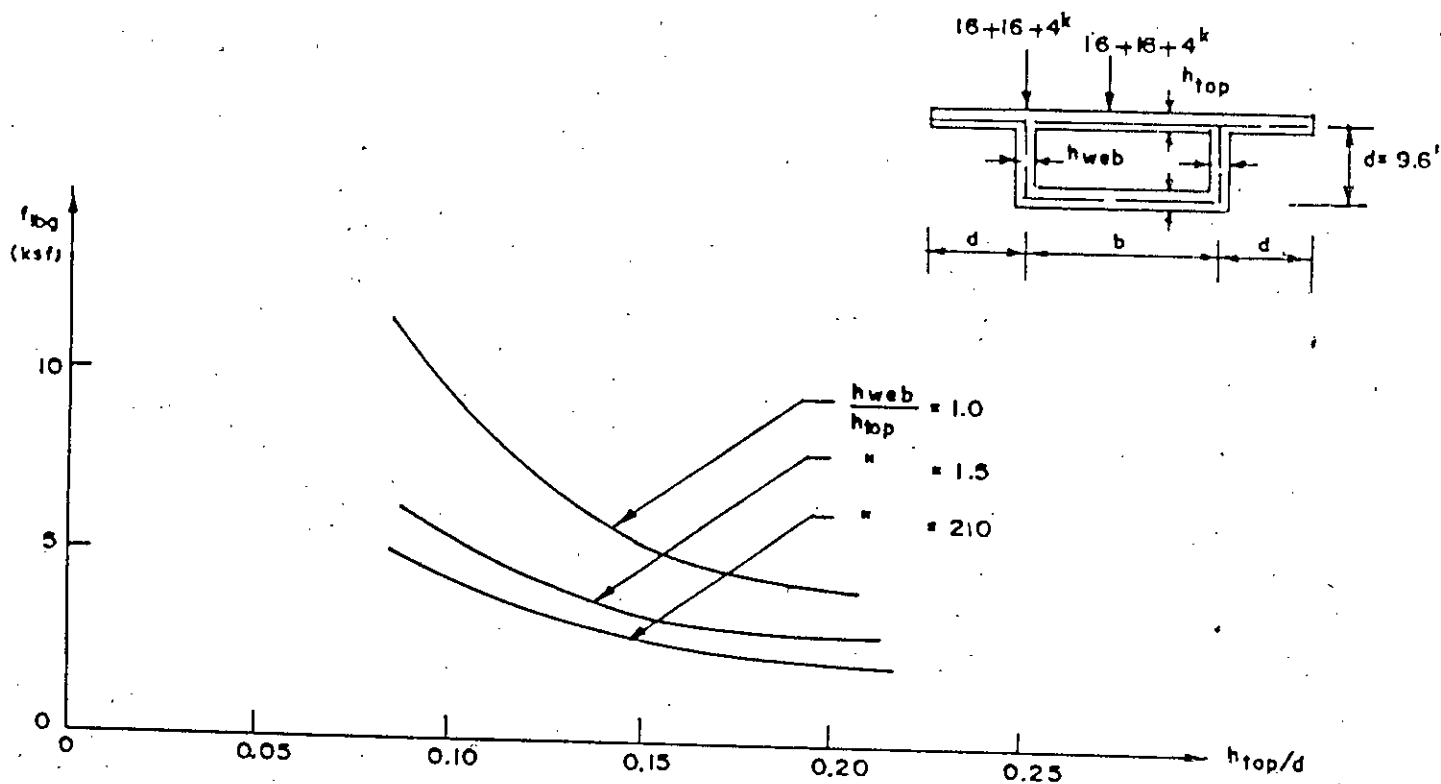thickness. Span = 84', b/d = 2.0.

Fig. 5.17 Variation of longitudinal bending stress at bottom of loaded web for different web thicknesses to flange thickness, span = 96', b/d = 1.0.
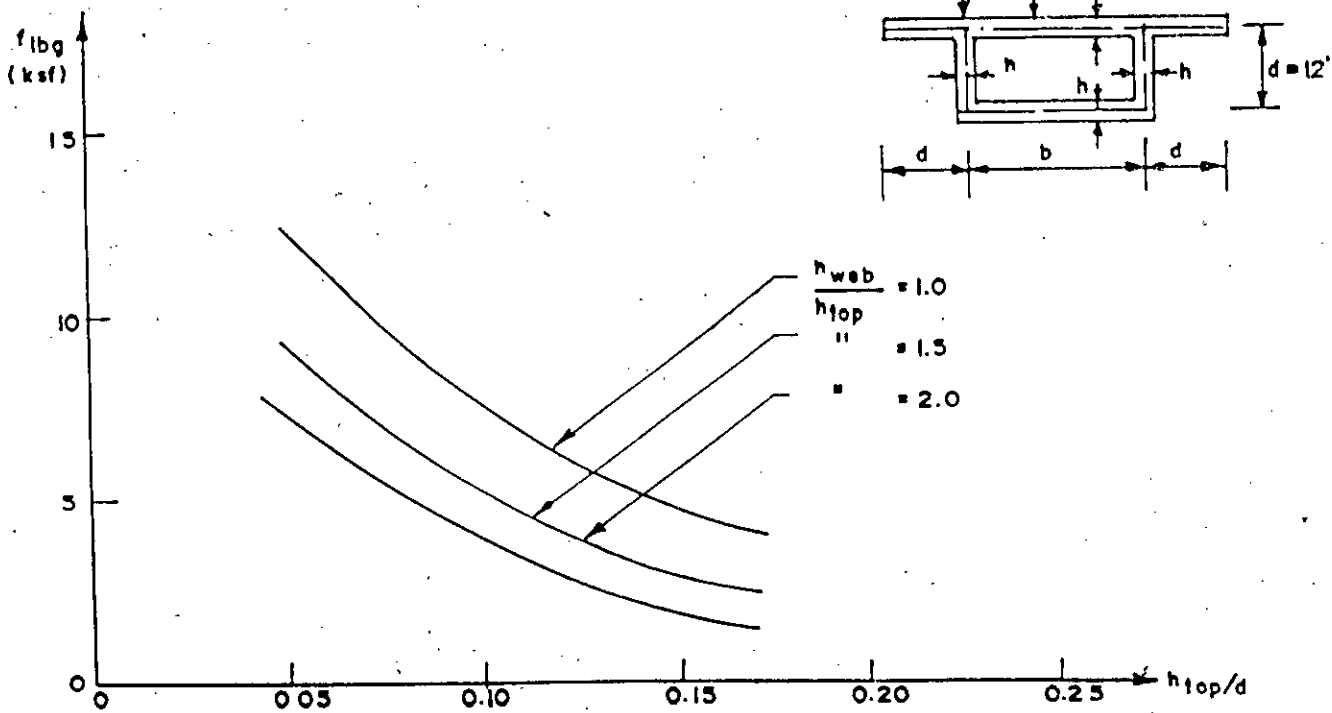
Fig. 5.18 Variation of longitudinal bending stress at bottom of loaded web for different web thicknesses to flange thickness, span = 96', b/d = 1.5.

Fig. 5.19   Variation of longitudinal bending stress at bottom
of loaded web for different web thicknesses
to flange thickness, span = 96', b/d = 2.0.

Fig. 5.20   Variation of longitudinal bending stress at bottom
of loaded web for different web thicknesses
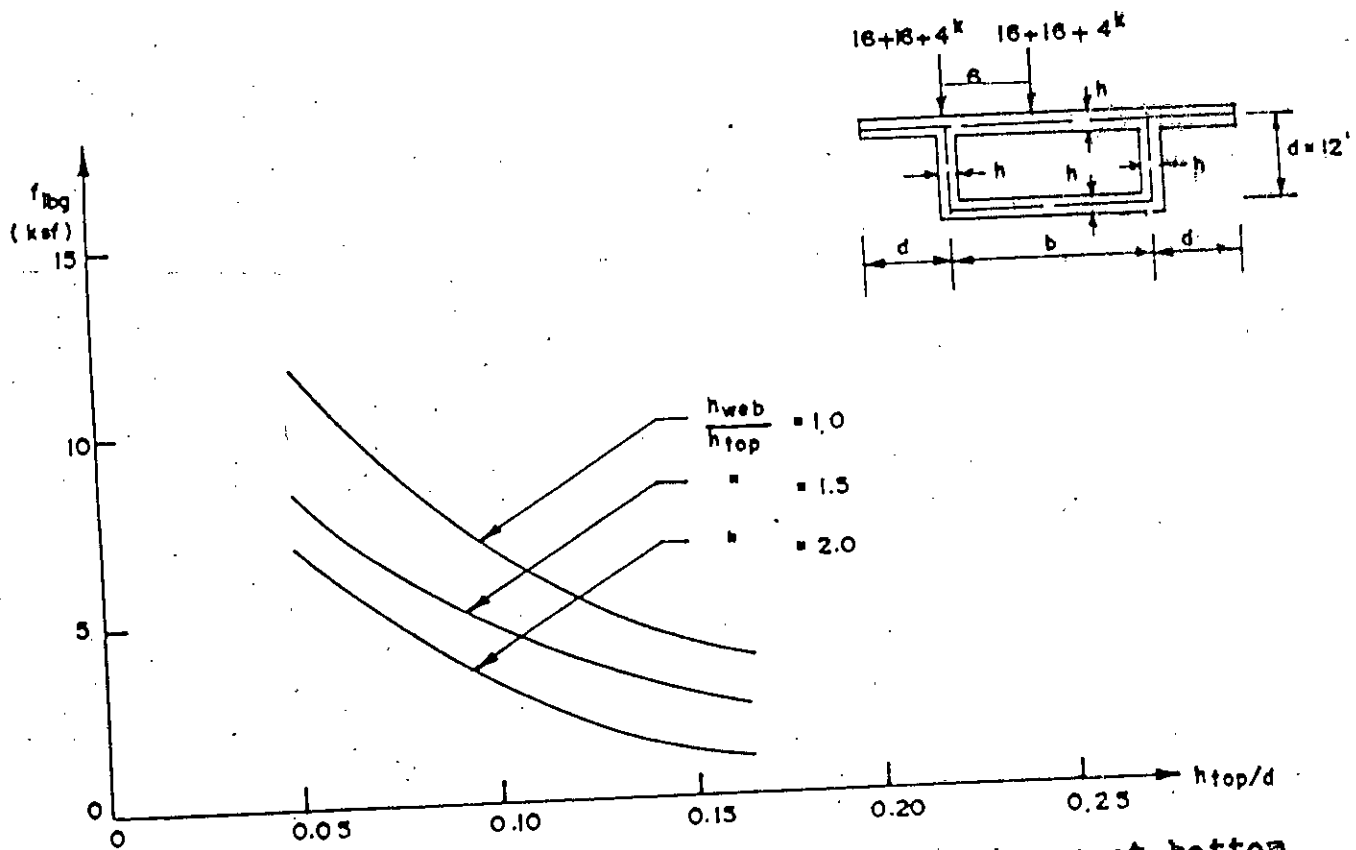to flange thickness, span = 120', b/d = 1.0.

Fig.5.21 Variation of longitudinal bending stress at bottom
of loaded web for different web thicknesses to flange
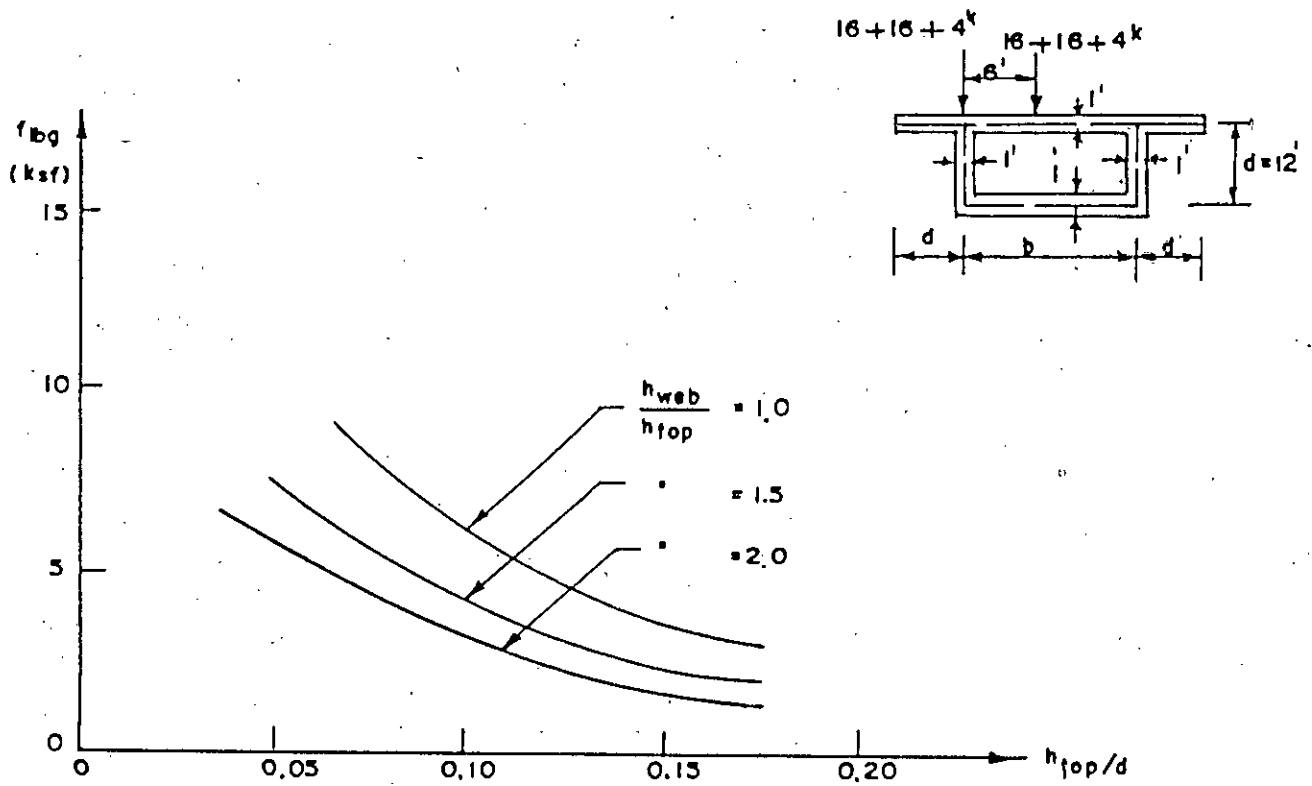thickness, span = 120', b/d = 1.5

Fig. 5.22 Variation of longitudinal bending stress at bottom
of loaded web for different web thickness to
flange thickness. Span 120', b/d = 2.0.

5.4 CONCLUSIONS

From the results of this study the following conclusions can be made for the spine beam bridge decks used in this analysis.

i) Of all the available methods for analysis of spine beam bridge decks, the finite element method is the most sophisticated one. A spine beam may be analysed by omitting the physical presence of diaphragms to reduce computational time. This may be achieved by modelling the diaphragms by restraining the translational displacements of joints at the section. From the analytical model study, it is found that more than 50% time can be saved by modelling the diaphragms in this way.

ii) From the comparative study of the analysis of spine beams, it is concluded that the simple beam theory does not give any information about the torsional and distortional warping and transverse bending due to eccentric loading which are quite significant in case of spine beams.

iii) The assumptions of the simple beam theory (Art. 3.2.1) are not valid in case of spine beams. But the results obtained by this theory are more conservative in case of symmetric loading.

iv) Longitudinal bending stress as obtained by Finite element method is higher at top and bottom of web than that obtained by simple beam theory. But this variation is due to shear lag

effect.

v) Variation of longitudinal bending stresses at midspan for the three spine beams of 84', 96' and 120' span as obtained by simple beam theory and finite element method (where the lower values for shorter span) are as follows:

a) For symmetrical loading variation is in the range of -4 to -8% at top of webs.

b) For eccentric loading variation is in the range of -20 to -35% at bottom and -29 to -49% at top of loaded web. For unloaded web, this variation is in the range of 34 to 119% at bottom and 35 to 77% at top of webs respectively.

vi) The method of Kollbrunner, Hajdin and Heilig [10,7] and the beam on elastic foundation analogy are used for the analysis of individual action of torsion and distortion and the combined effect of bending, torsion and distortion are obtained by super imposing the results as obtained by these methods with the simple beam theory. After superimposing the results the variation of longitudinal stresses with the finite element method are as follows:

a) The variation is in the range of -16 to 34% at top of loaded web at midspan, i.e the combiend stresses are 16 to 34% lower than that of obtained by the finite element method.

b) At bottom of loaded web, the variation is in the range of -4 to 14%.

vii) From the parameter study it is found that the longitudinal bending stress decreases with the increase of web thickness and the ratio is more than one.

5.5 RECOMMENDATION FOR FUTURE STUDIES

This study is used for linear analysis of spine beam bridge deck, it should be extended to the following in the future studies.

i) This study was concerned with simply supported single-cell spine beam bridge decks. It should be extended to studies of multi-cell, multi-span deck.

ii) Long span structures are of prestressed segmental construction, the future studies may be extended to the studies of these types of bridge decks.

iii) Analysis of spine beam brdge deck is recommended to be carried out upto the failure stage of the deck, which requires non-linear analysis of the deck.

iv) Analysis may be extended to the spine beam bridge deck having intermediate diaphragms.

REFERENCES

The American Association of State Highway and Transportation Official (AASHTO), 'Standard Specification for Hihgway Bridges' 13th Edition, 1983.

2. Irons B. and S. Ahmad 'Techniques of Finite Elements' Ellis Horwood Ltd., Publishers - Chichester.

3. B.I. Maisel and F. Roll, 'Technical Report' 'Methods of Analysis and Design of Concrete Box Beams with Side Cantilevers. Publication of Cement and Concrete Association, November 1974.

4. Cheung, Y.K. 'Finite Strip Analysis of Box-Girder' Second International Symposium on Concrete Bridge Design. ACI Publication, SP-26, 1971.

5. Cope, R.J. and Mills, J.H., 'Finite Element Analysis of Spine Beam and Cellular Bridges', Bridge Programme Review Symposium Proc. P.T.R.C. Ltd., London, 1971.

6. Goldberg, J.E, and Leve, H.L., 'Theory of Prismatic Folded Plates', International Association for Bridge and Structural Engineering, Vol. 17, Zurich, 1957.

7. Heilig, R., 'A Contribution to the Theory of Box-girders of Arbitrary Cross-sectional Shape. Cement and Concrete Association, 1971, Translation No. 145.

8. Knittel, G., 'The Analysis of Thin-walled Box Girders of Constant Symmetrical Cross-section', September 1965. Available as Cement and Concrete Association Library Translation.

9. Kollbrunner, C.F. and Basler, K., 'Sectorial Quantities and Stresses in Open thin-walled Cross Sections. Mitteilungen dev Technischen Kommission, Heft 28, Schweizer Stahlban-Vereinigung, Zurich. January 1964.

10. Kollbrunner, C.F. and Hajdin, N., 'Warping Torsion of Thin-walled Beams of Closed Section. Mitteilungen dev Technischen Kommission, Heft 32, 1966, Schweizer Stahlban Vereinigung, Zurich. (3).

11. Kupfer, H. 'Box Beam with Elastically Stiffend Cross-section under line and point loads. Stahlbetonbau, Berichteans Forschung and Praxis. Ed. Knittel, G. and Kupfer, H.W. Ernst U, Sohn, Berlin, 1967, pp. 251-263.

12. Melosh, R.J. Basis for Derivation of matrices for Direct Stiffness Method' A.I.A.A.J.I, 1963.

13. Murtuza, M.A. Analytical and Experimental Investigation of Concrete Spine Beam Bridge Deck. Ph.D. thesis, University of Liverpool, January 1982.

14. Richmond, B. 'Twisting of Thin Walled Box Girders. Proceedings of Institution of Civil Engineers, April 1966.

15. Reissner, E. Analysis of Shear lag in Box beams by the Principle of minimum potential energy. Quarterly of Applied Mathematics, October 1946. pp. 268-278.

16. Sawko, F. and Cope, R.J. Analysis of Spine Beam Bridges, Civil Engineering and Public Works Riview, 65, 1970.

17. Scordelis, A.C. A matrix Formulation of Folded Plate Equations, Proceedings of ASCE, Vol. 86, No. ST 10, Oct. 1960.

18. Swann, R.A. A Feature Survey of Concrete Box Spine-Beam Bridges. Cement and Concrete Association, June 1972, Technical Report 42, 469.

19. Suidan, M. and Schnobrich, W.C. Finite Element Analysis of Reinforced Concrete, Journal of the Structural Division, ASCE, ST 10, 1973.

20. Timoshenko, S. and Krieger, S.W. 'Theory of Plates and Shells' 2nd Edition, Mc Graw Hill Co.

21. Tung, H.H.D. 'Torsion analysis of Single Thin Walled Trapezoidal Concrete Box Girder Bridges', ACI, Special Publication, SP-23, 1969.

22. Vlasov, V.Z. 'Thin Walled Elastic Beams', U.S. Department of Commerce, P.S.T. Catalogue No. 428, 1959.

23. Wright, R.N. Abdel - Samad, S.R and Robinson, A.R. 'Beam on Elastic Foundation Analogy for Analysis of Box Girders' Journal of the Structural Division, A.S.C.E. July 1968.

24. Zienkienicz, O.C., 'The Finite Element Method' Mc Graw Hill Book Company, 3rd Edition, 1977.

APPENDIX - A

EXAMPLES OF ANALYSIS

BY

SIMPLE BEAM THEORY AND ST. VENANT TORSION THEORY

METHOD OF KOLLBRUNNER, HAJDIN AND HELLIG

AND

BEAM ON ELASTIC FOUNDATION ANALOGY

EXAMPLE ONE

A simply supported single cell spine beam with diaphragms only at the ends is taken. The span (L) is 84 ft. and H_{20}-S_{16} loading is considered at midspan. Fig. A.1 shows the geometry and loading and Fig. A.2 gives the bending moment, shear force and torsional moment diagrams due to live load. For simplicity, thickness of top flange, bottom flange and webs are taken to be the same. The analysis would be restricted to live load effects only.

To calculate the stress distribution, the following section properties are required. For bending:

Depth of centroid above mid-line of bottom flange

$$y = \frac{7.4 \times 4.2 \times 2 + 33.6 \times 8.4}{7.4 \times 2 + 33.6 + 17.8}$$

$$= 5.2 \text{ ft.}$$

$$I_x = \frac{2 \times 7.4^3}{12} + 2 \times 7.4(5.2-4.2)^2 + \frac{33.6}{12} + 33.6 \times (8.4-5.2)^2$$

$$+ \frac{17.8}{12} + 17.8 \times 5.2^2$$

$$= 912 \text{ ft}^4$$

From Figs. 3.2 and 3.4, first moments of area of the partial half cross-section about the centroidal x-axis are as follows:

At top of web (B), just to right of mid-line of web.

$(Ay)_{1/2} = - 8.4 \times 1 \times 3.2 = -26.88$ ft^3

At top of web (B), just to let of mid-line of web,

$(Ay)_{1/2} = -8.4 \times 1 \times 3.2 = - 26.88$ ft^3

At level of centroid, (y=0)

$(Ay)_{1/2} = - (2 \times 26.88 + 2.7^2/2) = -57.4$ ft^3

At mid-depth of web (y=0.7 ft)

$(Ay)_{1/2} = - 57.4 + 1^2/2 = - 56.9$ ft^3

At bottom of web (D), (y=5.2')

$(Ay)_{1/2} = - 56.9 + 5.2^2/2 = -43.38$ ft^3

For St. Venant torsion

$A_{enc} = 8.4 \times 16.8 = 141.12$ ft^2

By equation 3.5

$$C_{svt} = \frac{4 \times 141.12^2}{16.8/1 + 16.8/1 + 2 \times 8.4/1} = 1580.54 \text{ ft}^4$$

Bending stress due to live load.
At midspan, $M_x = 1232$ k-ft, $M_v = 0$
By equation 3.1, at midspan of top flange

$$f_{1bg} = - \frac{1232 \times 3.2}{912} = - 4.32 \text{ ksf}$$

At mid-line of bttom flange,

$$f_{1bg} = \frac{1232 \times 5.2}{912} = 7.02 \text{ skf}$$

At support (z=0, V_v = 40 kips)

By equation 3.2, at top of web, just to right of mid-line of web,

$V_{lbg} = -40 \times (-26.88)/(912 \times 1) = 1.18$ ksf

= magnitude of V_{lbg} at top of web just to left of mid-line of web.

At top of web,

$V_{lbg} = -40 \times (-26.88 \times 2)/(912 \times 1) = 2.36$ ksf

At level of centroid,

$V_{lbg} = -40 \times (-57.4)/(912 \times 1) = 2.52$ ksf

This is the maximum bending shear stress in the web.

At mid-depth of web

$V_{lbg} = -40 \times (-56.9)/(912 \times 1) = 2.5$ ksf

At bottom of web

$V_{lbg} = -40 \times (-43.38)/(912 \times 1) = 1.9$ ksf

= magnitude of V_{lbg} at bottom of web just to right of mid-line of web.

Torsional stresses due to live load.

At support (z=0), $T_{svt} = 552$ k'

By equation 3.3

$V_{svt} = 552/(2 \times 141.12) = 1.96$ ksf

= magnitude of V_{svt} in web and flange.

The bending and torsional stresses calculated above are shown in the diagrams of Fig. A.3, which gives both the sign and the direction of action of stresses.

Torsional warping analysis by the methods of Kollbrunner, Hajdin and Heilig:

Position of shear centre,
By equation B.2

$$I_v = 1 \times 33.6^3/12 + 1 \times 17.8^3/12 + 7.4 \times 2 \times 1^3/12 + 7.4 \times 8.4^2 \times 2$$

$$= 4677 \text{ ft}^4$$

$$K_{13} = (1/4) \times 16.8 \times 1 \times 1 \times (1 \times 16.8/3 + 3 \times 8.4 \times 1)$$

$$= 129.36 \text{ ft}^5$$

$$K_{14} = 16.8 \times 8.4 \times 1((1^2/6 - 1^2/4)$$

$$= -11.76 \text{ ft}^5$$

$$K_{15} = 1 \times 1 \times 1/2 \times (16.8^2/6 + 8.4^2)$$

$$= 56.8 \text{ ft}^5$$

$$K_{16} = 8.4 \times 1 \times 1 \times 1(8.4 + 16.8)$$

$$= 211.68 \text{ ft}^5$$

$$K_{17} = 16.8 \times 1 \times (1+1) + 2 \times 8.4 \times 1 \times 1$$

$$= 50.4 \text{ ft}^3$$

$$\text{Therefore } d_{shc} = \frac{16.8^2 \times 8.4}{4677}((129.36 - 11.76 + 58.8 + 211.68)/50.4)$$

$$= 3.9 \text{ ft.}$$

Evaluation of sectorial co-ordinate in torsional warping (W_{twr}):

$$C_{svt} = 1580.54 \text{ ft}^4$$

$$A_{enc} = 141.12 \text{ ft}^4$$

and so $C_{svt}/(2 A_{enc}) = 1580.54/(2 \times 141.12)$

$$= 5.6 \text{ ft}^2$$

Hence in equation B.1

In top flange, (Points A,B,C)

$$a_8 = dsc = 3.9 \text{ ft}$$

In web, (points B,D), $a_s = b/2 = 8.4$ ft

In bottom slab, (points D,E), $a_s = d-dshc = 4.5$ ft

At A, $S_{per} = 0$, from which $W_{twr} = 0$

At B, $W_{twr} = $ $(3.9-5,.6/1)$ ds_{per}

$= -1.7 \times 8.4 = -14.28$ ft²

At C, $W_{twr} = -14.28$ a_s ds_{per}

$= -14.28+3.9 \times 8.4 = 18.48$ ft²

At D, $W_{twr} = -14.28+$ $(8.4-5.6/1)$ ds_{per}

$= -14.28+2.8 \times 8.4$

$= 9.24$ ft²

At E, $W_{twr} = 9.24 + (4.5-5.6/1)ds_{per}$

$= 9.24+8.4 \times (-1.1) = 0$

Evaluation of Torsional warping moment of inertia of cross-section (C_{twr}):

Simpson's integration method is used to evaluate the integral in equation B.3.

$$C_{twr} = \frac{16.8 \times 1}{6}(2 \times 14.28^2)+ \frac{2 \times 8.4 \times 1}{6}(14.28^2+4 \times ((-14.28+18.48)/2)^2$$
$$+ 18.48^2)+ \frac{2 \times 8.4 \times 1}{6}(14.28^2+4((-14.28+9.24)/2)^2+9.24^2)$$
$$+ \frac{16.8 \times 1}{6}(2 \times 9.24^2)$$

$= 4078$ ft⁶

Evaluation of Torsional Warping Bimoment (B_{twr}):

In equation B.10

Central torsional moment of inertia of cross-section (C_{cen}):

$C_{cen} = 33.6 \times 1 \times 3.9^2 + 2 \times 8.4 \times 8.4^2 + 16.8 \times 1 \times 4.5^2$

$\quad = 2036.66 \text{ ft}^4.$

In equation B.8

$$K_{19} = \frac{C_{cen}}{C_{cen} - C_{svt}} = \frac{2036.66}{2036.66 - 1580.54} = 4.46$$

In equation B.9

$C_{twr} = 4.46 \times 4078 = 18188 \text{ ft}^6$

In equation B.7, with Poisson's ratio taken as 0.18

$G/E = 1/(2(1+.18)) = 0.424$

Hence $K_{18} = (0.424 \times 1580.54/18188)^{1/2} = 0.192/\text{ft}$

In equation B.4, at midspan, Torsional warping bimoment

$$B_{twr} = \frac{331.2}{0.192 \times 4.46} \times \sinh(0.192 \times 42)/(\cosh(.192 \times 42))$$

$\quad = 386 \text{ k-ft}^2$

Evaluation of torsional warping stresses (f_{twr}) at midspan:

In equation B.11

$f_{twr} = 386/4078 \times W_{twr} = 0.0948 \ W_{twr} \text{ ksf}$

At A, (Fig. A.4), $f_{twr} = 0$

At B, $f_{twr} = -1.35 \text{ ksf}$

At C, $f_{twr} = +1.75 \text{ ksf}$

At D, $f_{twr} = .880 \text{ ksf}$

Fugure A.5 shows the torsional warping stress.

Discussion of calculated stresses:

The torsional warping stresses (f_{twr}) of Fig. A.5 are compared with the longitudinal bending stresses (f_{lbg}) of Fig. A.3a in magnitude.

At top of web, at midspan,

f_{twr}/f_{lbg} = .67/4.32 =0.32, i.e. 32%

At ends of cantilevers, at midspan,

f_{twr}/f_{lbg} = 1.75/4.32 =0.4, i.e. 40%

At bottom of web, at midspan,

f_{twr}/f_{lbg} = 0.88/7.02 = .12 i.e 12%

The above increases in longitudinal stress (where f_{lbg} and f_{twr} are additive) will be larger when the effect of distortional warping is considered.

Distortional analysis by the beam on elastic foundation analogy:

Evaluation of distortional warping coordinate (W_{dwr}):

By equations C.2, C.3 & C.4

$$K_6 = \frac{16.8 \times 1}{8.4 \times 1} \left(\frac{16.8+2 \times 8.4}{16.8} \right)^3 = 16$$

$$K_7 = \frac{16.8 \times 1}{8.4 \times 1} = 2$$

$$K_{25} = \frac{3+16}{3+2} = 3.8$$

From Fig. B.1, at top of web,

W_{dwr} = (16.8x8.4)/(4(1+3.8)) = 7.35 ft²

At bottom of web, W_{dwr} = -7.35x3.8 = -27.93 ft²

At end of cantilever,

W_{dwr} = (16.8+2x8.4)x7.35/16.8=14.7 ft²

The above values of W_{dwr} are shown in Fig. A.6

Evaluation of distortional warping moment of inertia of cross-section (C_{dwr}):

By equation C.1 and C.5

$K_4 = (3+2(16+2)+16x2)/(6+16+2)=2.96$

$C_{dwr} = 16.8^2 x 8.4^3 x 1 x 2.96/48 = 10315.9$ ft^6

Evaluation of the frame stiffness (EI_{fra}):

By equation C.6-C.10, with Poisson's ratio taken as 0.18

$I_{top} = 1^3/(12(1-0.18^2)) = .0861$ ft^4/ft

$I_{bot} = 0.0861$ ft^4/ft

$I_{web} = 0.0861$ ft^4/ft

$K_{26} = 1+(2x16.8/8.4+3x2)/(2+6/2) = 3$

$I_{tra} = 24x0.0861/(3x8.4)=0.082$ ft^2

Evaluation of distortional warping bimoment (B_{dwr}):

By equation C.12 and C.13

$K_{27} = (0.082/(4x10315.9))^{1/4} = 0.0375$/ft

B_{dwr} at midspan:

$72x16.8/(16x.0375)x(Sinh(.0375x84)+Sin(.0375x84))/(Cosh(.0375x84)+Cos(.0375x84))$
$= 1859$ ksf

Evaluation of distortional warping stresses (f_{dwr}) at midspan

In equation C.11.

$f_{dwr} = B_{dwr} W_{dwr}/C_{dwr}$

$= 1859/10315.9 W_{dwr} = 0.18 W_{dwr}$ ksf

At A, (Fig. C.1), $f_{dwr} = 0$

At B, $f_{dwr} = 0.18x(-7.35) = -1.32$ ksf

At C, $f_{dwr} = 0.18x(-14.7) = - 2.65$ ksf

At D, $f_{dwr} = 0.18(-27.93) = -5.0$ ksf

At E , $f_{dwr} = 0$

The stresses are shown in Fig. A.7

Evaluation of transverse bending stresses (f_{trb}) at midspan:

In equation C.17,

$$K_{30} = \frac{3+16.8/8.4}{3+16.8/8.4} = 1$$

In equation C.18

EI_{fra} B_{trb} = (72x16.8x.0375)/8x(Sinh(.0375x84)

$\qquad$ - Sin(.0375x84))/(Cosh(0.0375x84)+Cos(.0375x84))

$\qquad$ = 5.18 kips

In equation C.15, at top of web

M_{trb}, B = 5.18/(2(1+1)) = 1.3 k-ft/ft

In equation C.16, at bottom fof web,

M_{trb}, D = -1.3 k-ft/ft

In equation C.14, at top of web, in top flange,

Max. f_{trb} = $6xM_{trb}/h^2$
$\qquad$ = $6x1.3/1^2$ = 7.8 ksf

At bottom of web, f_{trb} = 7.8 ksf

These stresses are shown in Fig. A.8

Discussion of Calculated Stresses:

The magnitudes of distortional warping stresses (f_{dwr}), torsional warping stresses (f_{twr}) are compared to longitudinal bending stresses (f_{lbg}).

At top of web, at midspan,

(f_{twr}+f_{dwr})/f_{lbg} = (1.35+1.32)/4.32 = 0.6 i.e. 60%

f_{dwr}/f_{lbg} = 1.32/4.32 = 0.3, i.e: 30%

At ends of cantilevers, at mid-span

(f_{twr}+f_{dwr})/f_{lbg} = (1.75-2.65)/4.32 = 0.2, i.e. 20%

$f_{dwr}/f_{lbg} = 2.63/4.32 = 0.6,$ i.e 60%

At bottom of web, at mid-span

$(f_{twr}+f_{dwr})/f_{lbg} = (0.88+5)/7 = 0.84,$ 84%

$f_{dwr}/f_{lbg} = 5/7 = 0.7,$ i.e, 70%

The above increases in longitudinal stress (where f_{lbg}, f_{twr} and f_{dwr} are additive) are significant in design, even if the torsional warping stress (f_{twr}) is neglected.

In addition:

In the top flange, at the web,

$f_{trb}/(f_{lbg}+f_{twr}+f_{dwr}) = 7.8/(4.32+1.35+1.32)$

$$= 1.11, \text{ i.e } 111\%$$

In the bottom flange, at the web,

$f_{trb}/(f_{lbg}+f_{twr}++f_{dwr}) = 7.8/(7+0.88+5) = 0.6,$ i.e, 60%

Thus the transverse bending stresses are of the same order as the resultant longitudinal stresses at midspan, and are therefore significant in design. It is important to consider Poisson's ratio effects in this situation.
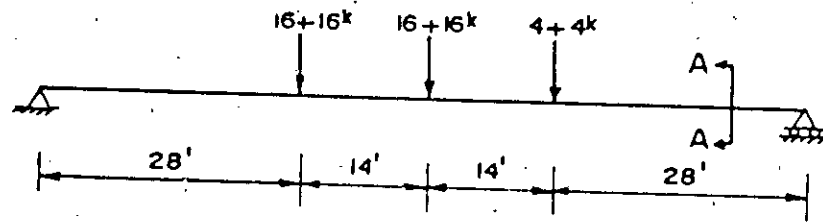
(a) Elevation of Beam
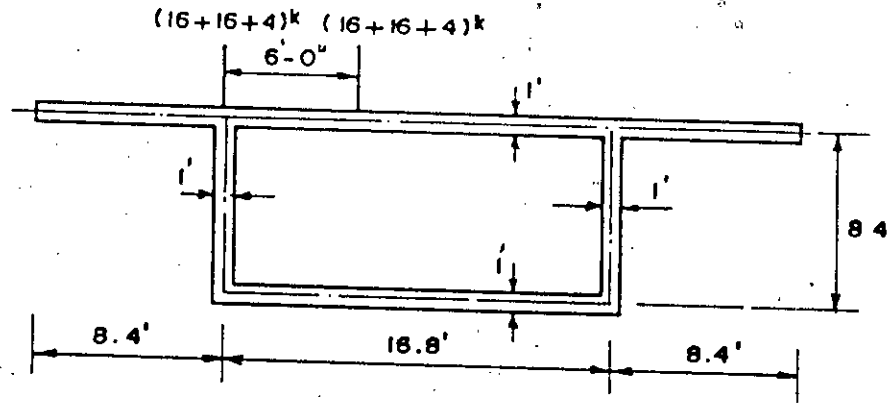
Section A-A

Fig. A.1 Loading and geometry.
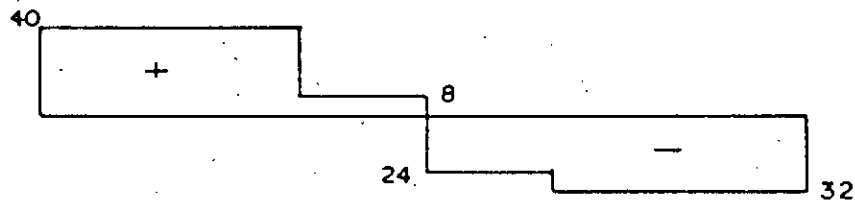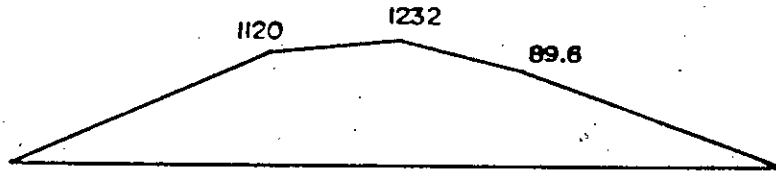
(a) Shear force diagram (kips).

(b) Bending moment diagram (k-ft).
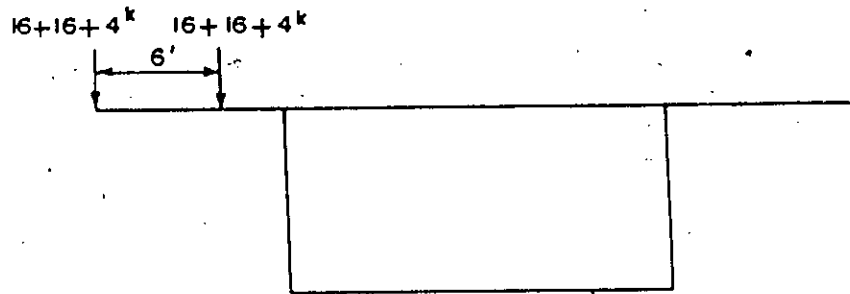
Position of loading for torsional analysis.
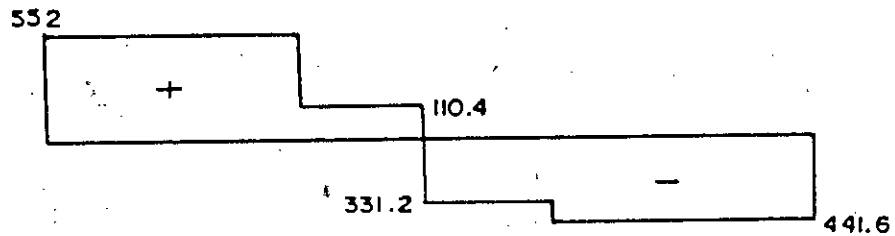
(c) Torsional mom nt diagram (k-ft).

Fig. A.2   Shear force, bending and torsional
moment diagram due to live load.
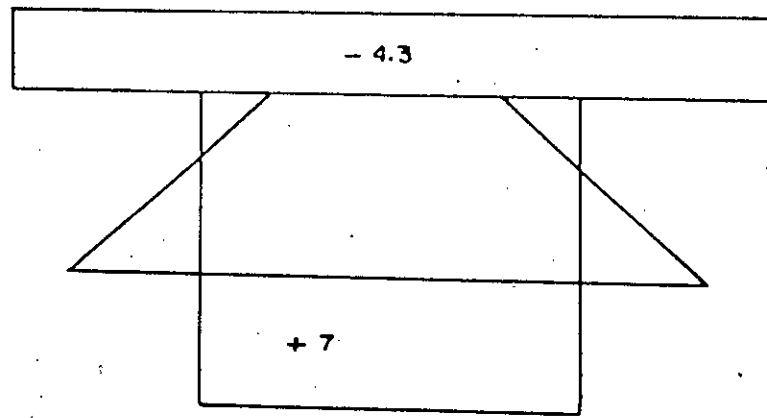
(a) Longitudinal bending stress at midspan
     section (ksf).
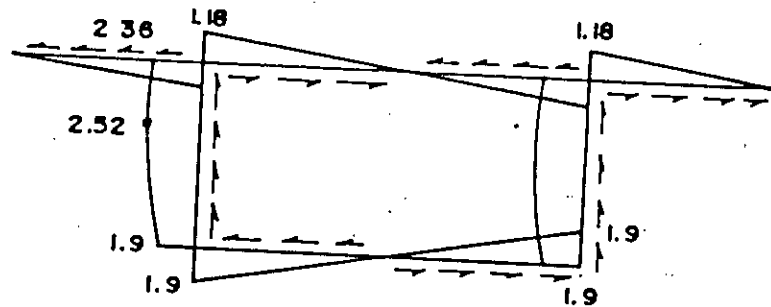
(b) Bending shear stress (V_{lbg}) on negative face
     of support section (ksf).
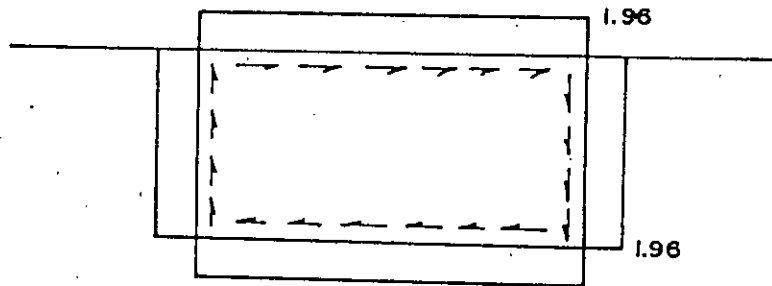
(c) Torsional shear stress (V_{svt}) on negative face of support section (ksf).
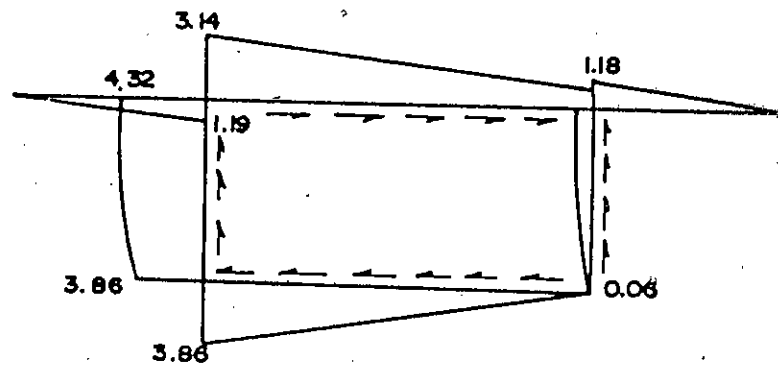
(d) Combined shear stress on negative face of support section (ksf).

Fig. A.3 Bending, shear and torsional stresses (ksf).
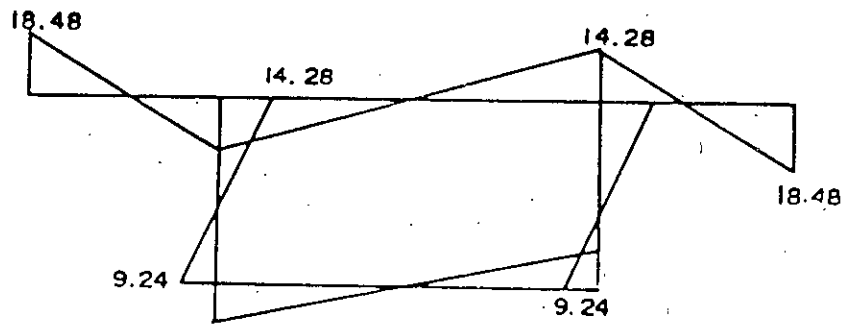
Fig. A.4 Diagram of torsional warping
coordinate (W_{twr}) (ft^2).
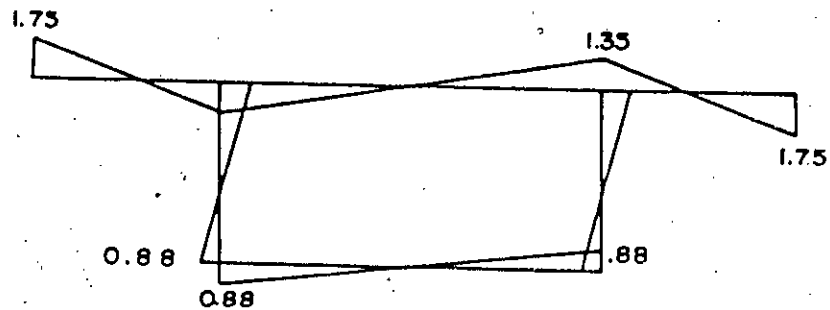
Fig. A.5 Torsional warping stress (f_{twr}) at midspan
section (ksf).
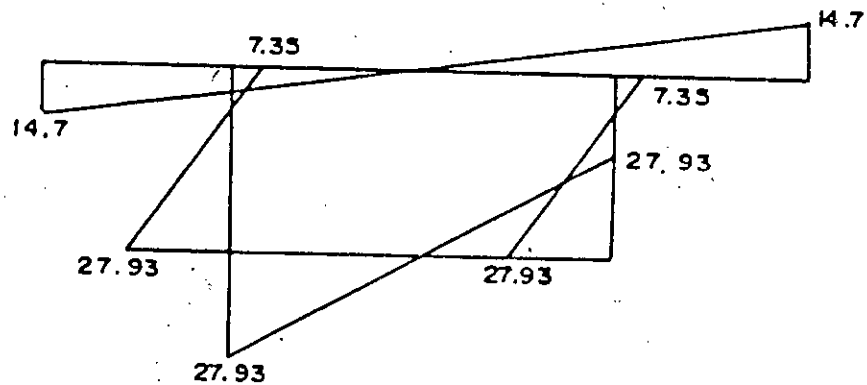
Fig. A.6, Diagram of distortional warping coordinate
(W_{dwr}), (ft^2).
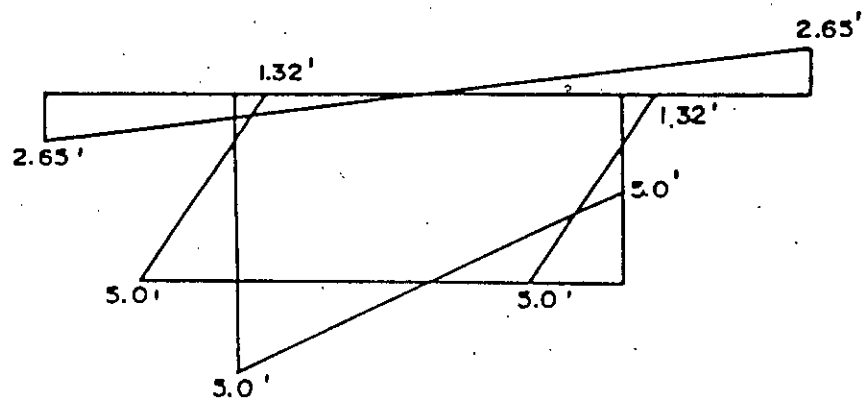
Fig. A.7   Distortional stress (f_{dwr}) at midspan
section (ksf).
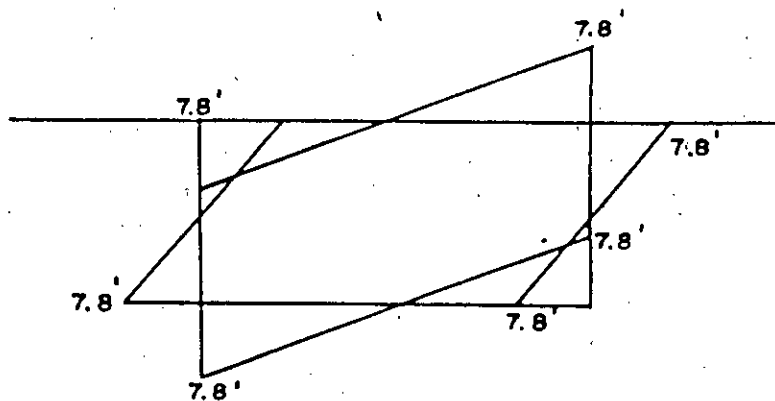
Fig. A.8   Maximum transverse bending stress (f_{trb})
at midspan section drawn on positive side (ksf).

EXAMPLE TWO

A simply supported single cell spine beam with diaphragms only at the ends is taken. The span (L) is 96 ft and HS_{20} loading is considered at midspan. Fig. A.9 shows the geometry and loading and Fig. A.10 gives the bending moment, shear force and torsional moment diagrams due to live load. For simplicity, thickness of top flange, bottom flange and webs are taken to be the same. The analysis would be restricted to live load effects only.

Analysis by simple beam theory and St. Venant Torsion Theory.

To calculate the stress distribution, the following section properties are required.

For longitudinal bending:

Depth of centroid above mid-line of bottom flange.

$y = (8.6 \times 2 \times 4.8 + 38.4 \times 9.6)/(8.6 \times 2 + 38.4 + 20.2)$

$= 5.95$ ft.

$I_x = (8.6^3/12) \times 2 + 8.6 \times 2 \times (1.15)^2 + 38.4 \times 3.65^2 + 20.2/12$

$\quad + 20.2 \times 5.95^2 = 1357$ ft^4

From Figs. 3.2 and 3.4, first moments of area of the partial half-cross-section about the centroidal x-axis as follows.

At top of web (B), just to right of mid-line of web.

$(Ay)_{1/2} = -9.6 \times 3.65 \times 1 = -35.04 \text{ ft}^3$

At top of web (B), just to left of mid-line of web.

$(Ay)_{1/2} = -9.6 \times 3.65 \times 1 = -35.04 \text{ ft}^3$

At level of centroid, $(y = 0)$

$(Ay)_{1/2} = (-2 \times 35.04 + 3.05^2/2) = -74.7 \text{ ft}^3$

At mid-depth of web $(y=0.7 \text{ ft})$

$(Ay)_{1/2} = -74.7 + 1.15^2/2 = -74.\text{ft}^3$

At bottom of web (D), $(y = 5.95)$

$(Ay)_{1/2} = -74.7 + 1 \times 5.95^2/2 = -57 \text{ ft}^3$

For St. Venant torsion

$A_{enc} = 9.6 \times 19.2 = 184.32 \text{ ft}^2$

By equation 3.5, torsional moment of inertia of cross-section,

$$C_{svt} = \frac{4 \times 184.32^2}{19.2/1 + 19.2/1 + 2 \times 9.6/1} = 2359 \text{ ft}^4$$

Bending stresses due to live load

At midspan, $M_x = 1448 \text{ k-ft}$, $M_y = 0$

By equation 3.1, at midspan of top flange.

$$f_{lbg} = -\frac{1448 \times 3.65}{1357} = -3.9 \text{ ksf}$$

At mid-line of bottom flange,

$$f_{lbg} = \frac{1448 \times 5.95}{} = 6.35 \text{ ksf}$$

1357

At support (z=0, V_y = 39.5ᵏ

By equation 3.2, at top of web, just to right of mid-line of web,

V_{lbg} = -39.5(-35.04)/1357 = 1.01 ksf

= magnitude of V_{lbg} at top of web just to left of mid-line of web.

At top of web,

V_{lbg} = - 39.5(-35.04x2)/(1357x1) = 2.02 ksf

At level fo centroid,

V_{lbg} = -39.5x(-74.7)/(1357x1) = 2.2 ksf

This is the maximum bending shear stress in the web

At bottom of web

V_{lbg} = -39.5(-57)/(1357.1) = 1.66 ksf

= magnitude of V_{lbg} at bottom of web just to right of mid-line of web.

Torsional stresses due to live load

At support (z=0), T_{svt} = 640 k-ft

By equation 3.3

V_{svt} = 640/(2x184.32) = 1.74 ksf

= magnitude of V_{svt} in web and flange.

The bending and torsional stresses calculated above are shown in the diagrams of Fig. A.11, which gives both the sign and the direction of action of stress.

Torsional warping analysis by the method of Kollbrunner, Hajdin and Heilig.

Position of shear centre

By equation B.2

I_y = $1 \times 38.4^3/12 + 1 \times 20.2^3/12 + 2 \times 8.6 \times 1^3/12 + 2 \times 8.6 \times 9.6^2$

= 6992 ft⁴

K_{13} = $1/4 \times 19.2 \times 1 \times 1 \times (1/3 \times 19.2 \times 1 + 3 \times 9.6 \times 1)$

= 169 ft⁵

K_{14} = $19.2 \times 9.6 \times 1 \times (1/6 \times 1^2 - 1/4 \times 1^2)$ = -15.36 ft⁵

K_{15} = $1/2 \times 1 \times 1 \times 1 \times (1/6 \times 19.2^2 + 9.6^2)$ = 76.8 ft⁵

K_{16} = $9.6 \times 1 \times 1 \times 1 \times (9.6 + 19.2)$ = 276.48 ft⁵

K_{17} = $19.2 \times 1 \times (1+1) + 2 \times 9.6 \times 1 \times 1 = 57.6$ ft³

$$d_{shc} = \frac{19.2^2 \times 9.6}{6992} \; ((169 - 15.36 + 76.8 + 276.48)/57.6)$$

= 4.45 ft

Evaluation of sectorial co-ordinate in torsional warping referred to shear centre (W_{twr}):

C_{svt} = 2359 ft⁴

A_{enc} = 184.32 ft²

and so $C_{svt}/(2 A_{enc})$ = 6.4

Hence in equation B.1

In top flange, (Points A,B,C)

a_s =, d_{shc} = 4.45 ft

In web, (Points B,D), a_s = b/2 = 9.6 ft

In bottom slab, (points D,E), $a_s = d-d_{s h c} = 9.6-4.45 = 5.15$ ft

At A, $S_{per} = 0$, from which $W_{t w r} = 0$

At B, $W_{t w r} = $ $(4.45-6.4/1)$ ds_{per}

           $= - 1.95 \times 9.6 = - 18.72$ ft^2

At C, $W_{t w r} = -18.72+$ a_s ds_{per}

       $= -18.72 + 4.45 (19.2-9.6)$

         $= 24$ ft^2

At D, $W_{t w r} = -18.72+$ $(9.6-6.4/1)ds_{per}$

         $= -18.72+3.2 \times 9.6 = 12$ ft^2

At E, $W_{t w r} = 12 +$ $(5.15-6.4/1)ds_{per}$

         $= 12+ (-1.25 \times 9.6) = 0$

Fig. A.12 shows the $W_{t w r}$ diagram.

Evaluation of torsional warping moment of inertia of cross-section ($C_{t w r}$):

Simpson's integration method is used to evaluate the integral in equation B.3

$C_{t w r} = 19.2 \times 1 \times (2 \times 18.72^2)/6+2 \times 9.6 \times 1 \times (18.72^2+4((-18.72+24)/2)^2$

     $+ 24^2)/6+2 \times 9.6 \times 1 \times (18.72^2+4((-18.72+12)/2)^2+12^2)/6$

     $+ 19.2 \times 1 \times (2 \times 12^2)/6$

     $= 7945$ ft^6

Evaluation of torsional warping bimoment ($B_{t w r}$):

In equation B.10

$C_{c e n} = 38.4 \times 4.45^2 \times 1+2 \times 9.6 \times 1 \times 9.6^2+19.2 \times 1 \times 3.15^2$

     $= 3039$ ft^4

In equation B.8

$K_{19} = 3039/(3039-2359) = 4.47$

In equation B.9

$C_{twr} = 4.47 \times 7945 = 35502$ ft⁶

In equation B.7, with Poisson's ratio taken as 0.18

$G/E = 1/(2(1+0.18)) = 0.424$

Hence $K_{18} = (0.424 \times 2359/35502)^{1/2}$

$= 0.168/ft$

In equation B.4, at midspan torsional warping bimoment,

$B_{twr} = 396.8 \times Sinh(0.168 \times 48)/(Cosh(0.168 \times 48))/(0.168 \times 4.47)$

$= 528$ k-ft²

Evaluation of torsional warping stresses

(f_{twr}) at midspan:

In equation B.11

$f_{twr} = 528/7954 \times W_{twr} = 0.066 W_{twr}$ ksf

At A, (Fig. A.12), $f_{twr} = 0$

At B, $\qquad f_{twr} = -1.24$ ksf

At C, $\qquad f_{twr} = 1.6$ ksf

At D, $\qquad f_{twr} = 0.8$ ksf

Figure A.13 shows the torsional warping stresses

Discussion of calculated stresses

The torsional warping stress (f_{twr}) of Fig. A.13 are compared

with the longitudinal bending stresses (f_{lbg}) of Fig. A.11a in

magnitude.

At top of web, at midspan,

$f_{twr}/f_{lbg} = 1.24/3.9 = 0.32$, i.e 32%

At ends of cantilevers, at midspan,

$f_{twr}/f_{lbg} = 1.6/3.9 = 0.4$, i.e. 40%

At bottom of web, at mdispan,

$f_{twr}/f_{lbg} = 0.8/6.35 = 0.12$, 12%

The above increases in longitudinal stress(where f_{lbg} and f_{twr} are additive) will be larger when the effect of distortional warping is considered.

Distortional analysis by the beam on elastic foundation analogy.

Evaluation of distortional warping co-ordinate W_{dwr}:

By equations C.2, C.3, and C.4

$$K_6 = \frac{19.2}{9.6} ((19.2+19.2)/19.2)^3 = 16$$

$$K_7 = \frac{19.2 \times 1}{9.6 \times 1} = 2$$

$$K_{25} = \frac{3+16}{3+2} = 3.8$$

From Fig. C.1, at top of web,

$W_{dwr} = 19.2 \times 9.6/(4(1+3.8)) = 9.6$ ft²

At end of cantilever,

$$W_{dwr} = \frac{19.2+19.2}{19.2} \times 9.6 = 19.2 \text{ ft}^2$$

The above values of W_{dwr} are shown in Fig. A.6

Fig. A.14: Diagram of distortional warping co-ordinate (W_{dwr}) at midspan.

Evaluation distortional warping moment of inertia of cross-section (C_{dwr}):

By equations C.1 and C.5

$K_4 = (3+2(16+2)+16.x2)/(6+16+2) = 2.96$

$C_{dwr} = 19.2^2 \times 9.6^3 \times 1 \times 2.96/48 = 20112 \text{ ft}^6$

Evaluation of frame stiffness (EI_{tra}):

By equation C.6-C.10, with Poisson's ratio taken as 0.18

$I_{top} = 1^3/(12(1-0.18^2)) = 0.0861 \text{ ft}^4/\text{ft}$

$I_{bot} = 0.0861 \text{ ft}^4/\text{ft}$

$I_{web} = 0.0861 \text{ ft}^4/\text{ft}$

$K_{26} = 1+(2 \times 19.2/9.6+3 \times 2)/(2+6/2) = 3$

$I_{tra} = 24 \times 0.0861/(3 \times 9.6) = 0.07175 \text{ ft}^2$

Evaluation of distortional warping bimoment (B_{dwr}):

By equations C.12 and C.13

$K_{27} = (0.07175/(4 \times 20112))^{1/4} = 0.0307/\text{ft}$

B_{dwr} at midspan $= 72 \times 19.2/(16.0 \times .0307) \times (\text{Sinh}(0.0307 \times 96)$

$+\text{Sin}(0.0307 \times 96))/(\text{Cosh}(0.0307 \times 96)$

$+\text{Cos}(0.0307 \times 96))$

$= 2548 \text{ k-ft}^2$

Evaluation of distortional warping stresses (f_{dwr}) at midspan

In equation C.11

f_{dwr} = (2548/20112)xW_{dwr} = 0.1267 W_{dwr} ksf

At A (Figure C.1), f_{dwr} = 0

At B, f_{dwr} = 0.1267(-9.6) = - 1.22 ksf

At C, f_{dwr} = 0.1267(-19.2) = -2.44 ksf

At D, f_{dwr} = 0.1267 (36.48) = 4.62 ksf

At E, f_{dwr} = 0

These stresses are shown in Fig. A.15

Evaluation of transverse bending stresses (f_{trb}) at midspan:

In equation C.17,

$$K_{30} = \frac{3+2}{3+2} = 1$$

In equation C.18

EI_{trs} B_{trb} = (72x19.2x0.0307)x(Sinh(.0307x96)-Sin(.0307x96))/(8(Cosh(.0307x96)+Cos(.0307x96)))

= 4.75 kips

In equation C.15, at top of web

M_{trb} B = 4.75/(2(1+1)) = 1.19 k-ft/ft

In equation C.16, at bottom of web,

$M_{trb}, D = -1.19$ ksf/ft

In equation B.14, at top of web, in top flange

$f_{trb} = 6 \times M_{trb}/h^2$

$= 6 \times 1.10/1^2 = 7.12$ ksf

At bottom of web, $f_{trb} = 7.12$ ksf

These stresses are shown in Figure A.16

Discussion of calculated stresses:

The magnitudes of distortional warping stresses (f_{dwr}), torsional warping stresses (f_{twr}) are compared to longitudinal bending stress (f_{lbg}).

At top of web, at midspan,

$(f_{twr} + f_{dwr})/f_{lbg} = (1.24+1.22)/3.9 = .6$, i.e 60%.

$f_{dwr}/f_{lbg} = 1.22/3.9 = 0.3$, i.e. 30%.

At ends of cantilevers, at midspan

$(f_{twr} + f_{dwr})/f_{lbg} = (1.6-2.44)/3.9 = .2$ i.e. 20%

$f_{dwr}/f_{lbg} = 2.44/3.9 = 0.62$, i.e 62%.

At bottom of web, at midspan,

$(f_{twr}+f_{dwr})/f_{lbg} = (0.8+4.62)/6.35 = .85$, i.e 85%

$f_{dwr}/f_{lbg} = 4.62/6.35 = 0.72$, i.e 72%

The above increases in longitudinal stress (where f_{lbg}, f_{twr} and f_{dwr} are additive) are significant in design, even if the torsional warping stress (f_{twr}) is neglected.

In addition,

In the top flange, at the web

$$f_{trb}/(f_{lbg}+f_{twr}+f_{dwr}) = 7.12/(3.9+1.24+1.22) = 1.11 \text{ i.e } 111\%$$

In bottom flange, at the web,

$$f_{trb}/(f_{lbg}+f_{twr}+f_{dwr}) = 7.12/(6.35+.8+4.62) = 0.60, \text{ i.e: } 60\%.$$

Thus the transverse bending stresses are of the same order as the resultant longitudinal stresses at midspan, and are therefore significant in design. It is important to consider Poisson's ratio effects in this situation.

(a) ELEVATION OF BEAM

(b) SECTION A—A
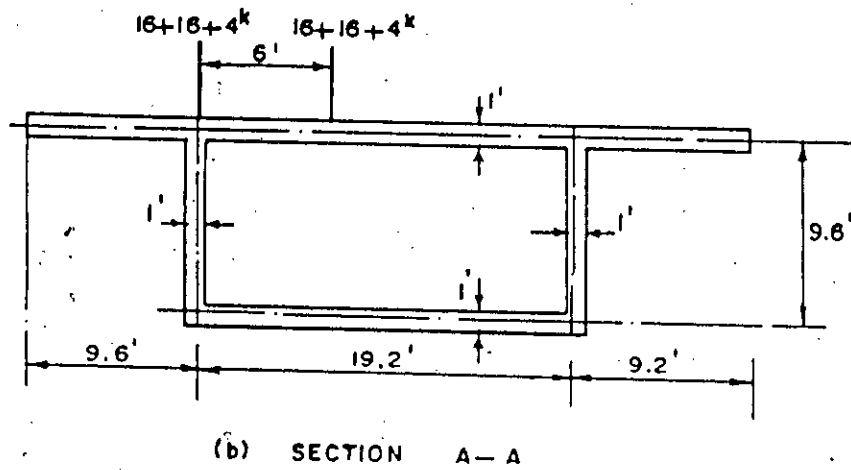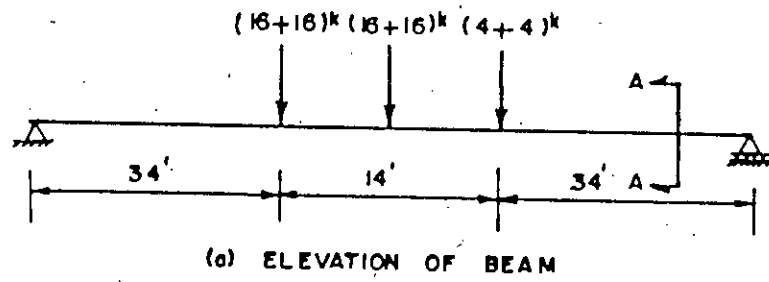
Fig. A.9 Loading and geometry.
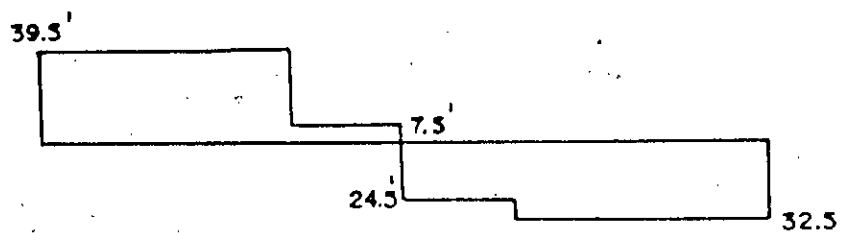
(a) Shear force diagram (kip).
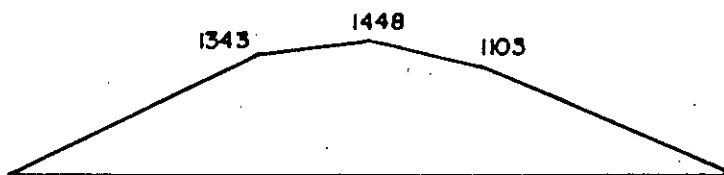
(b) Longitudinal bending moment diagram (k-ft).
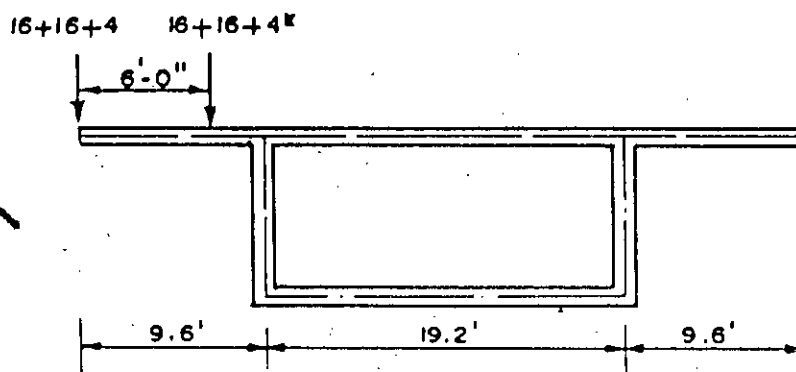
Position of loading for torsional analysis.
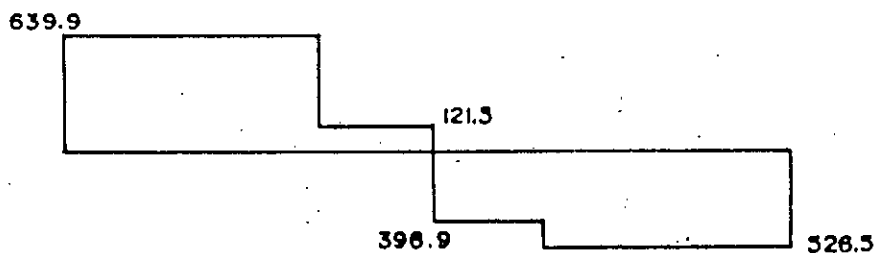
(c) Torsional moment diagram (k-ft).

Fig. A.10 Shear force, bending and torsional moment diagram due to live load.
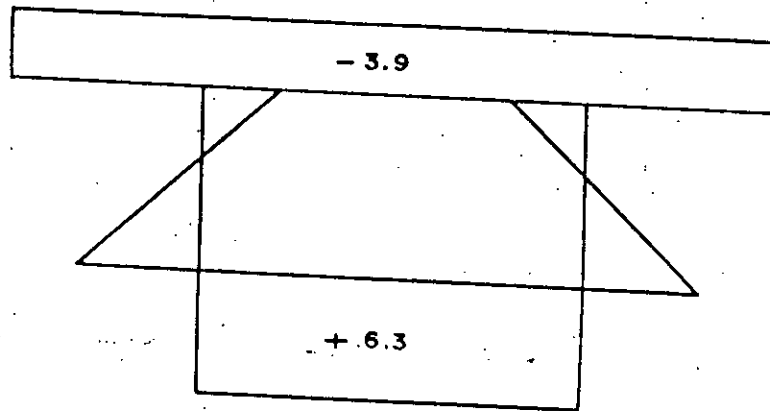
(a) Longitudinal bending stress at midspan section (ksf).
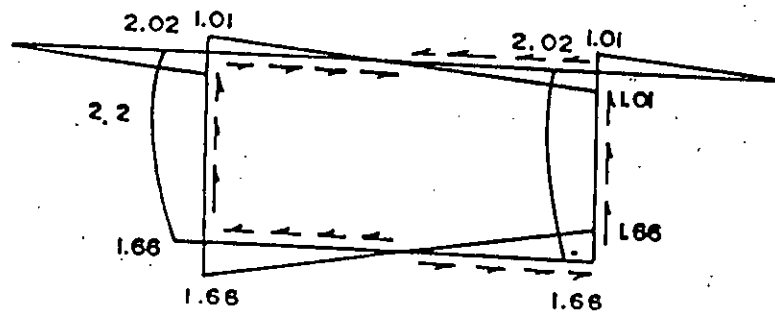
(b) Bending shear stress (V_{lbg}) on negative face of support section (ksf).
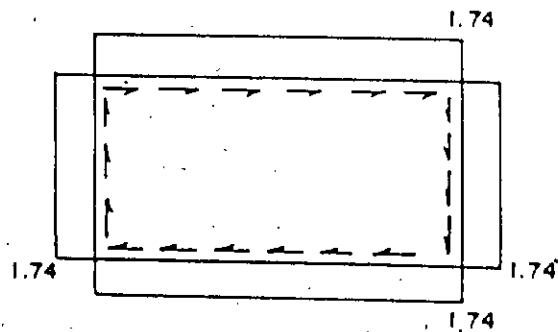
(c) Torsional shear stress (V_{svt}) on negative face of support section (ksf).
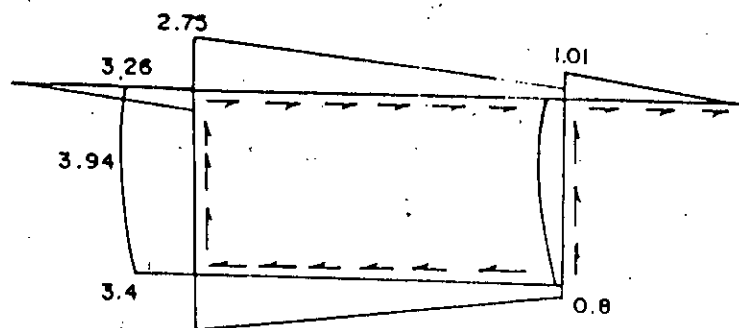
(d) Combined shear stress on negative face of support section (ksf).

Fig. A.11 Bending, shear and torsional stresses (ksf).
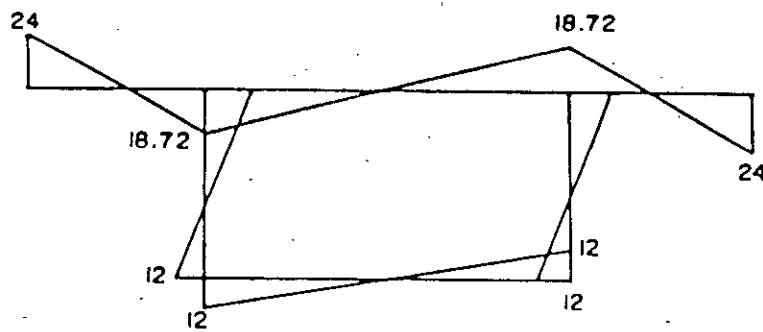
Fig. A.12 Diagram of torsional warping coordinate
(W_{twr}), (ft^2).
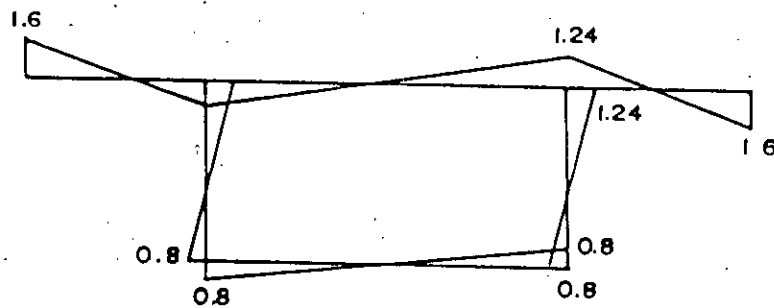
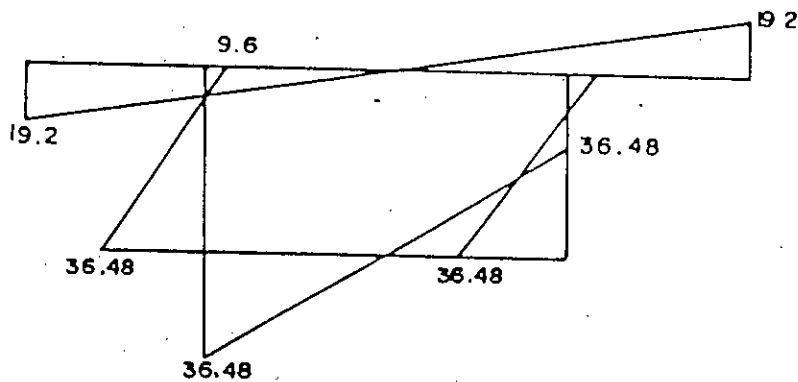
Fig. A.13 Torsional warping stress (f_{twr}) at
midspan. section (ksf).

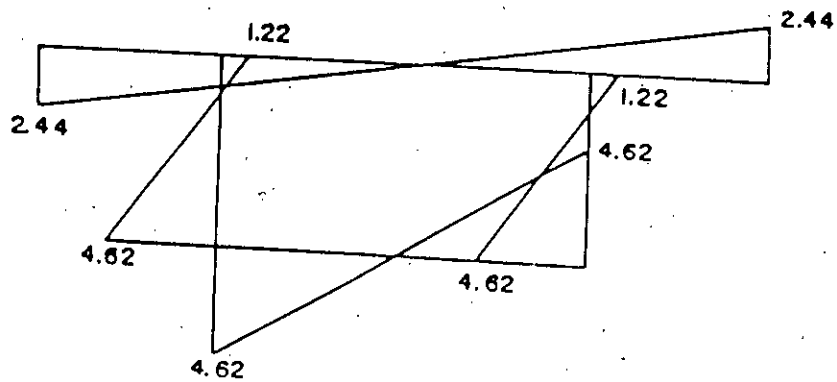Fig. A.14 Diagram of distortional warping coordinate
(W_{dwr}), $(ft2)$.

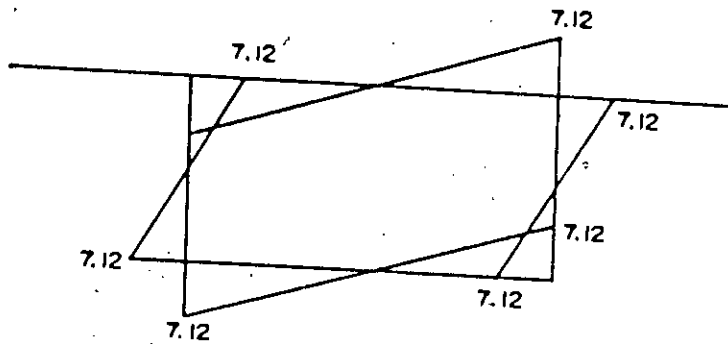Fig. A.15 Distortional tress (f_{dwr}) at midspan
section (ksf)

Fig. A.16 Maximum transverse bending stress (f_{trb})
at midspan section on positive side
(ksf).

EXAMPLE THREE

A simply supported single cell spine beam with diaphragms only at the ends is taken. The span (L) is 120 ft and HS$_{20}$ loading is considered at midspan. Fig. A.17 shows the geometry and loading and Fig. A.18 gives the bending moment, shear force and torsional moment diagrams due to live load. For simplicity, thickness of top flange, bottom flange and webs are taken to be the same. The analysis would be restricted to live load effects only.

Analysis by simple beam theory and St. Venant Torsion Theory.

To calculate the stress distribution, the following section properties are required.

For bending:

Depth of centroid above mid-line of bottom flange

$y = (11 \times 1 \times 2 \times 6 + 48 \times 1 \times 12)/(48 + 11 \times 2 + 25)$

$= 7.45'$

$I_x = 2 \times 11^3/12 + 2 \times 11 \times (7.45-6)^2 + 48/12 + 48 \times (12-7.45)^2$

$+ 25/12 + 25 \times 7.45^2$

$= 2655 \ ft^4$

Bending stresses due to live load:

At mid-span, $M_x = 1880$ k-ft, $M_v = 0$

By equation 3.1, at midspan of top flange

$f_{bg} = - (1880 \times 4.55)/2655 = -3.2 \ ksf$

At mid-line of bottom flange,

f_{1bg} = 1880x7.45/2655 = 5.27 ksf

There stresses are shown in Fig. A.19.

Torsional Warping analysis by the method of Kollbrunner, Hajdin and Heilig:

Evaluation of Shear Centre:

By equation B.2,

I_y = 1x48³/12+1x25³/12+2x11/12+2x11x12²

= 13,688 ft⁴.

K_{13} = 1x24x1x1(24x1/3+3x12x1)/4=264 ft⁵

K_{14} = 24x12x1(1x1²/6-1²/4) = -24 ft⁵

K_{15} = 1x1x1(1x24²/6+12²)/2 = 120 ft⁵

K_{16} = 12x1x1(12+24) = 432 ft⁵

K_{17} = 24x1x(1+1)+2x12x1x1 = 72 ft³

d_{ahc} = 24²x12x(264-24+120+432)/(13688x72)

= 5.55 ft.

Evaluation of sectorial co-ordinate in torsional warping (W_{twr}):

Torsional moment of inertia of cross-section

C_{avt} = 4x(12x24)²/(24/1+24/1+24/1)

= 4608

A_{enc} = 12x24 = 288 ft²

and so C_{avt}/(2 A_{enc}) = 4608/(2x288)

= 8 ft²

Hence in equation B.1

In top flange, (Points A,B,C)

$a_s = d_{shc} = 5.55'$

In web (Points B,D), $a_s = b/2 = 12$ ft

In bottom slab, (Points D,E), $a_s = d - d_{shc} = 6.45$ ft

At A, $S_{per} = 0$, from which $W_{twr} = 0$

At B, $W_{twr} = \quad (5.55-8.6/1)ds_{per}$

$\qquad = -12 \times 2.45 = -29.4$ ft²

At C, $W_{twr} = -29.4 + 12 \times 5.55$

$\qquad = 37.2$ ft²

At D, $W_{twr} = -29.4 + 12 \times (12-8.0)$

$\qquad = 18.6$ ft²

At E, $W_{twr} = 0$

Figure A.20 shows the W_{twr} diagram.

Evaluation of torsional warping moment of inertia of cross-section (C_{twr}): Simpson's integration method is used to evaluate the integral in equation B.3.

$C_{twr} = 24 \times 1 (2 \times 29.4^2)/6 + 2 \times 12 \times 1 \times (29.4^2 + 4((-29.4+37.2)/2)^2$

$\qquad + 37.2^2)/6 + 2 \times 12 \times 1 \times (29.4^2 + 4((29.4+18.6)/2)^2 + 18.6^2)/6$

$\qquad + 24 \times 1 \times (2 \times 18.6^2)/6$

$\qquad = 24226$ ft⁶

Evaluation of torsional warping bimoment (B_{twr}):

In equation B.10, central torsional moment of inertia,

$$C_{cen} = 48 \times 1 \times 5.55^2 + 2 \times 12 \times 1 \times 12^2 + 24 \times 1 \times 6.45^2$$

$$= 5933 \text{ ft}^4$$

In equation B.8

$$K_{19} = 5933/(5933-4608) = 4.47$$

In equation B.19

$$C_{twr} = 4.47 \times 24226 = 10,8290 \text{ ft}^6$$

In equation B.7,

$$G/E = 1/(2(1+0.18)) = 0.424$$

Hence,

$$K_{18} = (0.424 \times 4608/108290)^{1/2}$$

$$= 0.134/\text{ft}$$

In equation B.4, torsional warping bimoment,

$$B_{twr} = 529.2/(0.134 \times 4.47) \times (Sinh(0.134 \times 60)/Cosh(0.134 \times 60))$$

$$= 864 \text{ k-ft}^2$$

Evaluation of torsional warping stresses (f_{twr}) at mispan:

In equation B.11

$$f_{twr} = 864 \, W_{twr}/24226 = 0.0356 \, W_{twr}$$

At A, Fig. (A.20), $f_{twr} = 0$

At B, $\qquad\qquad\qquad f_{twr} = 1.05 \text{ ksf}$

At C, $f_{twr} = 1.33$ ksf

At D, $f_{twr} = 0.66$ ksf

At E, $f_{twr} = 0$

Fig. A.21 shows the torsional warping stress:

Discussion of calculated stresses:

The torsional warping stresses (f_{twr}) of Fig. A.21 are compared with the longitudinal bending stresses (f_{lbg}) of Fig. A.19 in magnitude.

At top of web, at midspan,

$f_{twr}/f_{lbg} = 1.05/3.2 = 0.32$ i.e 32%

At end of cantilevers, at midspan.

$f_{twr}/f_{lbg} = 1.33/3.2 = 0.40$, i.e 40%

At bottom of web, at midspan,

$f_{twr}/f_{lbg} = 0.66/522 = 0.12$, i.e 12%

The above increases in longitudinal stress where f_{lbg} and f_{twr} are additive) will be larger when the effect of distortional warping is considered.

Distortional analysis by the beam-on-elastic foundation analogy:
Evaluation of distortional warping co-ordinate (W_{dwr}):
By equation C.2, C.3 & C.15

$K_6 = 24 \times 1 ((24+2 \times 12)/24)^3/(12 \times 1) = 16$

$K_7 = 24 \times 1/(12 \times 1) = 2$

$K_{25} = (3+16)/(3+2) = 3.8$

From Fig. C.1, at top of web,

$W_{dwr} = 24 \times 12/(4 \times (1+3.8)) = 15$ ft²

At bottom of web, $W_{dwr} = 3.8 \times 15 = 57$ ft²

At end of cantilever,. $W_{dwr} = (24+2 \times 12) \times 15/24 = 30$ ft²

The above values of W_{dwr} are shown in Fig. A.22.

Evaluation of distortional warping moment of cross-section (C_{dwr}):

By equation C.1 and C.5

$K_4 = (3+2(16+2)+16 \times 2)/(6+16+2)$

$= 2.96$

$C_{dwr} = (24^2 \times 12^3 \times 1 \times 2.96)/48 = 61344$ ft⁶

Evaluation of frame stiffness:

By equation C.6 to C.10, with Poisson's ratio taken as 0.18

$I_{top} = 1^3/(12(1-.18^2)) = 0.0861$ ft⁴/ft

$I_{bot} = 0.0861$ ft⁴/ft

$I_{web} = 0.0861$ ft⁴/ft

$K_{26} = 1+((2 \times 24/12+3 \times 2)/(2+6 \times 1/2))$

$= 3$

$I_{fra} = (24 \times 0.0861)/(3 \times 12)=0.0574$ ft².

Evaluation of distortional warping bimoment (B_{dwr}):

By equations C.12 and C.13,

K_{27} = $(0.0574/(4 \times 61344))^{1/4}$ = 0.022

B_{dwr} = $72 \times 24 \times ((Sinh(0.022 \times 120) + Sin(0.022 \times 120))/$

$(Cosh(0.022 \times 120) + Cos(0.022 \times 120))/(16 \times 0.022)$

= 4283 k-ft^2

Evaluation of distortional Warping Stresses (f_{dwr}) at midspan:

In equation C.11

f_{dwr} = $(4283/61344)$ W_{dwr}

= 0.0698 W_{dwr} ksf

At A, Fig. (A.22), f_{dwr} = 0

At B, f_{dwr} = 1.05 ksf

At C, f_{dwr} = 2.1 ksf

At D, f_{dwr} = 3.98 ksf

At E, f_{dwr} = 0

These stresses are shown in Fig. A.23.

Evaluation of transverse ebding stresses (f_{trb}) at midspan:

In equation C.17

K_{30} = $(3 + 24/12)/(3 + 24/12)$ = 1

In equation C.18

EI_{tra} B_{trb} = $(72x24x.022)x(Sinh(.022x120)-$

$Sin(.022x120)/((Cosh(0.022x120))+Cos(0.022x120))x8)$

= 4.09 kips

In equation C.15, at top of web

M_{trb}, B = $4.09/(2(1+1))$=1.023 k-ft/ft

In equation C.16, at bottom of web,

M_{trb}, D = -1.023 k-ft/ft

In equation C.14, at top of web, in top flange,

max f_{trb} = $6x1.023/1^2$ = 6.10 ksf

At bottom of web, f_{trb} = 6.1 ksf

These stresses are shown in Fig. A.24.

Discussion of calculated stresses:

The magnitude of distortional warping stresses (f_{dwr}), torsional warping stresses (f_{twr}) are compared to longitudinal bending stresses (f_{lbg}).

At top of web, at midspan,

(f_{twr} + f_{dwr})/f_{lbg} = $(1.05+1.05)/3.2$ = 0.65, i.e 65%

f_{dwr}/f_{lbg} = 1.05/3.2 = 0.30, i.e 30%

At ends of cantilever, at midspan,

(f_{twr} + f_{dwr})/f_{lbg} = $(1.33-2.1)/3.2$=0.24, i.e 24%

f_{dwr}/f_{lbg} = 2.1/3.2 = 0.65, i.e 65%

At bottom of web, at midspan,

$(f_{twr}+f_{dwr})/f_{lbg}$ = $(0.66+3.98)/5.22$

$= 0.88$, i.e 88%

f_{dwr}/f_{lbg} = $3.98/5.22=0.76$, i.e 76%.

The above increases in longitudinal stress (where f_{lbg}, f_{twr} and f_{dwr} are additive) are significant in design, even if the torsional warping stress f_{twr} is neglected.

In addition:

In the top flange, at the web, $f_{trb}/(f_{lbg}+f_{twr}+f_{dwr})$ = $6.10/(3.2+1.05+1.05)$

$= 1.11$, i.e, 111%

In the bottom flange, at the web,

$f_{trb}/(f_{lbg}+f_{twr}\_f_{dwr})$ = $6.10/(5.2+0.66+3.98)$

$= 0.60$, i.e 60%

Thus the transverse bending stresses are of the same order as the resultant longitudinal stresses at midspan, and are therefore significant in design. It is important to consider Poisson's ratio effects in this situation.
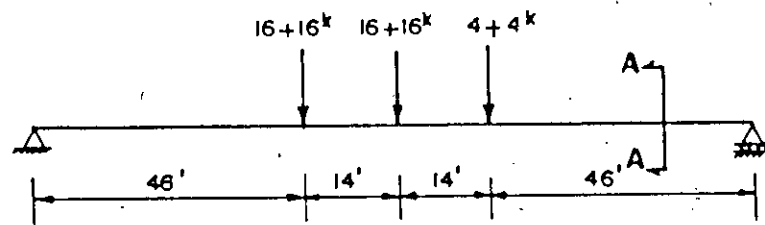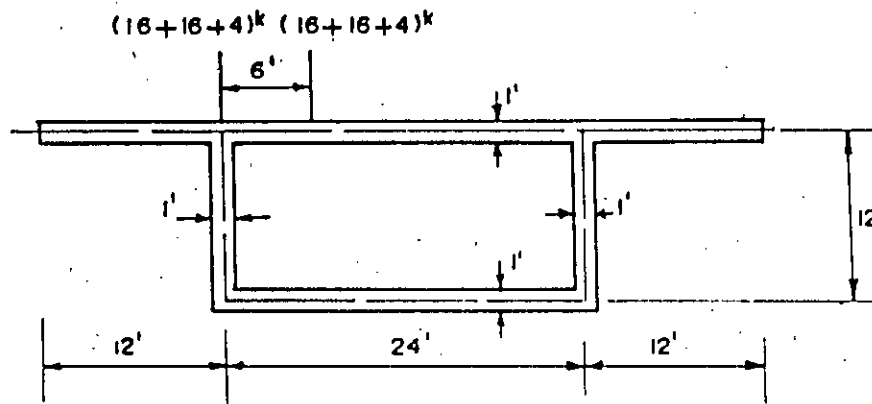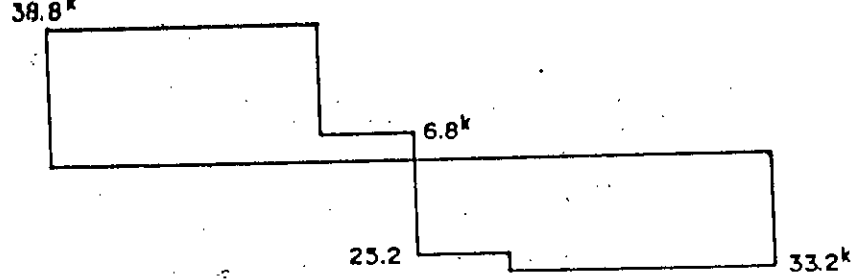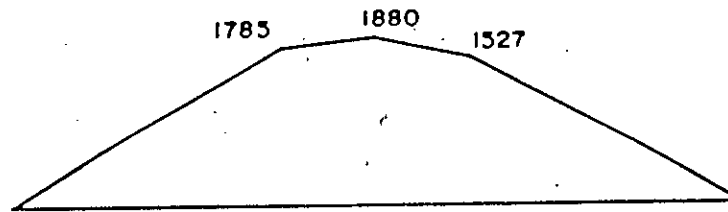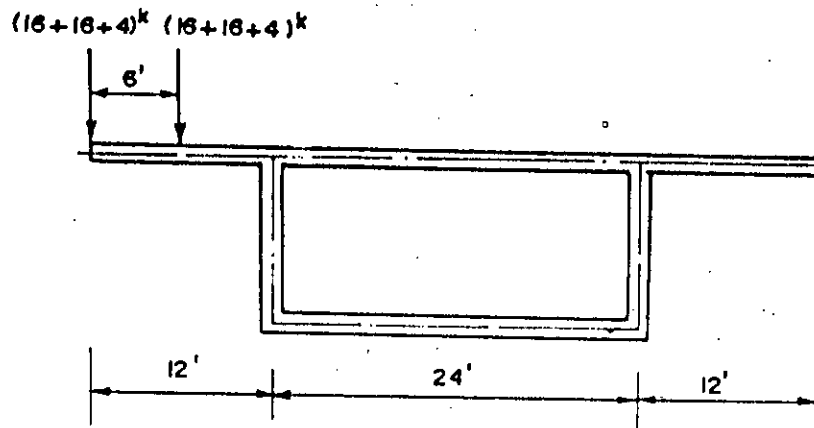
(a) Elevation of Beam

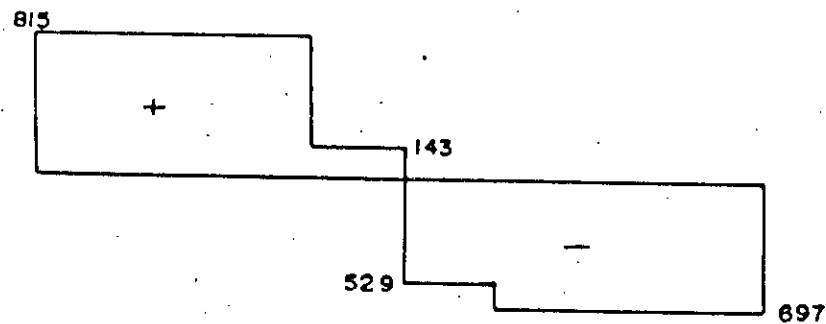(b) Section A-A

Fig. A.17 Loading and geometry.

(a) Shear force diagram (kips).

(b) Bending moment diagram (k-ft).

Position of loading for torsional analysis.

(c) Torsional moment diagram (k-ft).

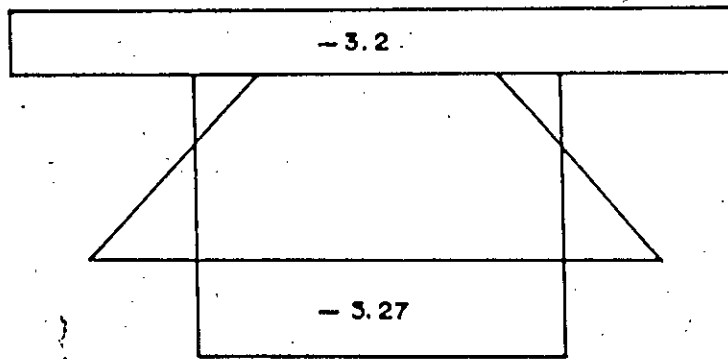Fig. A.18 Bending moment, shear force and torsional
moment diagram due to live load.
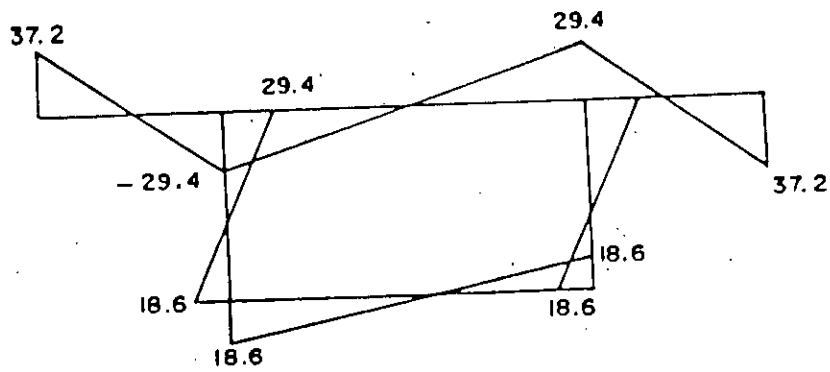
Fig. A.19 Longitudinal bending stress at
midspan (ksf).

Fig. A.20 Diagram of torsional warping coordinate (W_{twr}) (ft^2).
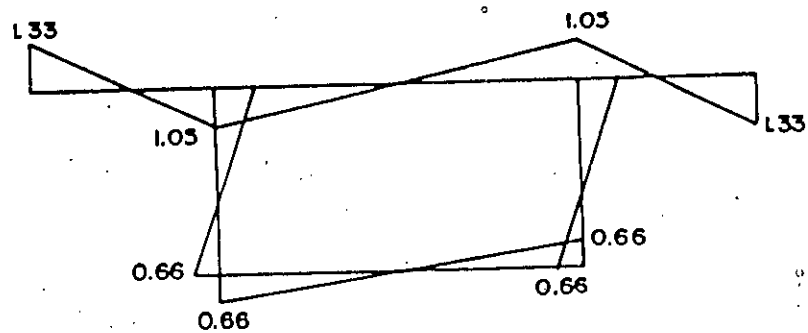

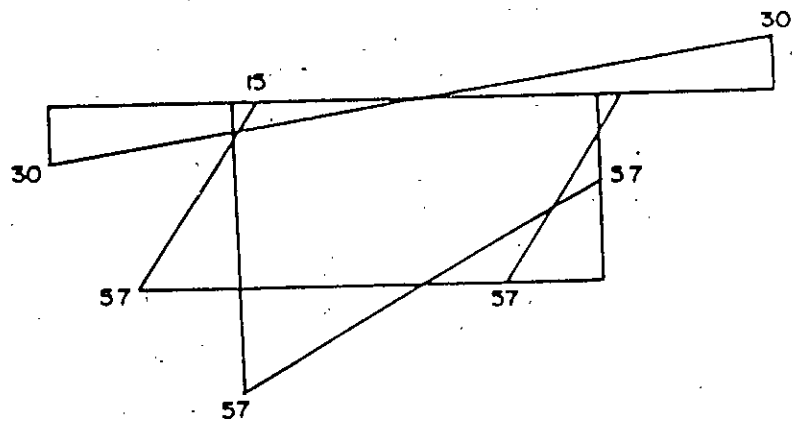Fig. A.21 Torsional warping stress (f_{twr}) at midspan section (ksf)

Fig. A.22 Diagram of distortional warping co-ordinate $(W_{dwr})(ft^2)$.
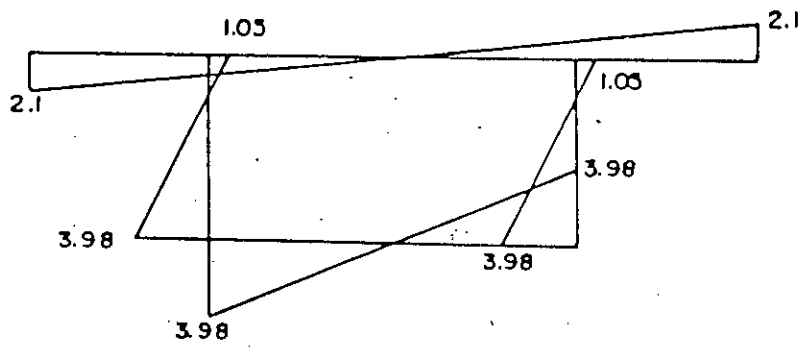
Fig. A.23 Distortional stress (f_{dwr}) at midspan
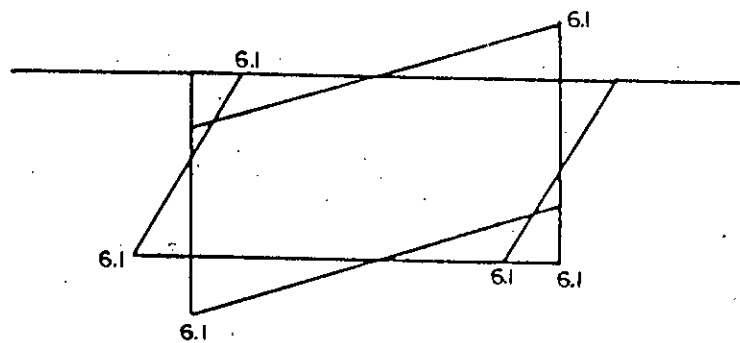section (ksf).

Fig. A.24 Maximum transverse bending stress
(f_{trb}) at midspan section (ksf).

APPENDIX-B
EXPRESSIONS USED IN TORSIONAL WARPING ANALYSIS BY
THE METHOD OF KOLLBRUNNER, HAJDIN AND HEILIG [9,6]

The sectorial coordinate w_{twr} is defined as

$$w_{twr} = \int (a_s - C_{svt}/(2 A_{enc}))ds_{per} \qquad (B.1)$$

where

a_s is the perpendicular distance from the shear centre to

the tangent to the mid-line of wall at the point

considered

C_{svt} is defined in equation 3.5

A_{enc} is defined in equation 3.3

h is the wall thickness

s_{per} is the peripheral coordinate along the mid-line of wall

To find a_s the following expression is used for the position of

the shear centre

$$d_{shc} = b^2 d/I_y (K_{13}+K_{14}+K_{15}+K_{16})/K_{17} \qquad (B.2)$$

where

d_{shc} = depth of shear centre below mid-line of top slab

I_y = moment of inertia of entire cross-section about the

centroidal y axis

$b, b_{cant}, d, h_{top}, h_{web}$ and h_{bot} are defined in Fig. 3.1

K_{13} = $1/4 b h_{bot} h_{web}(1/3 \ b h_{bot}+3 d h_{web})$

K_{14} = $b d \ h_{top}(1/6 \ h^2_{bot} - 1/4 \ h^2_{web})$

K_{15} = $1/2 \ h_{top} h_{bot} h_{web}(1/6 \ b^2+d^2)$

K_{16} = $b_{cant} h_{top} h_{web} \ h_{bot}(b_{cant}+b)$

K_{17} = $b h_{web}(h_{top}+h_{bot})+2 d h_{top} h_{bot}$

The torsional warping moment of inertia of cross-section C_{twr} is

9also required, and is defined as

$$C_{twr} = \int W^2_{twr} \, dA \qquad (B.3)$$

Relations between applied load, internal stress-resultants and twist.

$$B_{twr}(Z) = \frac{T_{ext}}{2K_{18}K_{19}} \cdot \frac{Sin(K_{18}z/l)}{Cosh\left(\dfrac{K_{18}\, l}{2}\right)} \qquad (B.4)$$

$$T_{svt}(z) = T_{ext}(-1+Cosh(K_{18}z)/(K_{19}\ Cosh(K_{18}L/2)))/2 \qquad (B.5)$$

$$T_{twr}(z) = \frac{T_{ext}}{2K_{19}} \cdot \frac{Cosh\ K_{18}\ z}{Cosh\dfrac{K_{18}\ l}{2}} \qquad (B.6)$$

where,

T_{ext} = Concentrated torsional moment subjected to midspan.

$B_{twr}(z)$ = bimoment of torsioanl warping at section Z

$T_{svt}(z)$ = torsional moment due to St. Venant shear stresses at section Z

T_{twr} = torsional moment due to torsional warping shear stresses at section Z

$$K_{18} = (G\ C_{svt}/E\ C_{twr})^{1/2} \qquad (B.7)$$

$$K_{19} = C_{con}/(C_{con}-C_{svt}) \qquad (B.8)$$

$$\bar{C}twr = K_{19}\ C_{twr} \qquad (B.9)$$

C_{con} = Central torsional moment of inertia of cross-section

$$= \int a^2_s \, dA \qquad (B.10)$$

Torsional Warping Stresses f_{twr}

$$f_{twr} = (B_{twr}\ W_{twr})/C_{twr} \qquad (B.11)$$

APPENDIX-C
EXPRESSIONS USED IN DISTORTIONAL WARPING BY
THE BEAM — ON-ELASTIC FOUNDATION ANALOGY

$$K_4 = \frac{3 + 2(K_6 + K_7) + K_6 K_7}{6 + K_6 + K_7} \tag{C.1}$$

$$K_6 = \frac{bh_{top}}{bh_{web}} \left(\frac{b + 2b_{cant}}{b}\right)^3 \tag{C.2}$$

$$K_7 = \frac{bh_{top}}{dh_{web}} \tag{C.3}$$

$$K_{25} = \frac{3 + K_6}{3 + K_7} \tag{C.4}$$

The distortional warping moment of inertia of cross-section:
C_{dwr} is given by the following expression:

$$C_{dwr} = \frac{b^2 d^3 h_{web}}{48} K_4 \tag{C.5}$$

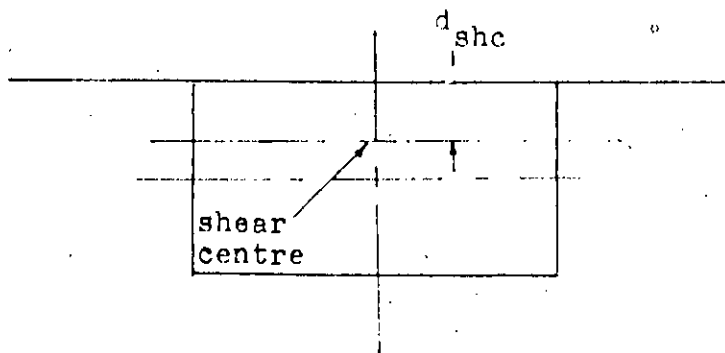The frame stiffness EI_{fra} is obtained from:
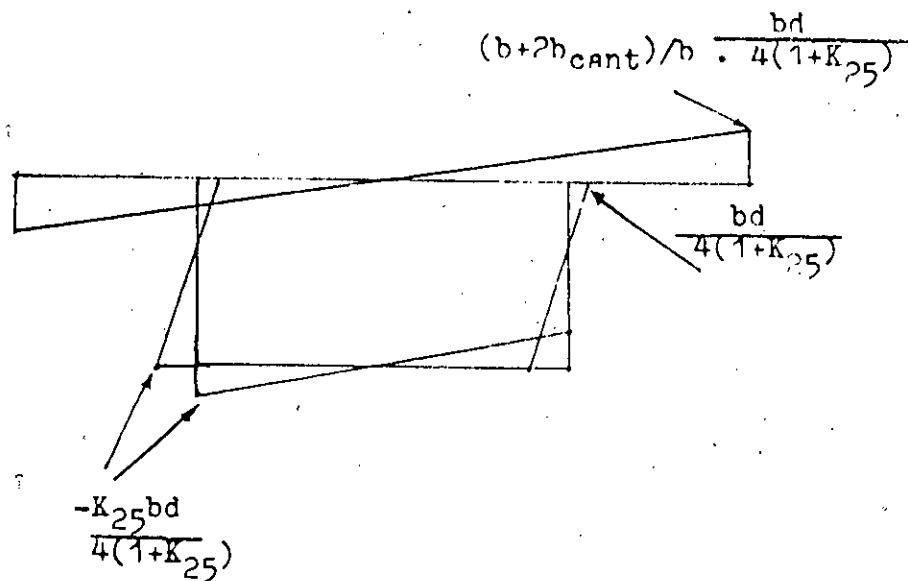
$$I_{fra} = \frac{24 \, I_{web}}{K_{26} \, d} \tag{C.6}$$

where,

$$K_{26} = 1 + \frac{2b/d + 3(I_{top} + I_{bot})/I_{web}}{\dfrac{I_{top} + I_{bot}}{I_{web}} + 6d/b \dfrac{I_{top} I_{bot}}{I^2_{web}}} \tag{C.7}$$

$$I_{top} = \frac{h^3_{top}}{12(1 - m^2)} \tag{C.8}$$

$$I_{bot} = \frac{h^3_{bot}}{12(1 - m^2)} \tag{C.9}$$

a) Position of shear centre.

b) Distortional warping coordinate w_{dwr}.

Fig. C.1 Position of shear centre and Distortional warping coordinate

$$I_{web} = \frac{h^3{}_{web}}{12(1-m^2)}$$ (C.10)

m = Poisson's ratio
E = Young's modulus of elasticity

Distortional Warping Stresses f_{dwr}

$$f_{dwr} = \frac{B_{dwr} W_{dwr}}{C_{dwr}}$$ (C.11)

$$B_{dwr} = \frac{F_v b}{16 K_{27}} \frac{Sinh (K_{27} \ l) + Sin (K_{27} \ l)}{Cosh (K_{27} \ l) + Cos (K_{27} \ l)}$$ (C.12)

$$K_{27} = \left(\frac{I_{fra}}{4 \ C_{dwr}}\right)^{1/4}$$ (C.13)

F_v = Concentrated load applied on web at midspan.

Transverse bending stresses f_{trb}

$$f_{trb} = 6/h^2 \quad M_{trb}$$ (C.14)

where

M_{trb} = transverse bending moment due to distortional load system
h = web thickness
f_{trb} = transverse bending stress at face of web

$$M_{trb}, \ B = \frac{E \ I_{fra} \ B_{trb}}{2(1 + K_{30})}$$ (C.15)

At bottom of web

$$M_{trb}, \ D = - \frac{K_{30} \ E \ I_{fra} \ B_{trb}}{2(1+K_{30})}$$ (C.16)

$$K_{30} = \frac{3+(b/d)(I_{web}/I_{top})}{3.+(b/d)(I_{web}/I_{bot})}$$ (C.17)

The midspan value of B_{trb} for the load case considered

$$B_{trb} = \frac{F_v b \ K_{27}}{8 \ E \ I_{fra}} \frac{Sinh \ (K_{27} \ L) - Sin(K_{27} \ L)}{Cos \ (K_{27} L) + Cos(K_{27} L)}$$ (C.18)